CONFIDENTIAL

THE INFLUENCE OF MICROSTRUCTURE ON THE HOT DUCTILITY OF FOUR LOW CARBON STEELS WITH RESPECT TO TRANSVERSE CRACK FORMATION IN CONTINUOUSLY CAST SLABS

by

Geraldo I. S. L. Cardoso

A Thesis Submitted to the Faculty of Graduate Studies and Research in Partial Fulfillment of the Requirements for the Degree of Master of Engineering

Department of Mining and Metallurgical Engineering
McGill University
Montreal, Canada

February 1990

ABSTRACT

The influence of Al, Mn and Ti on the hot ductility of four low C steels has been examined. The steels were solution treated at 1350°C, and tensile tested in the temperature range of 700 to 1000°C at a strain rate of $10^{-3}s^{-1}$. Specimens were cooled to test temperature either continuously or by oscillating about a mean cooling rate. Samples were quenched after fracture in order to relate the microstructure to the hot ductility behavior.

Ductility troughs were exhibited by all the steels. These could be related to the austenite-to-ferrite phase transformation and grain boundary precipitation behavior. When no precipitation took place at the austenite grain boundaries, as in the low Al containing steel, the trough occurred by intergranular failure due to stress concentration in the relatively weak grain boundary ferrite film. Fracture surfaces revealed microvoid coalescence, with voids associated with MnS inclusions. The thin ferrite film was found to be strain induced and first appeared at temperatures just below the equilibrium transformation start (Ae_3). Lowering the test temperature below the non-equilibrium transformation start (Ar_3) or by undercooling before reheating to test temperature introduced a relatively high volume fraction of statically transformed ferrite (i.e. non strain induced). The stress concentration in the ferrite was thus lowered and the ductility restored.

Increasing the Mn in the steels lowers the $\gamma \rightarrow \alpha$ transformation temperature, causing the trough to be moved to lower temperatures. It also decreases the volume fraction of MnS inclusions within the ferrite film, decreasing the depth of the trough. Increasing the Al level caused AlN to be precipitated at the austenite grain boundaries, extending the trough to higher temperatures into the single phase austenite region. These precipitates are believed to act as stress concentrators, and also pin the grain boundaries, thus allowing void formation and coalescence to take place, resulting in intergranular fracture. The application of thermal cycling during cooling to test temperature tended to increase AlN precipitation and extended the trough into the single austenite region, even for the low Al containing steel. Grain boundary sliding was shown to have contributed to embrittlement in both the single phase austenite and the duplex austenite-ferrite region.

The addition of Ti results in a fine austenite grain size after the solution treatment, compared to the C-Mn-Al steels, and impedes AlN precipitation. This

leads to improved ductility in the austenite region. The finer grain size also encourages the production of large quantities of strain induced ferrite, approaching the equilibrium levels. Consequently, recovery in ductility does not begin below the Ar_3, as is the case for the coarse grained steels, but occurs at only a short temperature interval below the Ae_3.

Finally, when austenite recrystallization occurs during deformation, any voids which have initiated at the boundaries are trapped within the newly recrystallized grains. Thus, intergranular failure cannot progress and the ductility is high.

RÉSUMÉ

L'influence de Al, Mn et Ti sur la ductilité à chaud de quatre aciers bas carbone est étudiée. Les aciers ont été recuits à 1350°C et déformés en traction dans le domaine de température 700-1000°C à la vitesse de 10^{-3} s^{-1}. Les échantillons ont été refroidis soit continuement jusqu'à la température de test soit cycliquement autour d'une vitesse de refroidissement moyenne. Faisant suite à la rupture, les éprouvettes furent trempées afin de relier la microstructure et la ductilité à chaud.

Pour tous les aciers, une poche de ductilité est observée. Ce comportement peut être relié à la transformation de phase austénite-ferrite et à la précipitation intergranulaire. Lorsqu'il n'y a pas de précipitation aux joints de grain de l'austénite, comme cela se produit pour l'acier à faible teneur en aluminium, la perte de ductilité est causée par une rupture intergranulaire due à une concentration des contraintes au niveau du film de ferrite de plus faible résistance que la matrice austénitique. L'analyse des surfaces de fracture a mis en évidence une coalescence des micro-cavités, ces dernières contenant des inclusions de MnS. Un film de ferrite de faible épaisseur apparait durant la déformation à des températures justes inférieures à la température d'équilibre de la transformation (Ae_3). Par un abaissement de la température en dessous de la température de transformation hors équilibre (Ar_3), ou par un refroidissement en dessous de la température de déformation suivi d'un réchauffage à la température de test, la ferrite est produite statiquement (c'est à dire non induit par la déformation) en plus grande quantité. En conséquence, la contrainte appliquée est distribuée entre les deux phases en présence et la ductilité est restaurée.

Une augmentation de la teneur en Mn dans ces aciers abaisse la température de transformation $\gamma \rightarrow \alpha$, par conséquent la poche de ductilité est déplacée vers des températures plus basses. La fraction volumique de MnS dans le film de ferrite décroit aussi diminuant la profondeur de la poche. Une augmentation de la teneur en Al permet la précipitation de AlN aux joints de grain de l'austénite élargissant la poche vers des températures plus élevées dans la phase austénitique. Ces précipités jouent le rôle de concentrateurs de contraintes et retiennent les joints de grain permettant ainsi la formation des cavités et leur coalescence, ceci produisant une rupture intergranulaire. L'application de cycles thermiques oscillants durant le refroidissement à la température de test, résulte en une augmentation de la

précipitation de AlN et un élargissement de la poche de ductilité vers la phase austénite simple, même pour l'acier à faible teneur en Al. Nous avons aussi montré que le glissement intergranulaire contribue aussi à la fragilisation à la fois dans les domaines austénitique simple et biphasé austénite-ferrite.

Après le traitement de recuit, l'addition de Ti produit une taille de grain austénitique plus fine que dans le cas de l'acier contenant seulement de l'aluminium et empêche la précipitation de AlN. Ceci conduit à une augmentation de la ductilité dans la phase austénitique. Une taille de grain plus fine favorise aussi la formation d'une plus grande quantité de ferrite induite par déformation, à des niveaux approchant l'équilibre. Par conséquent, la restauration de la ductilité ne débute pas en dessous de Ar_3 comme cela se produit pour les aciers à gros grains, mais se produit sur un court intervalle de température en dessous de Ae_3.

Finalement, lorsque la recristallisation de l'austénite se produit pendant la déformation, la concentration de contraintes le long des joints de grain décroit et la ductilité est importante, ceci parce que les fissures associées avec la coalescence des cavités sont isolées dans les grains nouvellement recristallisés.

RESUMO

A influência da adição de Al, Mn e Ti na dutilidade a quente de quatro aços baixo carbono foi estudada. Os aços foram austenitizados a 1350°C e submetidos a ensaios de tração na faixa de temperatura compreendida entre 700 e 1000°C, com uma velocidade de deformação igual a $10^{-3}s^{-1}$. Os corpos de prova foram resfriados para a temperatura de teste a uma taxa constante ou com uma oscilação térmica em torno de uma velocidade de resfriamento média. Os corpos de prova foram temperados imediatamente após a ruptura, com o objetivo de se analisar a microestrutura de alta temperatura do material, e compará-la com os resultados da dutilidade a quente.

Para todos os aços foram observados "vales" de dutilidade (isto é, regiões de fragilização), os quais podem ser correlacionados com a transformação de fase austenita→ferrita e com precipitação intergranular. Na ausência de precipitados nos contornos de grão austeníticos, como no caso do um aço com baixo teor de alumínio, a fragilização ocorreu via fratura intergranular, devido a concentração de tensão em um filme de ferrita de menor resistência que a matriz austenítica. A análise das superfícies de fratura indicou coalescência de microporosidades, estas últimas contendo inclusões de MnS. Verificou-se que o filme de ferrita é induzido por deformação, e que é observado em temperaturas de teste ligeiramente abaixo do ponto de início de transformação austenita-ferrita previsto em equilíbrio termodinâmico (Ae_3). O decréscimo da temperatura de ensaio abaixo do ponto de início da transformação de fase em condicões de não-equilíbrio (Ar_3) introduziu ferrita nucleada estaticamente (isto é, não induzida por deformação), aumentando a fração volumétrica de ferrita na microestrutura. Foi observado que, nessas condições, ocorre uma recuperação na dutilidade, devido à uma melhor distribuição da tensão aplicada entre as fases presentes. O mesmo efeito é observado se os corpos de prova são resfriados abaixo do ponto Ar_3, e posteriormente reaquecidos para a temperatura de deformação.

Um aumento no teor de Mn nos aços implica em um abaixamento na temperatura de transformação $\gamma\rightarrow\alpha$, resultando em um deslocamento do "vale" de dutilidade na mesma direção. O teor mais elevado de Mn também conduziu à uma menor fração volumétrica de inclusões de MnS no filme de ferrita, diminuindo a profundidade do "vale". Um acréscimo no teor de Al no material, propiciou a

precipitação de AlN nos contornos de grão austeníticos, estendendo a região de fragilização para temperaturas mais elevadas, onde austenita é a única fase presente. Estes precipitados atuam como concentradores de tensão e retardam o movimento dos contornos de grão, permitindo a formação e posterior coalescência de microporosidades, resultando em uma fratura intergranular. A aplicação de oscilação térmica durante o resfriamento para a temperatura de teste resultou em um acréscimo na precipitação de AlN, estendendo o "vale" de dutilidade para temperaturas ainda mais altas no campo austenítico, mesmo para aços com baixo teor de Al. Análises metalográficas e das superfícies de fratura indicaram que o deslizamento de contornos de grãos contribuíram para a fragilizacão no domínio austenítico, assim como na região bifásica.

A adição de Ti resultou em um grão austenítico menor (comparado com os aços contendo somente alumínio) e também impediu a precipitação de AlN, eliminando a fragilização na região austenítica. O menor tamanho de grão também favoreceu à formação de uma maior quantidade de ferrita induzida por deformação, a níveis próximos daqueles previstos para as condições de equilibrio. Consequentemente, a recuperação da dutilidade não ocorreu abaixo do ponto Ar_3 (como nos aços com estrutura mais grosseira), mas se efetuou em um curto intervalo de temperatura abaixo do ponto Ae_3.

Finalmente, quando a recristalização da austenita ocorre durante a deformação, a dutilidade é elevada e a concentração de tensão nos contornos de grão é reduzida, devido ao fato de que as trincas (associadas com o coalescimento de porosidades) são isoladas no interior dos novos grãos recristalizados.

ACKNOWLEDGEMENTS

The author would like to express his sincere appreciation to his thesis supervisor, Prof. Stephen Yue, for his guidance, example of industriousness, stimulating discussions and constant encouragement throughout the course of this research.

I am very honored and fortunate to have met Prof. Barrie Mintz, an expert on the field of hot ductility, who was on sabbatical at McGill University from The City University, London. I am deeply grateful for his spontaneous help and suggestions during the writing of this thesis. His kindness and generosity will remain as an example for my life.

I would like to thank Prof. John J. Jonas, who initially accepted me as a member of his dynamic research group, for his encouragement and provision of laboratory facilities.

Much gratitude is due to the graduate students and post-doctoral fellows for their sympathy and creation of a pleasant working environment during the period that this research was carried out. I am indebted to my friends and former colleagues, in particular Eider A. Simielli, for the immense help given to me at the start of my research program, in introducing me to the operation of an MTS machine, and to Dr. Alain M. Guillet, for his enthusiastic encouragement and for his consistently good suggestions.

I would like to express my appreciation to Mr. E. Fernandez, technician of the hot deformation group, for his important input in the design of the tensile tools, and for machining these pieces. For the specimen preparation, I acknowledge the assistance of Mr. M. Knoepel, supervisor of the machinery shop.

Special thanks go to Companhia Siderúrgica de Tubarão (CST) - Brazil, for the granting of a study leave at McGill during the period that this work was developed.

I would like to express my gratitude to Mr. J. Young of STELCO, for supplying two of the steels investigated and Dr. L. Collins of MTL - CANMET who carried out the dilatometric measurements.

The moral support and encouragement received from all my family and friends in Brazil and Canada is deeply appreciated.

Last, but not least, I would like to acknowledge my wife, Maria Águeda, and my son, Hermano, for their kindness, affection and the love devoted to me. This thesis is dedicated to them.

TABLE OF CONTENTS

LIST OF FIGURES

LIST OF TABLES

CHAPTER 1

INTRODUCTION

In the last two decades, the continuous casting process has experienced a rapid development in the production of semifinished steel products, replacing the conventional route of ingot casting plus rolling. In order to become more cost effective, other related processes are being developed in the steel industry with the objective of saving energy and eliminating stages in the processing route, such as direct rolling and hot charging. However, eliminating these stages presents problems for certain grades of steel, due to occurrence of surface cracks on the semifinished products.

This study originated from an industrial problem related to transverse cracks in Al killed steel slabs. These cracks usually appear during the straightening or unbending operation of the continuously cast strand, where the steel is deformed at strain rates of the order of $10^{-3}s^{-1}$, within the temperature range of 700 to 1000°C. It has been shown to be associated with embrittlement of the austenite grain boundaries and is believed to be related to either the austenite-to-ferrite phase transformation and/or grain boundary precipitation of nitride particles.

The general objective of this work is to investigate the mechanisms of embrittlement in four low carbon steels, under the thermomechanical conditions typical of the straightening situation. In particular, the aims of this research are:

(i) To determine the influence of increasing the soluble Al in the steels from 0.026 to 0.085% on the hot ductility of a low carbon steel.

(ii) To investigate the effect on hot ductility of decreasing the austenite-to-ferrite transformation temperature by increasing the Mn from 0.39 to 1.39% in a low Al containing steel.

(iii) To establish the influence of a Ti addition on the hot ductility of a high Al containing grade. Titanium is a complex microalloying addition, since it has been shown to refine the austenite grain size, raise the austenite-to-ferrite transformation temperature and hinder the precipitation of AlN.

In these investigations, several different thermal cycles were employed, which either simulated the slab surface temperature during unbending and/or emphasized the effects of precipitation and ferrite nucleation.

In Chapter 2, the characteristics of transverse cracks and the conditions for crack formation are presented. This is followed by a review and analysis of the microstructural aspects that control the hot ductility of steels, based on laboratory investigations relating hot ductility to the problem of transverse cracking.

The materials and the experimental procedures used in this research are given in Chapter 3. The hot tensile testing system with fast quenching capability is described, as well as the techniques for microstructural analysis, such as optical metallography, electron microscopy and dilatometry.

The experimental results are given in Chapter 4, where the ductility is correlated with the microstructure of specimens quenched immediately after fracture. Included in this section are the results of fractography, optical metallography of sections close to fracture, and the characteristics of the precipitates and inclusions present, from the examination of replicas.

In Chapter 5, the mechanisms of embrittlement and ductility recovery in the low carbon steels investigated are discussed with respect to the microstructures developed during deformation.

CHAPTER 2

LITERATURE REVIEW

2.1 - INDUSTRIAL ASPECTS

2.1.1 - Continuous casting

More than a century after the first trial was performed, the continuous casting process emerged in the late sixties as a new route for the production of semi-finished steel shapes, i.e. slabs, blooms and billets, largely replacing ingot casting plus rolling (slabbing/blooming) operations [1]. Over the last two decades, with the driving force of two world oil crises, the tonnage of steel produced by continuous casting has been increasing enormously, particularly in countries that are currently investing in modernization of their steel production [2].

The main reasons for the rapid development of continuous casting are the inherent advantages of lower cost, higher yield and flexibility of operation. In fact, as compared with ingot casting plus rolling, the product is not only 10-15% cheaper [3], but is also of a higher as-cast quality [4].

A simplified schematic diagram of a typical continuous casting machine is shown in Fig. 2.1. The liquid steel is poured from a ladle via a tundish into a water cooled copper mould. At this "primary cooling" stage, the solidification of the molten steel begins. The mould oscillates vertically to prevent the sticking of the strand. At the mould exit the strand is supported and guided by top and bottom rolls and water sprays continue the solidification process in this so called "secondary cooling" stage. The most widely used machine is as represented in Fig. 2.1. The key feature is the curved mold and the subsequent curvature of the strand imposed by the supporting rolls. At the point of full solidification, straightening takes place, i.e. the strand movement becomes horizontal. The strand is then cut, usually by oxygen torch, to obtain semifinished products of specified lengths. Other types of machines have been used which produce strands in completely horizontal or vertical configurations, or are equipped with straight or curved molds [5,6]. However, it appears that the curved mold-curved strand combination is the most suitable for large production of steels, in terms of product quality and cost of installation.

2.1.2 - Quality of continuously cast products

Defects such as inclusions, blow holes and segregation can affect the quality of the continuously cast products [7]. However, cracks have the most deleterious influence on quality and have significantly retarded the development of continuous casting.

Cracking in the continuously cast strand can arise through a variety of causes as the strand moves through the machine and is subjected to withdrawal, unbending/straightening, bulging and other stresses. Moreover, from the mold to the point of straightening, changes in thermal gradient through the solidifying shell take place leading to stress generation as a result of differential expansion or contraction [4].

The types of crack that may be found in a continuously cast slab have been classified by Brimacombe and Sorimachi [8] in two broad categories: (i) internal and (ii) surface. For each category, they have defined subcategories using the criteria of defect position on the slabs, as shown in Fig. 2.2. For each of these subcategories, they have given the causes and influencing factors and suggested some corrective actions in terms of process and machine design.

Internal cracks lead to voids in the final product, and their vestiges can cause difficulties in subsequent manufacturing process. Surface cracks are oxydized by air and can result in oxide-rich seams in the rolled products. These type of cracks can be removed by scarfing or grinding, but the costs of inspection, surface treatment and yield loss affect the profitability of the operation.

There has been increasing emphasis on producing a high surface quality, in order to enable the direct rolling or at least hot charging of the continuously cast steel product to be performed, i.e. to avoid cooling for intermediate inspection and defect removal.

2.1.3 - Main source of stress in continuous casting

As mentioned previously, during continuous casting, the solidifying strand is submitted to varying thermal and mechanical loading conditions, both of which contribute to the generation of stresses and strains. There are two conditions that must be satisfied for cracking to occur at a given location [4]:

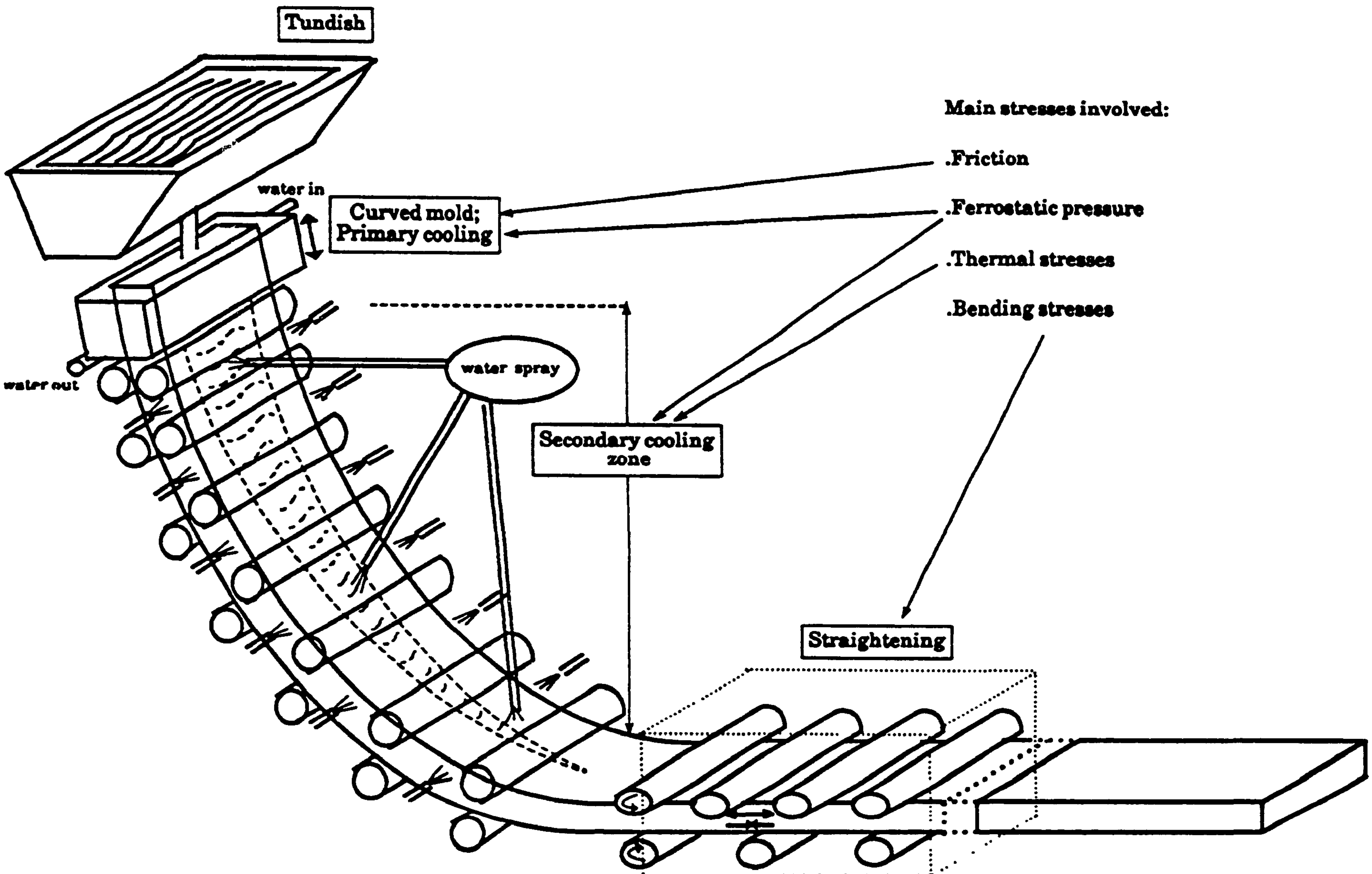

Fig. 2.1 - Simplified schematic diagram of a typical continuous casting machine (not to scale).

(i) the stress system must be tensile in nature; and

(ii) the fracture strength or strain of the steel must be exceeded.

Lankford [9] has described the main kinds of stresses to which the strand is submitted. Apart from operating irregularities (roll misalignment, non-uniform cooling, mold distortion, etc.), the most influential stresses in crack formation are indicated in Fig. 2.1, with respect to their location in the continuous casting machine. They are essentially:

. friction forces developed between the strand surface and the oscillating mold;

. thermal stresses, resulting from thermal gradients at different points on the strand, both longitudinal and through the cross section;

. ferrostatic pressure, promoted by the strand liquid core, which tends to bulge the solidified skin.

. bending stresses caused by straightening of the strand (both for curved and straight mold type machines). This is particularly severe for the case of a straight mold, where not only are bending stresses higher, but they are applied at a higher temperature near the exit of the mould, when the skin is still relatively thin. Some additional comments on this type of stress will be given in the next section.

As a result of the stresses applied on the solidifying strand, most of the cracks that are found in continuously cast products occur in the mold or mold vicinity, with the exception of transverse cracks, which appear to be formed during unbending, when the solidification process is more or less complete [8].

2.1.4 - Characteristics of transverse cracks

There is still some controversy about the origin of transverse cracks in slabs. The cracks generally appear at the bottom of oscillation marks [8,10-12], and may propagate below the slab surface along the prior austenite grain boundaries [10,12]. These oscillation marks appear as transverse ripples on the strand surface as a result of the mold oscillation. Some researchers have traced the origin of the cracks to just below the mould [4,8]. However, other investigators [5] observed that transverse cracks can be formed during bending tests applied in bars at $\simeq$800°C. Yamanaka et al. [13] have noted that, from the degree of decarburization and internal oxidation near the crack surface, the cracks may occur at temperatures below 1000°C. Mintz et al [11] suggest that the oscillation marks act as stress concentrators, serving as a path for crack propagation during unbending. Finally, Turkdogan [12] indicates that the cracks initiate at the valleys of "deep" oscillation marks. In this case the cracks are always filled with scale and show internal oxidation. The subsurface intergranular cracks, caused by sulfide, nitride, and carbonitride precipitates at the prior austenite grain boundaries (see Section 2.2.4) are neither oxidized nor related to oscillation marks. It can be inferred from this latter finding that the presence of oscillation marks is not a necessary condition for the formation of transverse cracks on the slab surface. If a slab is strained at a temperature of low ductility (see next section) the transverse cracks will form, even when the oscillation marks are shallow [12].

In general, transverse cracks appear on the inside radius face (top surface of the strand) of a curved mold machine [4,8,10,12], as a result of the tensile component of the bending stress applied by the straightener rolls. In a vertical bending machine, having an additional upper bending point, the cracks may form on either the inside or outside face [3].

The greatest strains to which the casting is subjected are those due to bending and/or straightening of the strand. In case of straightening, Lankford [9] suggested that the slab surface strains (ε) are given by:

$$\varepsilon = t/2R \tag{2.1}$$

where,

- t is the slab thickness (typically 200mm); and,
- R is bending radius, i.e. the machine radius of curvature (generally 10m [5]).

The strain rate (ε) can be estimated as [9]:

$$\dot{\varepsilon} = \varepsilon . \frac{V}{L} \tag{2.2}$$

where,

- V is the casting speed, which typically varies in the range of 0.8~1.8m/min [13]. Maximum casting speeds are defined by ensuring that the steel emerging from the mold is thick enough to withstand the ferrostatic pressure of the liquid core, preventing strand skin rupture (break-out).

- L is the "gauge" length, i.e. the distance over which the bending strain develops. The upper and lower limits of L are the distance between two consecutive straightener rolls and the slab thickness.

Using Eqs. 2.1 and 2.2, the strain developed during straightening of the strand is estimated to be 1~2% for a typical continuous casting machine, with the strain rate in the range of 7×10^{-3} to 5×10^{-4} s^{-1} [9].

As shown in Fig. 2.2, transverse cracks can occur on the surfaces but are also observed on the edges of the strand. The cracks are usually fine and may penetrate to a depth of 5-8mm below the slab surface [11]. It is often difficult to see these cracks on the as-cast slabs, and frequently they are detected by an inspection pass scarf [4,11].

Metallographic examinations of transverse crack regions of Nb bearing cast slabs have indicated extensive precipitation of Nb(CN) [14,15]. In C-Mn-Al steels, the cracks have been associated with the presence of AlN particles [15-18].

2.2 - HOT DUCTILITY OF LOW CARBON STEELS

The initiation and propagation of cracks on the slabs is almost certainly a manifestation of *reduced steel ductility* occuring concurrently with the application of a tensile stress. Three temperature zones of reduced ductility or embrittlement have been identified in laboratory simulations which have been used to investigate the mechanisms of crack formation during continuous casting [4,8,19,20]. These zones are located in the range between the melting point and 600°C, which covers the entire thermal history of a slab in the continuous casting machine. These temperature ranges of poor ductility , which are illustrated in Fig. 2.3, are nominally [19]:

- Zone I: High temperature zone (≃1340°C to solidus);

- Zone II: Intermediate temperature zone (900 to 1200°C);

- Zone III: Low temperature zone (600 to 900°C).

The high temperature zone is close to the solidus and the embrittlement has been attributed to segregation of residual elements to the interface between the solidifying dendrites (see next section), resulting in hot shortness and other types of cracks in cast products. The intermediate temperature zone of embrittlement is located entirely in the austenite range but only occurs at relatively high strain rates and is not considered deleterious in the case of continuous casting [4,8].

The position of the third zone varies from author to author, and depends largely on the grade being cast, but it generally occurs in the low temperature austenite region (<1000°C) and always includes the austenite-to-ferrite phase transformation. This coincides with the straightening operation temperature range during continuous casting. Thus, the origin of transverse surface cracks is regarded as being due to the application of straightening in the third embrittlement zone.

In the following sections, an attempt will be made to relate the ductility results available in the literature with microstructural aspects which take place during laboratory tensile testing simulations. Most of the material reviewed pertains to the low temperature zone of reduced ductility, which, as pointed out above, is most closely related with transverse cracks.

It should be added that, with very few exceptions, hot ductility investigations have been carried out by tensile testing, where the reduction of area at fracture is taken as the appropriate ductility parameter. Mintz et al. [11] pointed out that the test which simulates best the straightening operation is the hot bend test. However, because of the problem of quantifying the severity of surface cracking from a bend test, it has been rarely used, except in a few instances. Suzuki et al [21] note that the steels that produce significant slab rejections due to a high incidence of edge and transverse cracks in the actual continuous casting process, invariably show a ductility trough (i.e. reduction of area values < 60%) in hot tensile tests performed in the temperature range of 700 to 1000°C. Moreover, hot ductility failures in Zone III in tensile tests are similar to those of transverse cracks in that both are intergranular along the austenite grain boundaries.

2.2.1 - Influence of microsegregation of solute elements

Temperatures close to solidus

In an investigation of the mechanical properties of delta ferrite iron, Wray [22] demonstrated that high purity iron failed in a ductile manner when deformed in tension up to the melting point. His results also indicated that the iron solidifies homogeneously, i.e. a liquid layer is not present at grain boundaries below the

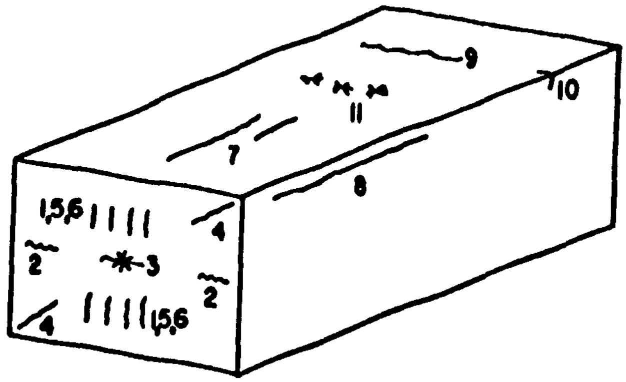

Cracks in continuously cast steel:

Internal cracks	Surface cracks
1 - Midway	7 - Longitudinal, mid-face
2 - Triple-point	8 - Longitudinal, corner
3 - Centreline	9 - Transverse, mid-face
4 - Diagonal	10 - Transverse, corner
5 - Straightening/bending	11 - Star
6 - Pinch roll	

Fig. 2.2 - Schematic drawing of strand cast section showing different types of cracks [8].

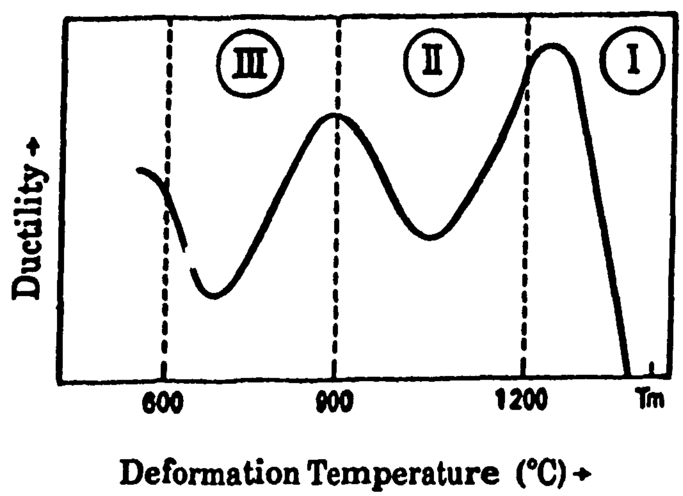

Fig. 2.3 - Schematic presentation of ductility troughs occurring in hot tensile test [19].

melting point. On the other hand, during the solidification of steel, residual liquid layers are observed at interdendritic interfaces, at temperatures below the solidus. It has been observed that this remaining liquid phase between dendrites is highly concentrated with segregating elements like S, P and C, giving rise to an alloy with a solidification temperature lower than that of the matrix [8,19-21].

Therefore, any stress that is applied to steel at temperatures 30-70°C below the solidus (Zone I of reduced ductility) will propagate cracks outward from the solidification front between dendrites [4,20]. In fact, the fracture strain of steels deformed in this condition is less than 1 percent [4,19-21,23], and remains at this low level until the interdendritic liquid film begins to freeze. This introduces the concept of "zero ductility temperature (ZDT)" [19-21], which is schematically illustrated in Fig. 2.4. The resulting fracture surface exhibits a smooth, rounded appearance, characteristic of the presence of a liquid film at the time of failure [19-21 and 23-25].

In order to verify the effect of impurity elements on the ZDT, Suzuki et al [21] have investigated impurity doped electrolytic irons containing 0.003% C. They concluded that the chemical species that strongly segregate to the dendritic interface (C, P, O and B in order of increasing influence), lower the zero ductility temperature, as illustrated in Fig. 2.5. Other investigators attribute the embrittlement mainly to the microsegregation of P and S [4,8,20]. In fact, Fuji et al [26] have detected higher P (0.18%) in the region of cracks than in the matrix (0.02%). This observation is supported by a laboratory study of Adams [27] who observed a P level of 0.2 to 0.5% at the austenite grain boundaries, for a matrix concentration of 0.02%. The same microsegregation behavior is observed for S. In addition, sulfur microsegregation in steels also leads to the formation of the Fe-FeS eutectic or FeS which have melting temperatures of 988 and 1190°C, respectively [28]. Addition of Mn is beneficial since it combines with S to form the less harmful and stable MnS precipitates, with a significantly higher melting point, thereby preventing liquid film formation at low temperatures. A Mn/S ratio greater than 20 minimizes cracking by this mechanism [9,20,21]. Apart from the addition of Mn and a lowering of the level of the segregating elements, Matsumiya et al. [29] have indicated that this type of embrittlement cannot be eliminated by any other adjustments in the chemical composition.

The mechanism described above is known as "hot tearing" or "hot shortness", and has been considered to be responsible for virtually all crack defects in continuously cast steel, with the exception of transverse cracks [8,20]. Since this thesis is concerned with transverse cracks, hot shortness will not be covered in any

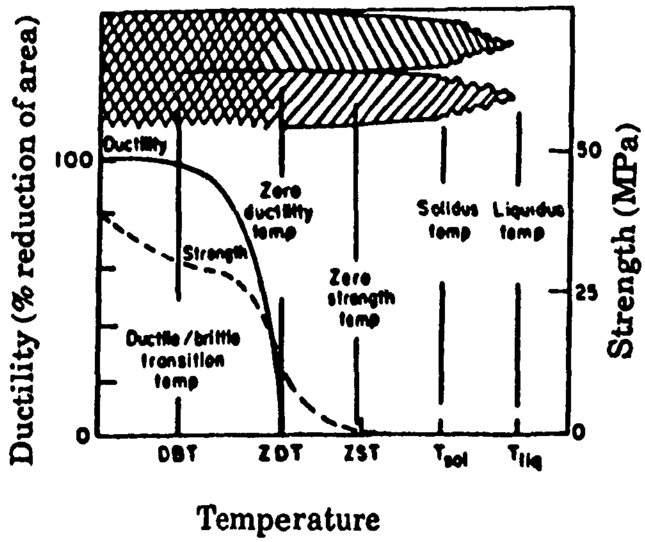

Fig. 2.4 - Mechanical properties in the high temperature zone of reduced ductility and corresponding schematic presentation of solid/liquid interface during casting [20].

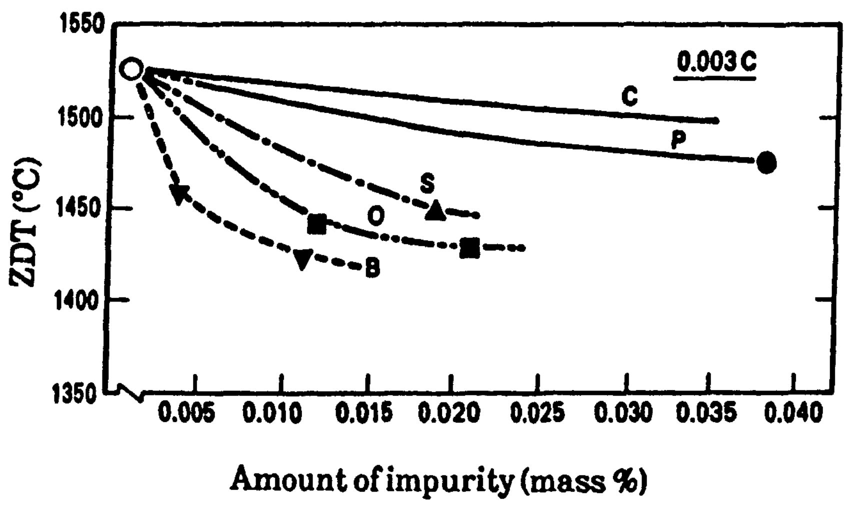

Fig. 2.5 - Effect of impurity elements on Zero Ductility Temperature (ZDT). Each element is doped in Fe-0.003%C binary alloy [21].

more detail in this literature survey. For further information, the reader is directed to references [19-21 and 23-25].

Temperatures corresponding to transverse crack formation

There are possible effects of microsegregation on transverse crack formation, i.e. in the low temperature zone of reduced ductility. A statistical analysis of commercial data by Mintz and Arrowsmith [14] have shown that P reduces the incidence of transverse cracking in Al-Nb containing steels, as well as improving hot ductility. This has also been confirmed by Hannerz in his statistical observations and laboratory investigations [15]. The origin of this beneficial effect has not been rigorously explained, but phosphorus segregation at the austenite grain boundaries may reduce the detrimental effect (see Section 2.2.4) of Nb(CN) grain boundary precipitation [14].

Sulfur segregation at 900°C at the austenite grain boundaries can result in a concentration as much as 200 times larger than that of the matrix [30]. It has been demonstrated [31] that segregated S exerts an attractive force on the electrons associated with the bonding of Fe atoms, thus reducing their strength. Other investigators [32-34] have proposed a model of grain boundary embrittlement, where decohesion of the precipitate (AlN, Nb(CN), etc.)/matrix interface is enhanced by the S segregation.

2.2.2 - Influence of austenite-to-ferrite phase transformation

In plain carbon steels, on cooling from the austenite region, ferrite starts to nucleate, tending to form a continuous film at the austenite grain boundaries. Since ferrite has a lower flow strength at the same temperature than austenite [35], deformation becomes concentrated in these thin films. It has been shown [13,19,36] that the ductility is at a minimum when the areas of the primary nucleating ferrite first link into a continuous film at the austenite grain boundaries. The thickness of this proeutectoid ferrite film is one of the controlling factors for ductility of steels deformed in the two-phase region. With lower temperatures or longer holding times, the increased thickness of the ferrite film (or increased ferrite volume fraction) is believed to be responsible for the improvement in ductility.

The austenite-to-ferrite phase transformation is influenced by alloying elements, cooling rate and prior austenite grain size. In low carbon and microalloyed steels the most influential elements are C [15,36] and Mn, i.e. increasing their concentration tends to decrease the transformation temperature, whereas increasing Al, Ti, Si and P tend to raise the temperature. A coarser grain size decreases the transformation temperature due to a smaller grain boundary area per unit volume, resulting in fewer sites for ferrite nucleation. High cooling rates decrease the transformation temperature because of the kinetics of the nucleation and growth process. Finally, some researchers have indicated that the onset of phase transformation can be enhanced by deformation [16,36,37]. It is therefore frequently a complicated matter to relate the ductility loss in the two phase region with the temperatures which characterize the phase transformation.

In addition to stress concentration in the softer ferrite phase, the presence of primary ferrite encourages preferential precipitation within the ferrite film, because nitrides and carbonitrides, which can be very detrimental to ductility (see Section 2.2.4) have a much lower solubility in ferrite than in austenite. The temperature range over which this ferrite film can form is believed to be wide and the cracks will propagate below the slab surface to the depth corresponding to the lower temperature limit of this critical range and/or where the tensile stress field imposed by the straightening operation becomes too low [12].

2.2.3 - Microalloying additions to steels

Microalloyed steels (HSLA) have experienced a rapid development in the last two decades. The combined properties of high strength, improved toughness and good weldability obtained in these steels are based on the small additions (generally <0.1%) of Nb, V and Ti. These microalloying elements precipitate in austenite, during cooling from the melt, in the form of carbide, nitride or carbonitride particles, when their solubility products have been exceeded.

Reheating temperatures prior to hot rolling are always around 1300°C, and most of these precipitates (Nb(CN), V(CN) and TiC) redissolve (TiN is the only precipitate that does not redissolve). During normalizing after hot rolling or controlled rolling at low temperatures in the austenite region, reprecipitation can be achieved either at the austenite grain boundaries or within the matrix, resulting in precipitation hardening and, ultimately, grain refinement.

Aluminum is added to steels because it can both grain refine and act as an effective and economical deoxidant. After deoxidation, any excess Al remains in solid solution, eventually combining with the available nitrogen to precipitate AlN, which can improve the properties of the steels in the same way as Nb, V, and Ti. Historically, because Al was used for many years as a deoxidizer before its role as a grain refining addition was appreciated, it is not always considered as a conventional microalloying addition [38]. Nevertheless, it should be regarded as a precipitate former, with mechanisms similar to that associated with Nb, V, and Ti. However, Al (as well as Ti) does not form a carbide, unlike Nb and V (and Ti when added in sufficient quantity). The aluminum nitrides are only able to grain refine, and no precipitation hardening is obtained in general. Unfortunately, although these elements are added to grain refine and strengthen the structure in the final product, they can (except for Ti) have a detrimental influence on hot ductility and encourage transverse cracking.

As mentioned in Section 2.2.1, the last portions of a steel to solidify are the solute enriched interdendritic zones, which subsequently become the austenite grain boundaries [11]. Turkdogan [12] notes that these zones are also enriched in microalloying elements and, as a result of that, the nitrides and carbonitrides will precipitate predominantly at the austenite grain boundaries. For a concentration of 0.02% Al and 0.04% Nb in the liquid steel, he estimated that the grain boundary concentration would be 0.13% Al and 1.15% Nb. Thus, precipitation at the boundaries may be very intense, and equilibrium conditions based on bulk compositions may not apply. This is important since it is the precipitation at the austenite grain boundaries which has the greatest influence on transverse cracking.

Based on the foregoing, grain boundary precipitation might be expected to be more intense during continuous casting than in a simulated laboratory test. Moreover, during heat treatments at temperatures above the solubility of precipitates in austenite, the particles dissolve and the interstitial elements (C and N) diffuse away from the austenite grain boundaries. However, the grain boundary region remains rich in the microalloying additions, since these, being substitutional additions, have lower diffusivities.

2.2.4 - Influence of precipitating forming elements on hot ductility

As mentioned earlier, the straightening operation in continuous casting occurs in the temperature range of 700 to 1000°C, corresponding to low temperatures in the austenite and γ-α phase transformation (Zone III of reduced ductility) regions. In this temperature zone, Suzuki et al. have observed no embrittlement in electrolytic (high purity) iron, although it occurred in C-Mn-Al and in microalloyed steels [19,39]. These results suggest that the embrittlement in low temperature austenite is intimately related to the presence of precipitates. In continuous casting, as pointed out in Section 2.1.4, extensive precipitation of nitride and carbonitrides has certainly been associated with transverse cracks.

A fracture mechanism based on the effect of precipitates has been proposed by Suzuki et al.[39] and is reproduced in Fig. 2.6(a). According to this mechanism, fine grain boundary precipitates act as stress concentrators, nucleating voids which are extended by grain boundary sliding (see Section 2.2.7). These voids ultimately coalesce, resulting in intergranular fracture. Another model, more specifically applicable for Nb(CN) precipitation in austenite, has been suggested by Maehara and Ohmori [40] and is given in Fig. 2.6(b). In this case the precipitation would occur simultaneously at the boundaries and in the interior of the grains. The growth of grain boundary precipitates results in a depletion of particles in the boundary proximity and the intragranular precipitation strengthens the matrix [41]. The stress is then concentrated in the softer precipitate free zones (PFZs), leading to fracture. A third model (Fig. 2.6(c)) more applicable to plain C-Mn or C-Mn-Al steels, relates the grain boundary embrittlement to the austenite-to-ferrite phase transformation, where the role of the precipitating particles is often secondary [13]. The stress is concentrated in the softer ferrite phase nucleated at the austenite grain boundaries. Inclusions (and precipitates, if present) are responsible for cavitation leading to void coalescence and failure. As indicated in Figs 2.6(a)-(c), the harmful precipitates are MnS, (Fe,Mn)S-O, AlN, BN and Nb(CN).

The thermal history to which the steel is submitted prior to testing significantly affects the amount of precipitates formed, as well as their morphology, as will be reviewed in Section 2.2.5. Funnell and Davies [42,43] have observed that the finer the grain boundary particles (usually < 100nm), the closer the interparticle spacing for a given volume fraction, and the worse the hot ductility. This is presumably because the smaller the intercritical distance between particles, the easier it is for void coalescence [11]. Furthermore, small particles can pin grain boundaries, preventing them from migrating, allowing time for the intergranular cracks to link together.

It is well established that the combined influence of N and Al is detrimental to the ductility [15,16,44,45]. As can be seen in Fig. 2.7, for a N content $\simeq 0.011\%$,

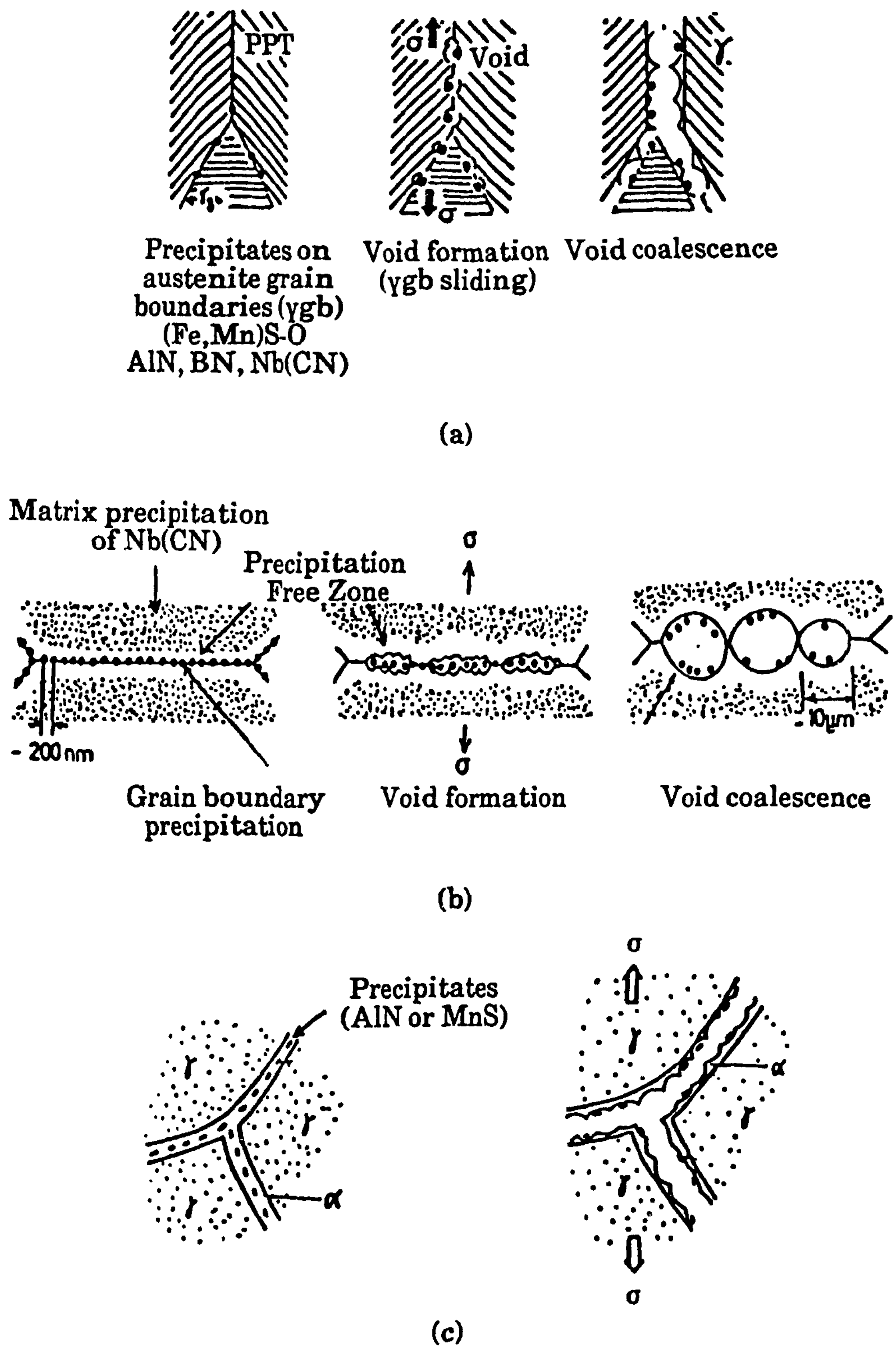

Fig. 2.6 - Models for embrittlement in the low temperature zone of reduced ductility, where transverse cracks are formed; (a) Ref [39], (b) Ref [40], (c) Ref [13].

increasing the Al concentration from .004 to .070% deepens the ductility trough and extends the embrittlement to higher temperatures. The same deleterious effect is observed when the Al content is kept constant at 0.04% and the N is increased from 0.003 to 0.011%. It can be inferred from these observations and other studies [45,46] that precipitation is controlled by the solubility product [Al]x[N], i.e. increasing the solubility product increases the amount of AlN precipitation, as well as raising the temperature at which precipitation starts. For higher values of [Al]x[N] in Fig. 2.7, the embrittlement is likely to have started in the single austenite region, whereas for the lower values the ductility trough probably occurred only in the austenite-plus-ferrite range.

The effect of Nb in the steels is very similar to that due to Al, i.e. higher Nb contents increase the embrittlement due to increased amount of Nb(CN) precipitation. However, Nb is more effective in extending the trough to higher temperatures in the austenite [14,16,17,19]. This behavior can be related to the temperatures at which maximum precipitation rates occur, which are 950°C for Nb(CN) [47], and 815°C for AlN [48], for typical Nb and Al additions in the steels.

Some ductility studies [49,50] show that C-Mn-Al steels behave like plain C-Mn grades with respect to the temperature region where embrittlement occurs, unless the Al content is high, i.e. Al$\geq$0.07% [11]. However, it is generally agreed that the addition of Al, even in much smaller amounts, to Nb bearing steels, significantly enhances the embrittlement [14,49]. One reason for this behavior is that precipitation of AlN in addition to Nb(CN) occurs at the austenite grain boundaries. Another possibility, based on the results of Mintz and Arrowsmith [14,51], is that the Al additions cause the Nb(CN) particles to become finer and more closely spaced at the austenite grain boundaries.

Vanadium, which is another nitride former, has not been considered as detrimental as Al and Nb [15,51]. If the V content in the steel is limited to 0.07%, the resultant ductility is comparable to that of plain C-Mn steels. This behavior can be related to the high solubility of vanadium nitride in austenite [51].

Titanium is the only microalloying element and nitride former which is unanimously considered effective in improving the ductility [15,17,50,51]. The reason for this is that stable TiN forms at much higher temperatures (higher than the austenite formation temperature), compared to other nitrides [12] and cannot be redissolved, except by melting. Therefore TiN precipitates are coarse at test

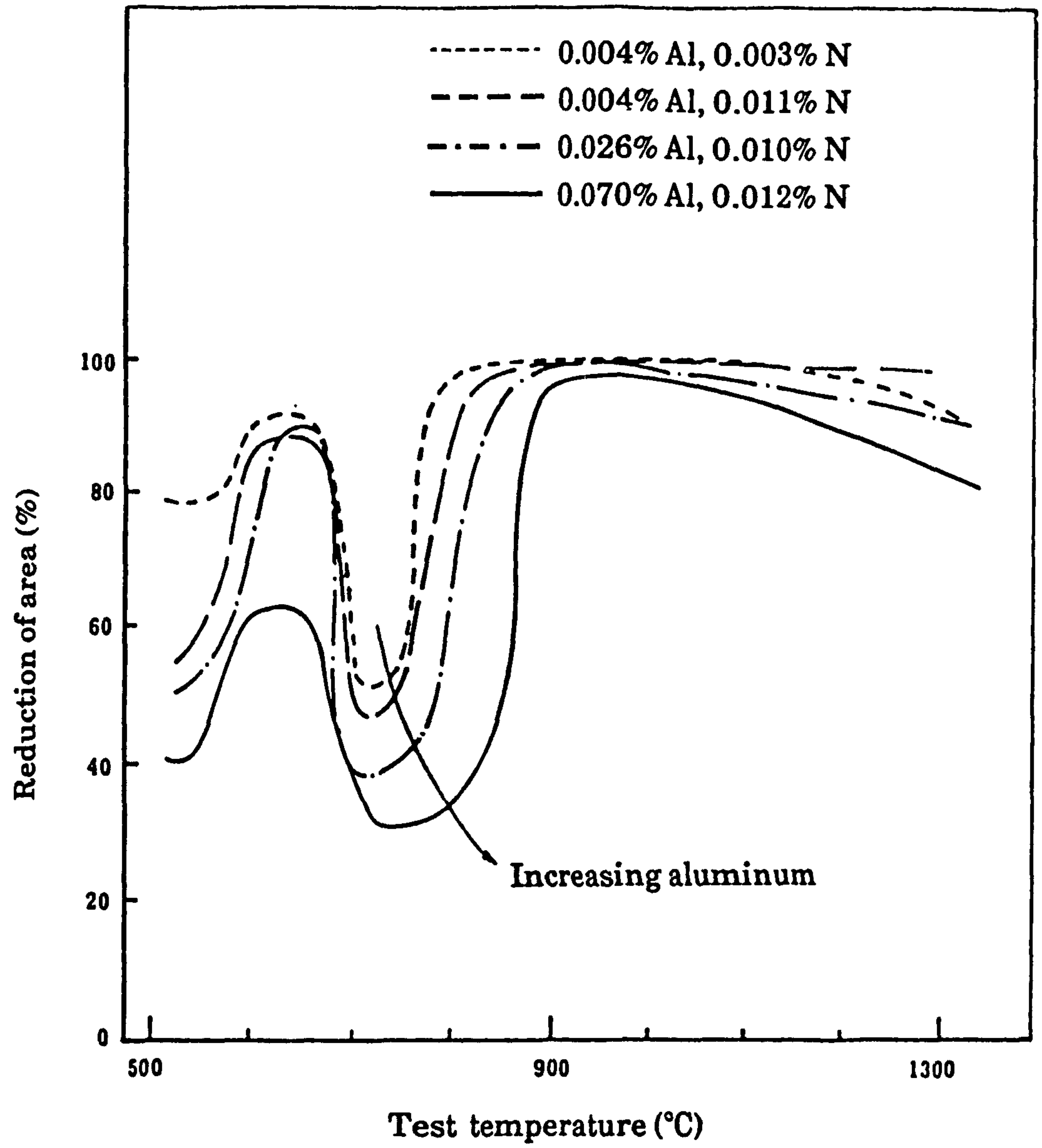

Fig. 2.7 - Influence of Al on hot ductility of a C-Si-Mn-Al steel solution treated at 1350°C, cooled to test temperature and tested at 0.05 mm s^{-1} [16].

temperatures between 700-1000°C [17,42,43] and randomly distributed throughout the matrix [52], as opposed to the grain boundaries. In addition, titanium removes nitrogen from solution, thus preventing the precipitation of detrimental AlN and Nb(CN) [15,17,51]. However, a Ti addition in a Nb bearing steel is less effective because niobium can also form carbides [51]. In tests performed after reheating to temperatures around 1300°C (below the dissolution of TiN) for a Ti added steel, grain coarsening is prevented. The resultant finer grain size (See Section 2.2.6) can further explain the beneficial effect of Ti on the hot ductility.

The effect of boron additions has not been clarified. Hannerz [15] indicates that it improves the ductility, acting in a similar way as Ti, since B strongly combines with N. However, the results of Suzuki et al. [53] show that BN precipitation resembles the behavior of AlN and Nb(CN), resulting in grain boundary embrittlement.

In addition to nitride and carbonitride precipitates, sulfide inclusions have been considered to be very deleterious to the ductility. For example, statistical correlations by Hannerz [15] have strongly indicated that the occurrence of transverse cracking and scarfing losses increases with increasing S content in the steels. Similar behavior has been found in hot ductility tests, i.e. the trough is widened and deepened with increasing S contents [9]. The sulfides usually occur as complex inclusions of the type (Fe,Mn)S [19,21]. Increasing the Mn in the steels, typically for Mn/S ratio greater than 20, reduces the embrittlement [9,19]. This improvement may be due an enrichment of Mn in the (Fe,Mn) inclusions, which results in coarser particles, nucleated preferentially in the matrix [9]. Suzuki et al [21] have shown that for $S<0.006\%$ or $Mn>0.7\%$, no embrittlement occurs in hot ductility simulations, even at low Mn/S ratio. The sulfide inclusions are often one order of magnitude larger than AlN and Nb(CN). Therefore they are not expected to reduce the ductility, based on the mechanisms described in the previous section (Fig. 2.6). However, the occurrence of sulfide particles (mainly MnS) have been observed at austenite grain boundary cracks [13]. Mintz et al. [11] suggest that in this case the fine AlN and/or Nb(CN) precipitates would prevent the boundaries from migrating, while the coarser MnS inclusion would encourage cavitation. This combined effect would facilitate intergranular failure.

Oxide inclusions, which are deleterious to ductility at room temperature, do not appear to impair hot ductility to the same extent as the nitrides and sulfide particles [20].

2.2.5 - Influence of thermomechanical history

Once the basic effects of the precipitate forming elements on hot ductility had been established, considerable effort was concentrated into determining the influence of thermal history and deformation on the precipitate sizes and distribution. As mentioned in the previous section, the embrittlement in the low temperature zone of reduced ductility has been associated with fine grain boundary precipitation.

Hot ductility investigations of transverse crack formation are generally carried out after annealing or solution heating at a high temperature (usually >1300°C) to dissolve the precipitates present. The specimen is then cooled to test temperature at a controlled rate (See Section 3.4.1).

Precipitate sizes and distribution can be influenced by whether the precipitates are formed statically prior to test, or dynamically during the deformation. Several studies have shown that, at the same temperature, the precipitation of AlN, Nb(CN) and V(CN) can be accelerated by deformation, compared to the precipitation rates obtained during isothermal transformations in undeformed structures [54-56]. Some investigators [49,57] have indicated that the increased precipitation rate is caused by the creation of favorable nucleation sites by the deformation process. These sites are probably dislocation networks and point defects (vacancies) which can accelerate the rate of diffusion.

It has been shown that for V and Al containing steels, ductility is reduced more by static precipitation than by dynamic precipitation. However, in Nb bearing steels, dynamic precipitation is more effective in increasing the embrittlement [49,58]. Dynamic precipitation has been observed either at the austenite grain boundaries or in the matrix, whereas static precipitation has been observed only at the austenite grain boundaries [49]. Dynamic precipitation is generally finer than static precipitation and hence can also be detrimental to hot ductility.

Increasing the volume fraction of fine precipitates has been shown to impair ductility and ductility improves only when the particles coarsen. For example, Funnell and Davies have shown that when fine AlN particles are present at the grain boundaries ductility is poor, but when a heat treatment is given to coarsen them, ductility improves [42,43]. Therefore, many hot ductility tests have been performed incorporating methods of precipitate coarsening. One way to achieve this with Al and Nb containing steels was demonstrated by Maehara et al. [59]. After cooling from the solution treatment (1300°C), the steels were given 5-10% predeformation strains at temperatures in the range 1000~1100°C, and at strain rates $\geq 10^{-2}s^{-1}$. Under these conditions, fine dynamic precipitates are formed. These precipitates coarsened markedly when the prestrain was followed by a low cooling rate (~0.5°C/s) to the test temperature in the range of 800~900°C, and the resultant ductility was high. Incidentally, the application of higher predeformation strains can result in grain refinement via dynamic recrystallization, again decreasing the embrittlement [60].

Other researchers used only thermal treatments to produce coarsening. Decreasing the cooling rate from the solution treatment to the test temperature increases the less detrimental static precipitation in Nb steels, and allows some coarsening of the particles to occur before deformation [14]. A similar effect is obtained by isothermal holding at 1100°C before cooling to test temperature [59]. In both conditions the undesired fine dispersion of dynamic Nb(CN) precipitates is avoided. However, differences in precipitation kinetics between AlN and Nb(CN) can lead to different results for the same cooling conditions. While fast cooling rates from the solution temperature promotes the more detrimental dynamically precipitated fine Nb(CN) particles, slow cooling enhances the more detrimental static precipitation of AlN. Moreover, AlN does not precipitate readily in the austenite, unless the solubility product is very high. For example, Crowther et al. [49] have shown that, in a C-Mn-Al steel having 0.015% Al and 0.006% N, a 1330°C solution treatement followed by cooling at 1°C/s, did not give rise to any AlN precipitation, even after holding for 6 hours at 850°C test temperature.

Some thermal treatments have been shown to be very detrimental to hot ductility. For example, cooling from the solution temperature to 800~900°C, followed by reheating to the test temperature of 1100°C, resulted in extensive grain boundary precipitation of AlN, leading to severe embrittlement [58]. Similar observations have been reported for Nb bearing steels solution treated around 1300°C, cooled to the zone of low temperature austenite and the duplex austenite-plus-ferrite region, and reheated and tested at 1000°C [17,58,61]. These treatments can be regarded as very simple simulations of the temperature cycling that occurs during cooling of the cast strands. More complete cycling simulations have lead to an accentuation of AlN

[18,62] and Nb(CN) [63] precipitation. These thermal oscillations can therefore have a remarkable effect on hot ductility, both widening and deepening the trough, with the embrittlement worsening the higher the amplitude of the cycling temperature [63]. It has been shown that these oscillation have a significant effect on transverse crack formation [18,62,64]. If, as the result of cycling, the slab surface temperature falls into the range 750~850°C, the steel can experience successive $\gamma \rightarrow \alpha$ and $\alpha \rightarrow \gamma$ transformations. Since the solubility of AlN in ferrite is much lower than in austenite, an increased amount of precipitation will be seen at the austenite grain boundaries at the hot ductility test temperature. This behavior is illustrated by Wilson and Gladman [39], based on the work of Nozaki et al. [62], and is reproduced in Fig. 2.8. The thermal oscillations through the austenite-to-ferrite transformation temperature increases the amount of N combined with Al (i.e. increases the volume fraction of AlN).

Based on precipitation characteristics, some practical countermeasures have been proposed to avoid the transverse cracking susceptibility. In terms of chemistry control, improvements can be obtained by reducing Al and Nb additions together with limiting the N levels, and/or the addition of Ti (a more stable nitride former), so decreasing AlN [15,18,42,43] and Nb(CN) [15,17] precipitation. In respect to process control, the reduction of temperature oscillation amplitude during the cooling of the strand can avoid extensive grain boundary precipitation [63].

2.2.6 - Effect of grain size

Among the several factors that can influence the hot ductility of steels, the austenite grain size is the most controversial. Most studies have indicated that a refinement of the grain size results in an improved ductility [10,51,60,65-67]. However, other investigations have found little effect [17] while some even show a deterioration of ductility (for example Ref. [42]). It appears that these contradictory findings are due to the difficulty in isolating the effect of grain size from the influence of precipitation presented above. Where the two have been separated, as in the case of investigations on plain C-Mn steels where grain boundary precipitation was absent, it has been concluded that refining the austenite grain size reduces both the width and the depth of the ductility trough [66,67].

Since the material which shows a brittle behavior invariably fails intergranularly, grain size would be expected to have an important influence on

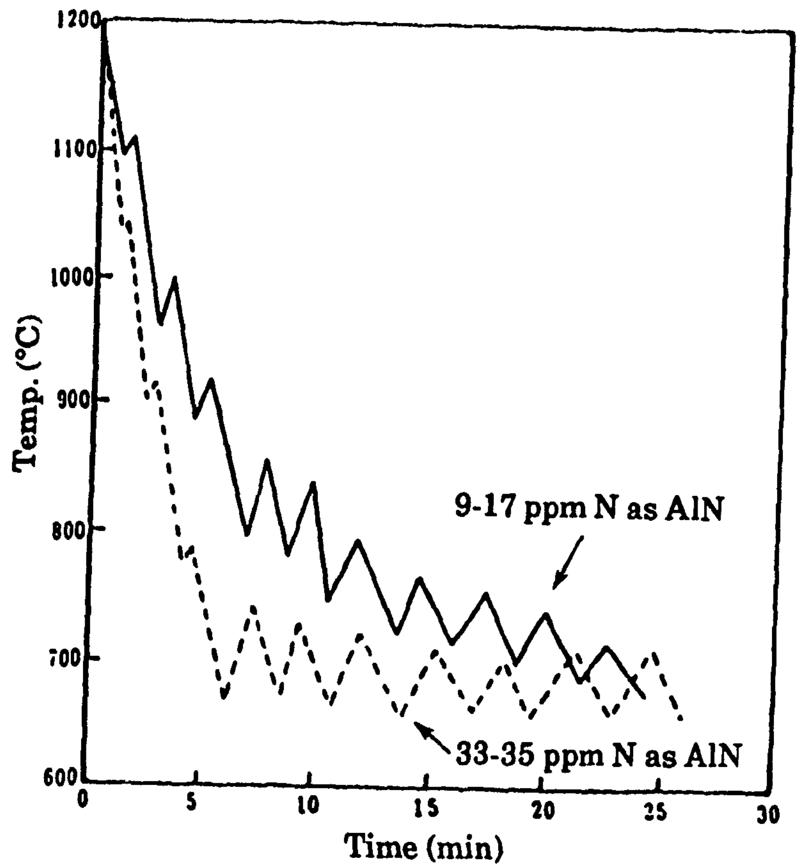

Fig. 2.8 - Effect of cooling cycle during continuous casting on AlN precipitation (schematic) [38], derived from Nozaki et al. [62].

ductility. One of the reasons for this is that, in fine grain material there is an increase in the number of triple points, which are barriers for crack propagation [68]. Furthermore, in coarse grained structures, crack lengths can be greater, thus aggravating the stress concentration at the boundaries [11].

There is no data available in the literature concerning the embrittling behavior of steels with austenite grain sizes of the order of those present in the cast slabs, i.e. 0.5 to 5 mm. However, as pointed out by Mintz and al. [11], the major benefit in hot ductility occurs with grain refinement in the range of 50 to 400 μm. Further deterioration in ductility for austenite grain sizes greater than 500 μm is likely to be only small [11].

The work of Schmidt and Josefsson [10] have indicated that, by adopting a suitable cooling pattern in the secondary zone of the continuous casting machine, the occurrence of transverse cracks can be reduced. They have shown that, if the slab surface temperature oscillates in such a way that it crosses the austenite-to-ferrite transformation sucessively, a fine grain layer is formed on the slab surface. In this condition the incidence of transverse cracks observed after the straightening was much lower than when the slab surface was composed of coarse grains.

The austenite grain size in continuously cast steel has been shown to be largely dependent on the C content. Coarse columnar grains occur in the peritectic range 0.10 to 0.15%C. It has been also observed that the incidence of transverse cracks is higher for plain C steels in this carbon range, and decreases for C<0.10 and C>0.15% [67]. However, in hot tensile simulations on micro-alloyed steels where the specimens are solution treated at ≃1300°C before being tested at the temperatures equivalent to those that occur during straightening, no significant change has been noticed in the austenite grain size, and/or dependency of the depth of the ductility trough with C contents in the steels [15,19,67]. The explanation for this behavior is given by Maehara et al. [67], who demonstrated that the influence of C on the grain size and consequently on ductility, is due to microstructural changes that occur only during solidification. Therefore, the real influence of C on transverse cracking can only be detected on specimens melted and solidified prior to test.

During the solidification of steels, the austenite grain growth is retarded if a second phase is present. This second phase is δ-ferrite or liquid, for steels with C levels lower or higher than the peritectic composition. The absence of the second phase, together with the fact that the austenite is formed at the highest temperature, result in the coarsest austenite grain sizes in steels with peritectic composition. In addition to this, Maehara et al. [67] have shown that medium carbon steels (C=0.10~0.15%) result in an uneven solidification in the mold, resulting in coarse grain layer on the slab surface, as illustrated in Fig. 2.9. This microstructural characteristic is consistent with the work of Schmidt and Josefsson [10], who, as noted above, have demonstrated that a layer of fine grains on the slab thickness was effective in reducing transverse crack susceptibility.

2.2.7 - Influence of strain rate

It is well established that, in the hot working temperature range, the mechanical properties of steels (in particularly the ductility) are strain rate sensitive. At the temperature region where the steel is processed during continuous casting, several embrittling mechanisms are operative. These mechanisms have represented schematically by Wray [35] for a medium carbon steel, in terms of temperature and strain rate, reproduced in Fig. 2.10. In this diagram , Zone A corresponds to the high temperature region of reduced ductility, where the embrittlement is caused by the presence of a liquid film in the interdendritic areas, and is independent of the strain rate [15,17]. Zone B is related to intergranular precipitation of (Fe,Mn)S particles, and leads to failure only at high deformation speeds. At strain rates lower than $10^{-2}s^{-1}$, these particles coarsen and do not impair the ductility [4,8,19-21].

As mentioned before, the tensile stress resulting from the straightening operation (which leads to transverse cracks) is applied at a strain rate of the order of $10^{-3}s^{-1}$ [9], and temperatures between 700-1000°C. In this strain rate-temperature range, three mechanisms (C,D,E) appear to operate simultaneously. Zone C is a result of ductile transgranular fracture and is intimately associated with dynamic recrystallization (see next section). Zone E is related to the austenite-to-ferrite phase transformation. As noted in Section 2.2.2, this embrittlement is caused by stress concentration in the thin ferrite films formed around the austenite grain boundaries, and appears to occur over a large range of strain rate. Zone D is responsible for intergranular failure in low temperature austenite, and has been associated with grain boundary sliding [19,21,35,42,43]. In this Zone the embrittlement increases with decreasing strain rate, as illustrated in Fig. 2.11 for a Nb bearing steel, tested in the temperature range of 700 to 1200°C and strain rates between $5x10^{-3}$ to 5 s^{-1} [39]. The explanation for this behavior is that, with decreasing strain rate, there is more

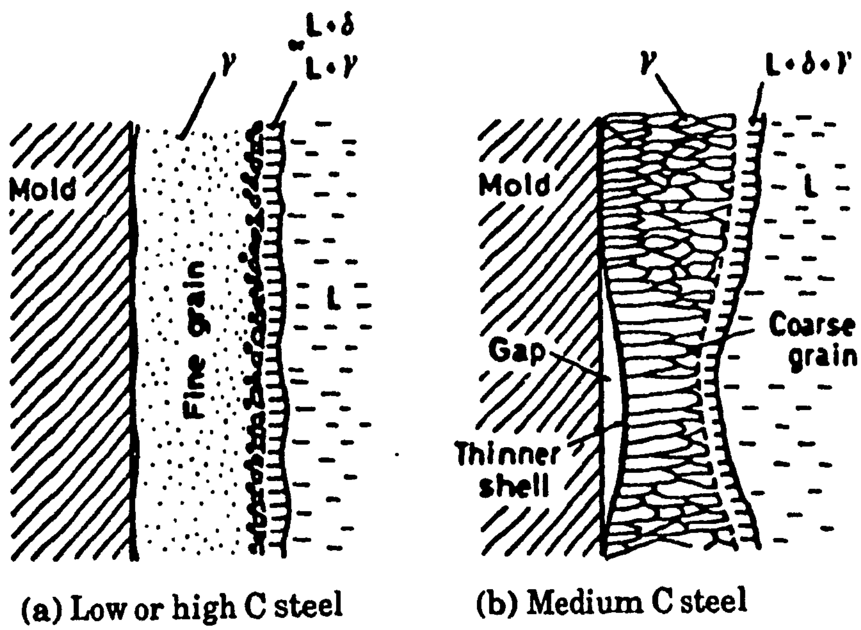

Fig. 2.9 - Schematic illustration showing austenite structure in solidified shell [67].

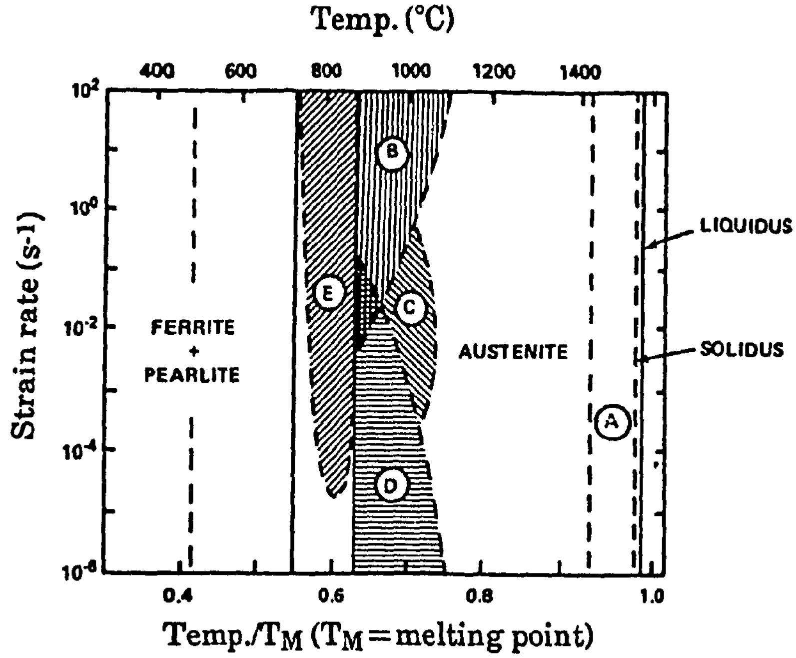

Fig. 2.10 - Possible fractures zones mapped for a 0.2%C plain carbon steel in strain rate-temperature space [35].

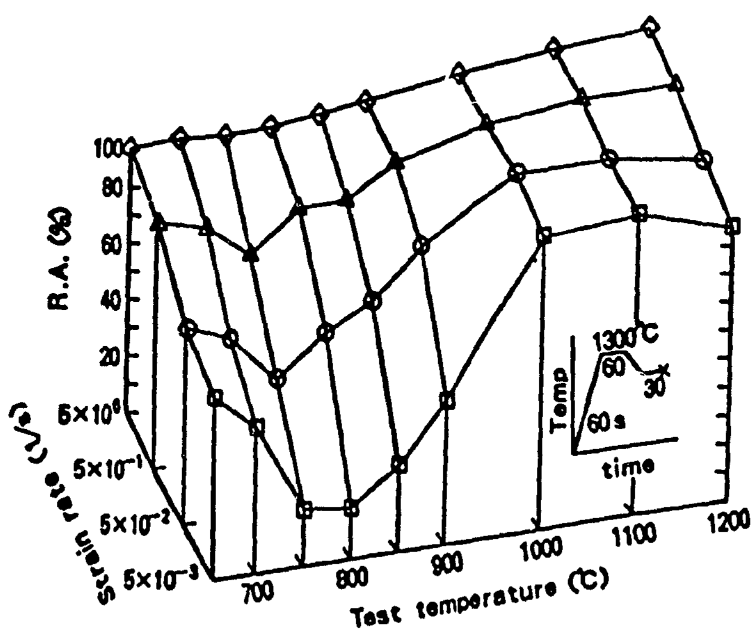

Fig. 2.11 - Dependence of ductility on the strain rate and test temperature for a Nb bearing steel [39].

time available for the growth of voids formed around the grain boundary precipitates [11]. Furthermore, the amount of grain boundary sliding is increased for lower strain rates [17]. It can be seen in Fig 2.11 that for a significant change in the reduction of area to occur in a Nb bearing steel, a variation of approximately one order of magnitude on the strain rate is required. Similar results have been reported for plain C-Mn steels [19]. Thus, even though hot ductility data indicates that increasing strain rate improves hot ductility, there is little scope for altering this variable in a continuous casting operation.

Grain boundary sliding is characteristic of creep rupture, and normally occurs at strain rates lower than $10^{-4}s^{-1}$ [69,70]. However, Ouchi and Matsumoto [17] have observed grain boundary sliding at strain rates as high as $10^{-1}s^{-1}$ in a 0.054% Nb containing steel deformed at 900°C. At the strain rates typical of creep, the fracture path for metals and alloys changes from transgranular to intergranular with increasing temperature [71]. Transgranular fracture occurs at low temperatures, i.e. below 0.3 T_M (T_M = melting point). At high temperatures the boundaries are weaker, and the fracture is intergranular [72]. This behavior has resulted in the concept of the equicohesive temperature, at which the grains and grain boundaries exhibit equal strength and the fracture mode changes from transgranular to intergranular [71].

Deformation at temperatures above the equicohesive temperatures results in two types of fracture. One possibility is by the relative movement of adjacent grains by a shear translation along their common grain boundaries, i.e, grain boundary sliding. In this case, wedge shaped cracks may form at the grain boundary triple points (grain corners) if the tensile stresses normal to the boundaries exceed 'he boundary cohesive strength [73]. These cracks, which are referred to as wedge or "w-type", are illustrated schematically in Fig. 2.12. Another possibility usually under low stress condition, is the occurrence of intergranular fracture by void formation at the grain boundaries. These cavities occur preferentially along the grain edges rather than at grain corners, and since they appear to be round when observed metallographically , these voids are referred to as "r-type" cavities [71]. As presented in Section 2.2.4, the models of grain boundary embrittlement used to explain the poor ductility of steel under continuous casting conditions, are derived from the above creep deformation concepts.

2.2.8 - Influence of dynamic recrystallization

Since the strains developed during the straightening operation are very small (<2%), dynamic recrystallization cannot take place in continuous casting. However, in hot tensile test simulations, it has been shown that when dynamic recrystallization is well established, the ductility is generally high [11,16,60].

Bernard et al. [16] have proposed a model based on grain refinement via dynamic recrystallization to explain the differences in the ductility behavior exhibited by a Nb bearing steel (0.050% Nb) compared to a plain C-Mn grade. Both steels were solution treated before cooling for testing in the temperature range 600 to 1200°C. In the C-Mn steel the trough covered the temperature range of 650 to 900°C, whereas for the Nb bearing steel the embrittlement is extended up to about 1050°C. They have shown metallographically, on samples quenched immediately after fracture, that high ductility in austenite corresponded to the attainment of fully recrystallized structures. Their model, which is presented in Fig. 2.13, considers that in the absence of recrystallization, the strain to fracture (ε_f) would be the same for the two steels. The strain to fracture increases with temperature and is schematically represented as the curves I and II in Fig. 2.13, referring to the initial coarse grained structure and to the fine recrystallized grain structure, respectively. The critical deformation for the onset of recrystallization (ε_c) is represented by curves III and IV, for the plain C-Mn and the Nb bearing steel, respectively. According to the model, for a given temperature, the progression of the specimen deformation in the austenite region can follow two routes:

1 - ε_c occurs before ε_f for the initial coarse grained structure. Therefore ε_f is moved from curve I to the the curve II, i.e the fracture occurs at a much higher strain.

2 - ε_f for the initial coarse grained structure occurs before the onset of recrystallization (ε_c) in the Nb bearing steel. Therefore the rupture is dictated by the low deformation level predicted by curve I and early fracture takes place.

As ε_c for the Nb bearing steel is greater than ε_c for the C-Mn grade, recovery in ductility for the former occurs at a higher temperature. Since Nb(CN) and possibly AlN can retard the austenite recrystallization [19,16,51] by pinning the grain boundaries, the above model can further explain the detrimental effects of nitrides on ductility in extending the trough to higher temperatures. However, as shown in the last section, increasing strain rate improves hot ductility in the temperature range of

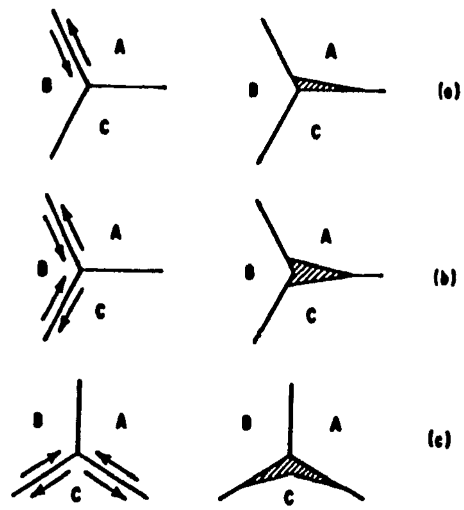

Fig. 2.12 - Schematic representation of the formation of w-type cracks at triple points by grain-boundary sliding [73].

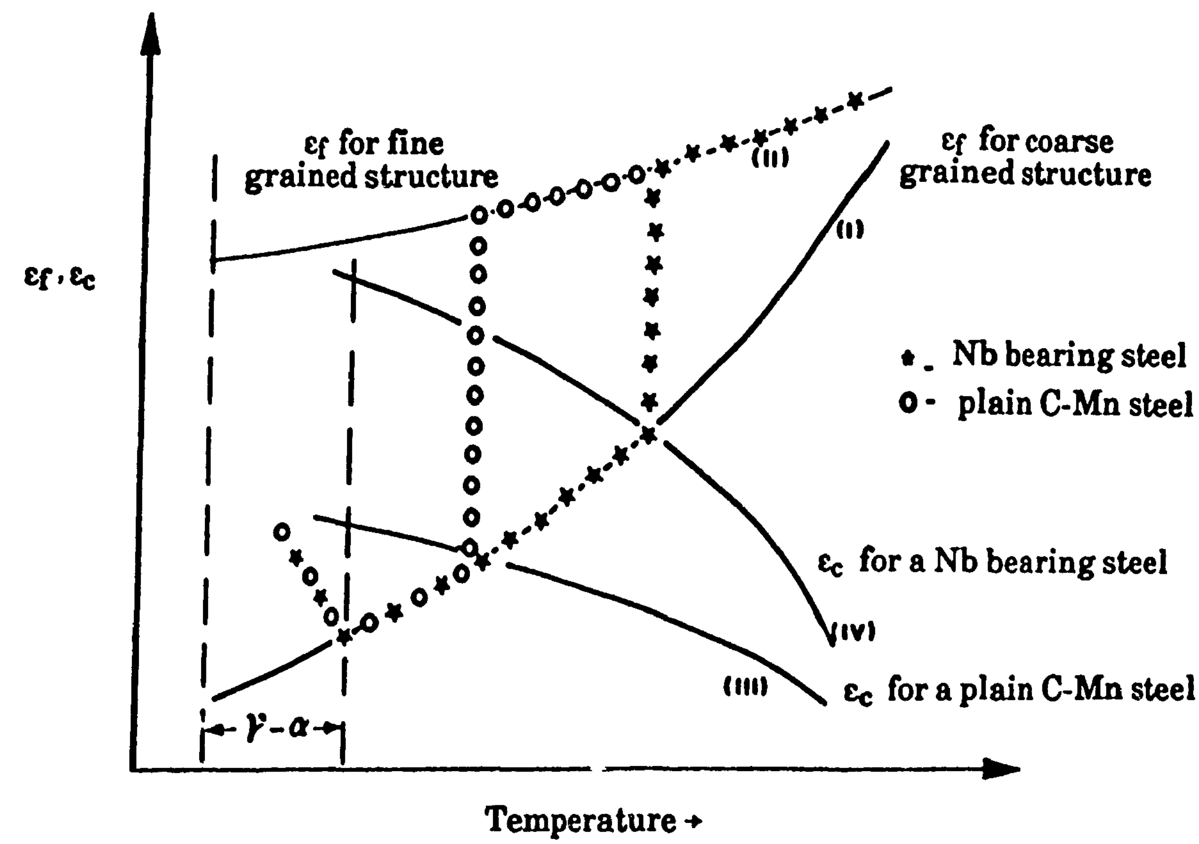

Fig. 2.13 - Schematic model of ductility recovery based on grain refinement via dynamic recrystallization [16].
ε_f=strain to fracture; ε_c=critical strain for dynamic recrystallization.

700 to 1000°C [21,39]. This fact is always used to argue against any influence of dynamic recrystallization in preventing embrittlement [17]. Since ε_c decreases with decreasing strain rate [55,56], tests performed at low strain rates might be expected to have a narrower ductility trough due to an earlier onset of dynamic recrystallization, whereas the opposite is observed. However, this argument may not be valid as Mintz et al. [74] have noted that the ε_f curve is more sensitive to strain rate than the ε_c curve and it is the relative movement of the two curves which controls the temperature at which dynamic recrystallization occurs.

CHAPTER 3

EXPERIMENTAL METHODS

The simple hot tensile test has been used in metallurgical laboratories to obtain a measure of the ductility during the straightening or unbending operation in continuous casting. This has been considered satisfactory in the prediction of the occurrence of transverse cracks during production [14]. Hot ductility is usually defined as the reduction of cross sectional area (R of A) at fracture of a cylindrical tensile specimen subjected to an appropriate thermal cycle and subsequently tested to rupture. Tensile testing was again employed in the present study, to investigate the hot ductility of three C-Mn-Al steels and one C-Mn-Al steel with a titanium addition.

The hot deformation behavior was examined over a temperature range encompassing the unbending temperature range and at a strain rate typical of slab straightening. Several thermal cycles were employed, which either simulated the slab surface temperature during unbending and/or emphasized the effects of precipitation and ferrite nucleation. The specimens were quenched immediately after rupture, thus allowing the high temperature structure to be correlated with ductility.

3.1 - EXPERIMENTAL MATERIALS

The initial objective of this study was to investigate the cause and mechanisms for the embrittling behavior exhibited by two low carbon aluminum killed steel grades produced by Stelco Inc. - Lake Erie Works, i.e. the "Low Al" and "High Al" steels in Table 3.1, which were cast with acid soluble aluminum (ASA) contents of .026 and .085 wt%, respectively. The "Low Al" steel, which exhibits a lower incidence of transverse cracks (about 10% of the number of slabs inspected in one year at the plant) was taken as reference. In the case of the "High Al" steel, about 50% of the inspected slabs are rejected or conditioned due to transverse cracks. These two grades were supplied by Stelco, in the as-cast condition, as pieces sectioned from continuously cast slabs of cross section 240 x 1180 mm.

As seen in the previous chapter, steels with increasing values of the product of ASA x total nitrogen will be more prone to embrittlement under continuous casting conditions, unless the precipitation of AlN in the austenite grain boundaries can be prevented. In order to examine this latter case, a third grade was tested which contained ASA and N levels similar to the "high aluminum" steel but with a 0.037% titanium addition. This titanium concentration was such that the Ti:N ratio (in wt%) was approximately 2.5 times the stoichiometric ratio, thus guaranteeing that almost all the nitrogen combined with the Ti, thereby reducing, or more likely eliminating AlN precipitation. As shown in Table 3.1, the ASA x N products are 1.04×10^{-4}, 4.25×10^{-4} and 3.8×10^{-4} for the "Low Al", "High Al" and "Ti treated" steels, respectively. It should be noted that, in the type of simulation used in this work (see Section 3.4.1), the TiN precipitation can also improve hot ductility by refining the austenite grain size. The Ti treated steel was prepared at the Metals Technology Laboratories (MTL) of the Department of Energy, Mines and Resources (CANMET, Ottawa), as a 50 kg air melted ingot with a 130 x 150 mm middle height cross section and a height of 240 mm after shearing off the shrinkage region from the ingot top. It was received in the as-cast condition.

The "high manganese" steel in Table 3.1 was used in a previous investigation by Guillet [25] and was included in this study to analyse the effect of lowering the austenite-ferrite transformation (due to the higher manganese content) on the hot ductility. This grade was also prepared at CANMET as an 50 kg air melted ingot, but was received as an as-hot rolled 17 mm thick plate.

Finally, it worth noting that studies by Bernard et al. [16] have indicated that ductility results obtained in simulations such as used in this work (as will be described in Section 3.4.1) are not affected by the initial condition of the material, i.e. either as-cast or hot rolled.

3.2 - SAMPLING AND SPECIMEN PREPARATION

The tensile specimens from the as-cast "High Al" and "Low Al" steel slabs and the "Ti treated" ingot were machined from regions near the slab/ingot surface with their longitudinal axes parallel to the casting direction (Figs. 3.1(a) and 3.1(b)). Thus, the strain in the tensile test was applied transverse to the solidification growth direction, more closely simulating the actual straightening situation. To minimize the number of inhomogeneities caused by surface defects and/or significant

Table 3.1 - Chemical composition (in weight %) of the steels investigated

Designation[1]	C	Mn	Si	P	S	ASA[2]	N	ASA x N	Ti
Low Al steel	.082	.39	.013	.007	.008	.026	.0040	$1.04\text{x}10^{-4}$	-
High Al steel	.079	.40	.019	.006	.008	.085	.0050	$4.25\text{x}10^{-4}$	-
Ti treated steel	.083	.38	.058	.008	.008	.095	.0040	$3.80\text{x}10^{-4}$	.037
High Mn steel	.078	1.39	.35	.010	.009	.016	.0078	$1.25\text{x}10^{-4}$	-

1) Cu, Ni and Cr were found in negligible residual levels
2) ASA = Acid soluble aluminum

segregation, the specimens were taken from the columnar crystal zone, thus avoiding the skin and center thickness regions. From the "High Mn" as-hot rolled steel plate, the tensile specimens were taken with their longitudinal axes parallel to the rolling direction.

The shape and dimensions of the specimens used in this work, which are given in Fig. 3.1(c), follow the ASTM standard, in which the gauge length is five times the diameter [75]. The specimen shoulders were lengthened to enable the installation of an alumina ring, as will be described in Section 3.3.3.

3.3 - EXPERIMENTAL EQUIPMENT

3.3.1 - Tensile test apparatus

The complete experimental system shown in Fig. 3.2 comprises of:

- an MTS 510 servohydraulic testing machine with a frame designed for a maximum load of 25 KN.
- a PDP11 computer, a VT-240 graphics terminal and an LA50 printer, all manufactured by Digital, interfaced to the MTS via a 468.20 processor unit. This provided the machine control and data acquisition, using an RT11 operating system and software written in MTS BASIC.
- a radiant furnace and temperature controller/programmer (to be described in the next section).

3.3.2 - Radiant furnace and temperature control

In order to perform experiments at high temperatures, a Research Inc. radiant furnace, equipped with an 16 KW power supply was used. This furnace is mounted on the columns of the MTS load frame and linked to a Micristar digital controller/programmer. The heat, generated by the four tungsten filament lamps which can be seen in the close up of the furnace (Fig. 3.3), is reflected to the center of the furnace (where the specimen is located) by four mirror finished elliptical reflectors of aluminum, positioned symmetrically about the center.

The temperature measurement was performed with a Pt/Pt-10% Rh (S type) open tip thermocouple. For reference, a second chromel-alumel (type K) closed tip

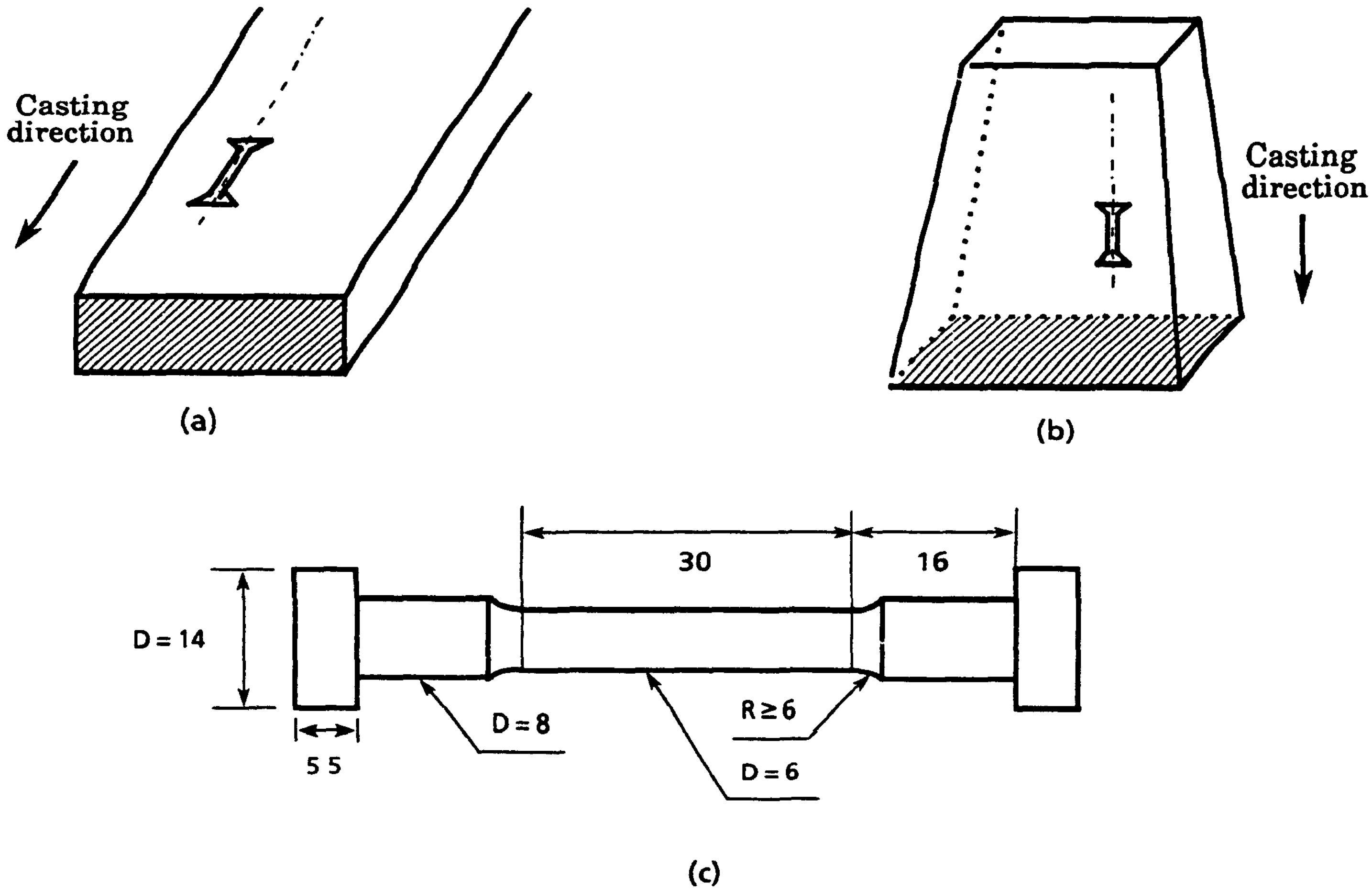

Fig. 3.1 - (a) Tensile specimen sampling with respect to slab casting direction ("high aluminum" and "low aluminum" steels);
(b) Tensile specimen sampling with respect to ingot casting direction ("Ti-treated steel");
(c) Specimen configuration (dimensions in mm).

thermocouple was installed, which is suitable for the test temperature range (700 to 1000°C) used in these experiments; both thermocouples contacted the specimen surface at the middle of the gauge length (see Fig. 3.3).

In some tests, the two thermocouples were installed in different positions on the specimen, and indicated that the maximum thermal gradient at any point along the gauge length was within ± 10°C. When the difference between the two independent readings was greater than 20°C in the test temperature, the experiment was discarded and repeated. It transpired that the main reason for such differences in temperature (i.e. >20°C) was either the rapid deterioration of any one of the heating elements with respect to the others, or a dirty reflector surface, resulting in asymmetrical reflection. Because of this, the elements had to be changed and the reflectors polished on a regular basis (about every 25 tests). In addition, it was observed that the chromel-alumel thermocouples deteriorated after approximately five tests, probably due to oxidation occurring during the initial solution heat treatment at 1350°C (see Section 3.4.1). This resulted in temperature readings higher than the actual temperature and thus necessitated a change in the type K thermocouple. Only one S type thermocouple was used throughout these experiments. As the Pt/Pt-Rh wires do not oxidize readily, no variation in temperature variation from the correct reading was noticed in this thermocouple. However, because the junction was relatively brittle, it fractured at about every 10 tests and had to be rewelded.

To minimize oxidation, the specimen and grips were kept within a quartz tube of 57 mm internal diameter with a continuous flow of "prepurified grade" argon (more than 99.998% pure). The argon inlet was located in the top of the tube and the outlet was one of the two holes drilled in the quenching guide (described in the next section) for installation of the thermocouple (the gap between the other thermocouple and the hole was sealed with a silicon based sealant).

As shown in Fig. 3.3, the quartz tube was supported at the bottom by the quenching guide and was sealed with a rubber "O"-ring placed outside the tube; the top of the quartz tube was also sealed by an "O"-ring, but, as the temperature was higher at the top, a metal shield (made of stainless steel sheet) filled with "fiberglass" was installed to prevent melting of the "O"-ring. The temperature difference between top and bottom of the tube was partly due to the fact that the hot argon tends

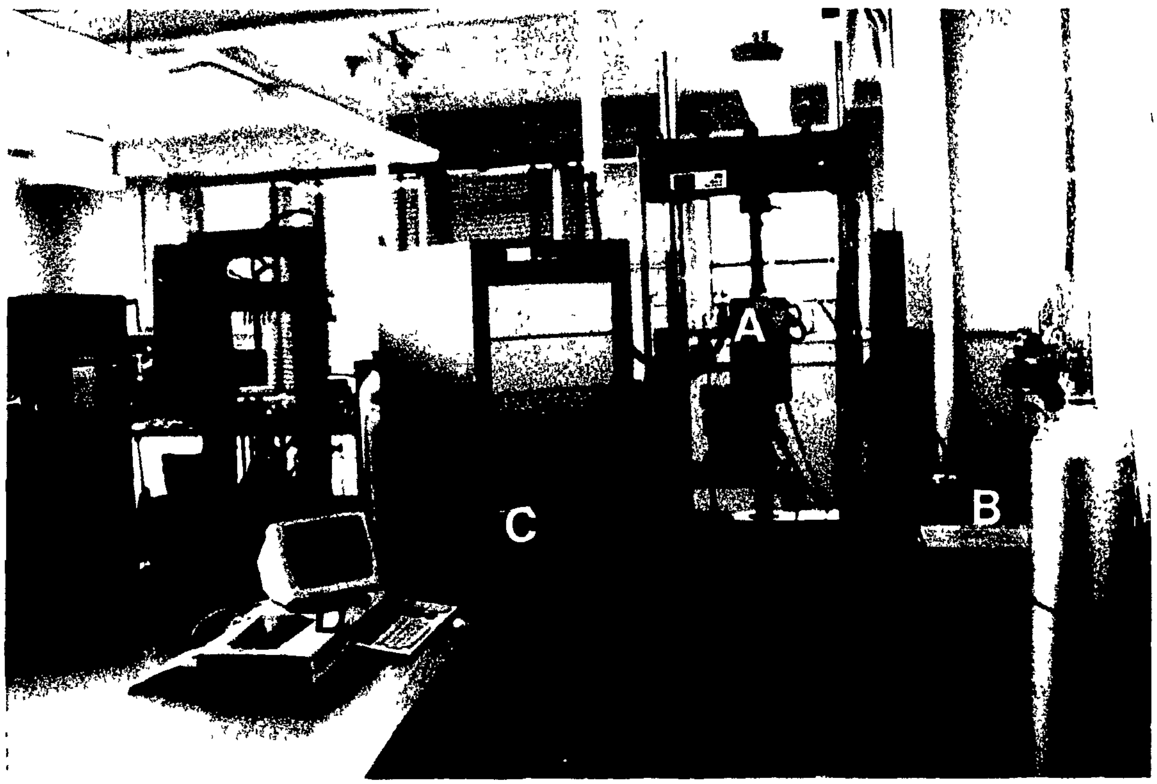

Fig. 3.2 - General view of the tensile testing system:
(A) radiant furnace;
(B) temperature controller/programmer;
(C) PDP-11 computer and 468 processor interface unit;
(D) VT-240 graphics terminal and LA-50 printer.

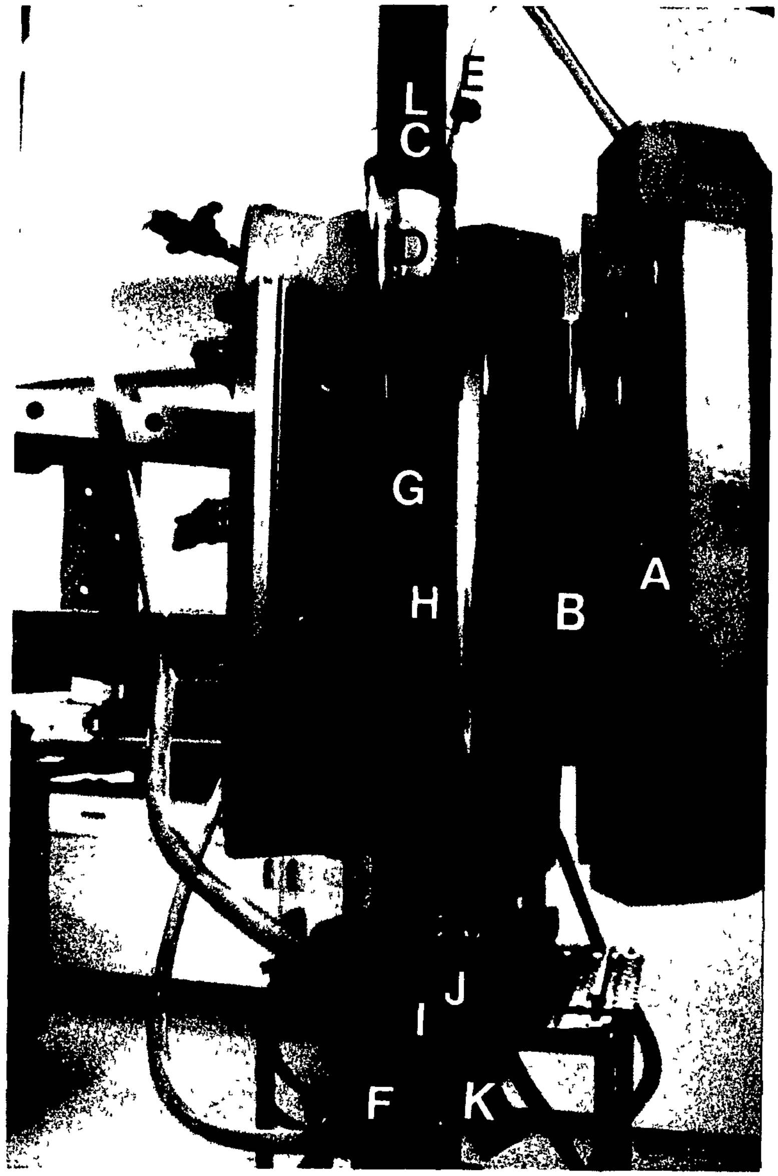

Fig. 3.3 - View of the radiant furnace and tensile grips:
(A) heating elements (tungsten filaments); (B) aluminum reflectors;
(C) quartz tube; (D) metal shield; (E) argon inlet; (F) argon outlet;
(G) tensile grips; (H) specimen; (I) quenching guide;
(J) copper cooling ring; (K) quenching guide plug;
(L) water cooled extension rods.

to rise, and partly because the cooling system is more efficient at the bottom compared to the top.

3.3.3 - Design of tensile grips and quenching system

For a test configuration where the tensile grips are heated together with the specimen in the chamber, there are few alloys that can withstand the combination of temperatures and flow stresses required to simulate continuous casting related processes. Candidate materials require a combination of high strength, good creep resistance and high melting point. Such an alloy is TZM, a molybdenum-base alloy containing 0.5 wt% Ti and 0.08% Zr (hence the initials TZM). This alloy fulfills the above mentioned requirements as well as having other key characteristics, such as the absence of a phase transformation in the solid state and high resistance to recrystallization or softening [76,77]. Another important property is good machinability and, in this respect, TZM is similar to that of medium carbon alloy steel at a hardness of HRc 30-35. At temperatures over 550°C TZM oxidizes very rapidly in air or oxidizing atmospheres, but it has a long life in high vacuums and is also inert in a pure argon atmosphere at all temperatures [76]. Because of these characteristics, TZM and other Mo-based alloys, have been employed for a variety of engineering applications, in which the service temperatures occasionally reach 1650°C [77]. It has been used succesfully by Guillet [25] under vacuum for hot tensile tests at temperatures as high as 1480°C and in the present work it has shown no visible indication of wear or deterioration.

The tensile grips/specimen configuration as well as a general view of the quenching system are shown in Fig. 3.3. The grip design is displayed in Figs. 3.4(a) and 3.4(b), with the approximate dimensions in mm; the original dimensions in inches, used for machining, are shown in parentheses. The lower grip, which is schematically shown in Fig. 3.4(a), is hollow and screws into a "quenching guide", the latter being connected to the lower extension rod which screws into the MTS actuator. The upper grip (displayed in Fig. 3.4(b), with a specimen installed) is a solid bar, which screws into the upper extension rod. This is in turn connected to the machine load cell.

The quenching guide represented in Fig. 3.5, made from high carbon steel ("drill rod"), has a hole drilled at an angle with the grip axis, thus permitting the sample to pass through to a quench cup. During the test, the quenching guide is sealed by a steel plug with an "O"-ring at its tip. Close to the end of the test, when the load approaches zero, the plug is removed, allowing the lower part of the broken specimen to drop through the quenching guide (via the hollow lower shaft) into a copper cup filled with cold water. During the quenching period, when the tensile system is opened to atmosphere, the argon flow is increased to prevent oxidation. After quenching, the plug is replaced and the gas flow decreased to the normal rate. The quenching guide is cooled by water passing through a copper ring.

To prevent sticking of the specimen onto the grip, a layer of high purity alumina powder was placed at the specimen/grip interface. This resulted in quenching times less than 1 second for about 90% of the tests. In the initial tests of this work, based on the method of Tacikowski [32,78], an alumina ring was placed on the specimen shoulder, to prevent sticking. The rings were manufactured from round solid bars (19 mm diameter) that were purchased in a "pressed and partially sintered" condition. They were machined and then sintered at 1600°C for 1 hour, leading to a thickness of 4 mm, internal diameter 8.5 mm and outside diameter 14 mm. Finally, a 7mm slot was cut out to allow installation on the specimen shoulder. However, in every test the ring fell with the specimen and often obstructed the quenching guide hole. Moreover, the sintered rings have high compression strength but low impact resistance and fractured after virtually every test, either during the specimen deformation or at the quenching stage. A final disadvantage of the ring compared to the powder is the higher cost.

3.4 - TENSILE TESTING CONDITIONS AND PROCEDURES

3.4.1 - Simulation of slab straightening during continuous casting

As seen in the previous chapter, the thermal history applied to the tensile specimens is a major variable affecting the hot ductility of the material. In most investigations, to simulate the continuous casting related processes, the specimens are first reheated to a high austenitizing temperature (>1300°C) and held there for a certain time to dissolve any precipitates present and to produce a coarse grain size, thus approaching the structure of a slab after solidification. A more ideal simulation involves melting the specimen and solidification just prior to testing. Such tests are often performed in Gleeble testing machines.

Suzuki et al. [21] have shown that the reheat temperature does affect the ductility results. Using a steel similar to the High Al grade tested in this

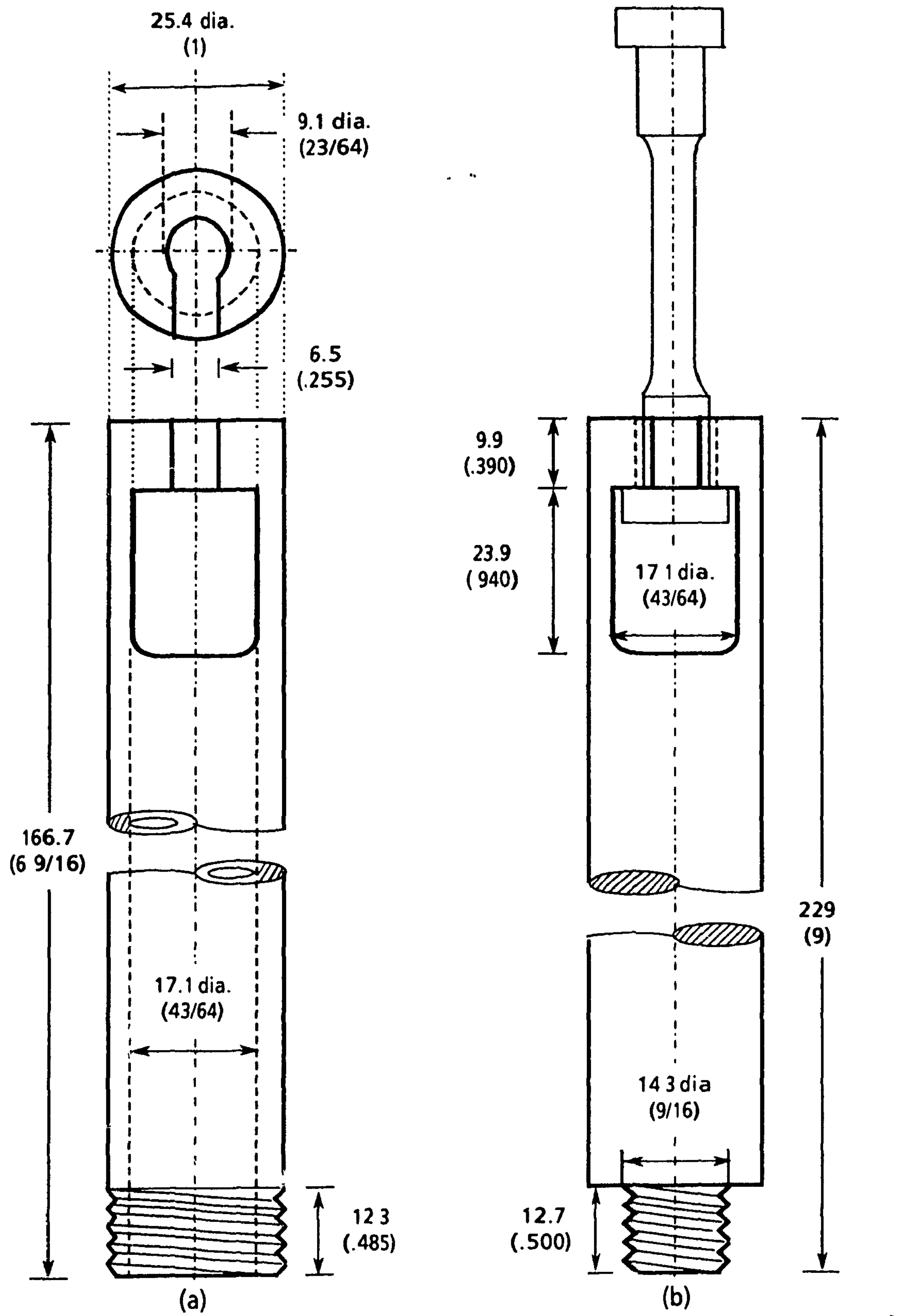

Fig. 3.4 - Shape and dimensions of the tensile grips, and specimen-grip configuration; approximate dimensions in mm (original dimensions in inches are shown in parentheses).
(a) Lower grip, which screws onto the quenching guide;
(b) Upper grip, which screws onto the water cooled extension rod.

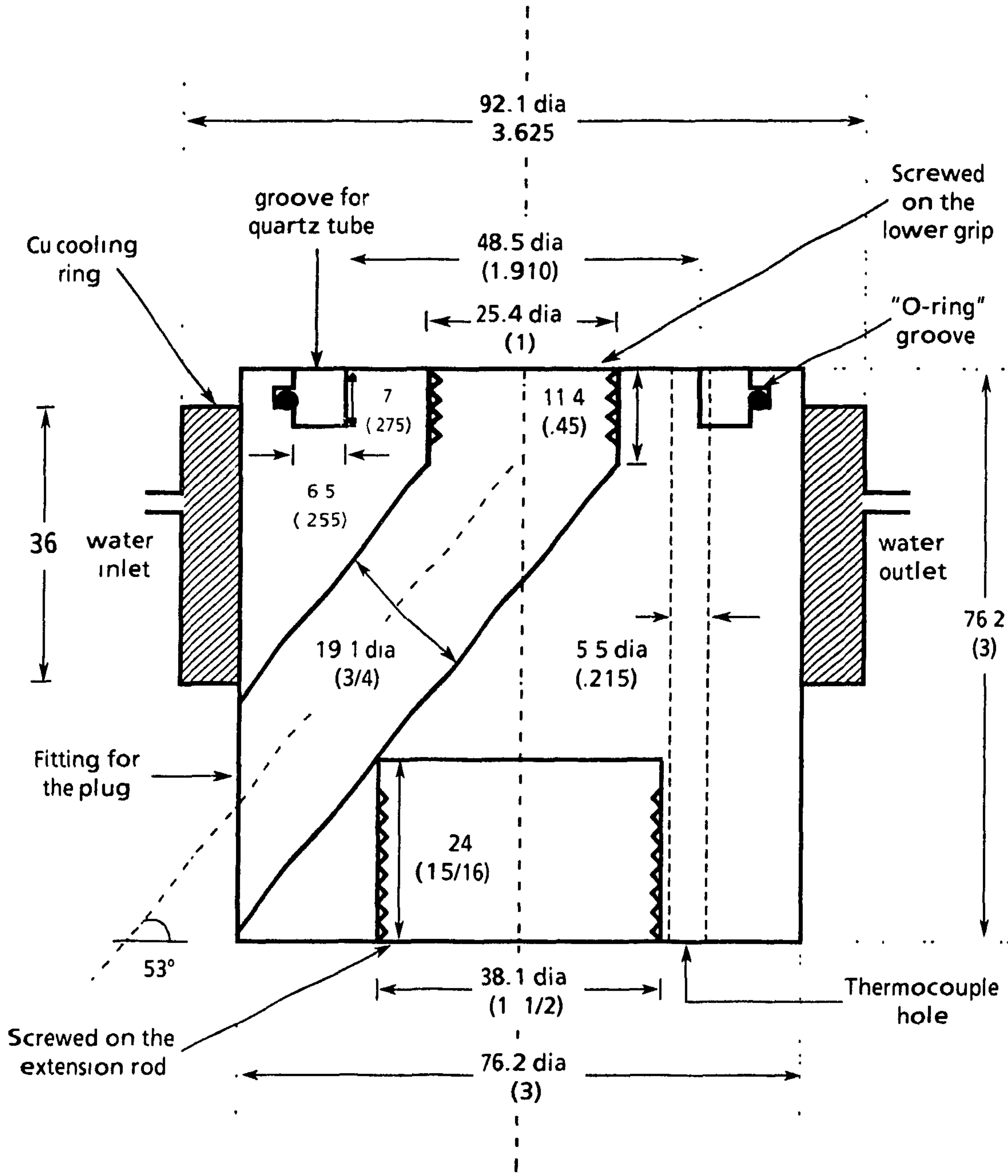

Fig. 3.5 - Sectional view of the quenching guide; approximate dimensions in mm (original dimensions in inches are shown in parentheses).

investigation, it was observed that the ductility trough was wider if the solution temperature was raised above 1200°C. It was also shown that reheating to 1400°C gave the same hot ductility behavior as "in-situ" melting and solidification (using a Gleeble apparatus). Bernard [44] indicated that the austenite grain size and the associated microsegregation pattern is independent of the solidification structure if the steel is reheated to a sufficiently high temperature (1350°C for his steels). According to his findings, above this critical reheat temperature, the grain size and morphology of the grain boundaries during the unbending stage is similar, in practical terms, to the ones obtained by melting and solidification prior to testing. As seen in the literature survey, this is not valid if the C content in the steels falls in the peritectic range ($C \simeq 0.10 \sim 0.15\%$).

The thermal cycles used in this work are schematically presented in Fig. 3.6. In all of them the specimen was heated to 1350°C in 15 minutes (approximately 1.5°C/s) and held at that temperature for 5 minutes in order to:

1) Coarsen and produce approximately the same austenite grain size in all the steels, except in the grain refined Ti-treated grade;

   this was confirmed by quenching a cylindrical sample (8 mm dia. x 10 mm) immediately after the solution treatment (using the quenching system attached to the compression set up developed by Simielli [79]) and measuring the coarsened austenite grain size.

2) Ensure the complete dissolution of all AlN present in all steels;

   the equilibrium solution temperatures of AlN were calculated from the relation given by Leslie et al. [48]:

$$\log (Al_s)(N_s) = -6770/T + 1\ 033 \qquad (3.1)$$

   where Al_S and N_S are the concentrations of aluminum and nitrogen in solution (wt%) at the equilibrium temperature T (in Kelvin). The austenitizing temperature used in this work is approximately 100°C above the calculated solution temperature for the "High Al steel", thus ensuring the complete dissolution of AlN in all the steels.

The three thermal cycles used in this study differ after the initial solution treatment. In the thermal cycle shown in Fig. 3.6(a), the specimen is cooled down to the test temperature at a constant rate of 1°C/s, which is approximately *the average cooling rate* of the continuously cast slab surface [63]. After 5 minutes of test temperature stabilization, the specimen is tested to rupture. This procedure represents the most common simulation of the unbending operation and is therefore designated the "reference cycle". The tests were performed from 700 to 1000°C (which encompasses the straightening temperature) at 50°C intervals, unless the ductility results and/or the microstructure indicated that smaller temperature intervals were necessary.

In the actual continuous casting process, the slab surface (where transverse cracks form) is cooled by water jets, and a complex thermal cycle occurs as a result of the alternate contact of water sprays and rolls on the strand surface, in addition to the heat transfer from the liquid metal in the center to the surface of the slab. Thus, the surface temperature actually oscillates about a mean cooling rate with an amplitude of 50 to 100°C [15]. This oscillation pattern has been reported to influence the precipitation behavior [63] as well as the austenite-ferrite phase transformation [17], and consequently influences hot ductility. To simulate this situation, two other thermal cycles were included in this work for the Low Al and High Al steels.

The "one-step cycling" variant is represented in Fig. 3.6(b), where the specimen is cooled, as before, at a constant rate of 1°C/s down to 100°C below the test temperature, held for either 1 or 5 minutes, then reheated in 30 s to the deformation temperature and tested after a 1 minute hold. With the temperature controller used in these experiments, 1 minute was the minimum time required for temperature stabilization. Figure 3.6(c) represents "two-step cycling" where the specimen was cooled down to the test temperature at an overall cooling rate of 1°C/s, but at 100°C above the deformation temperature a single cycle thermal oscillation was introduced with an amplitude of 100°C (with respect to the test temperature) and period of 90 s. After the oscillation, 1 minute was allowed for stabilization and the tests were again performed at constant temperature.

In addition to the above described thermal cycles, other variants were introduced to investigate or emphasize a particular phenomena in a few tests, such as one hour holding before deformation in the "reference cycle" (instead of the 5 minutes indicated in Fig. 3.6(a)) or multicycle thermal oscillations treatment (to be described in the results section).

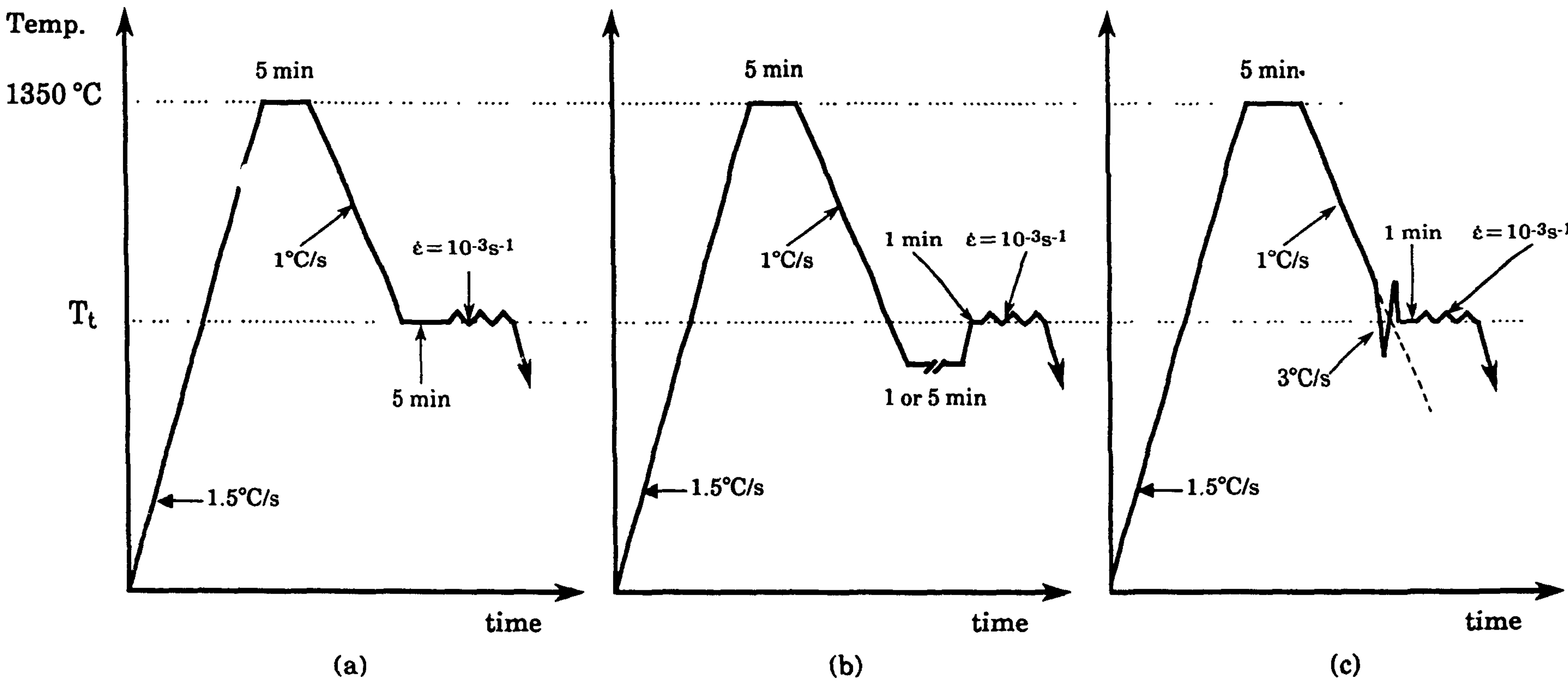

Fig. 3.6 - Thermo-mechanical cycles applied to the test specimens
(a) Reference cycle; (b) One-step cycling; (c) Two-step cycling.
T_t = test temperature = 700~1000°C.

The simulation of continuous casting related processes does not depend only on the temperature profile, but also on the applied strains. As mentioned in the previous chapter, the strain rate applied to the strand surface during bending/straightening can be estimated to be $7x10^{-3}$ to $5x10^{-4}$ s^{-1} for a typical continuous casting curved machine [9]. In this work, all tests were performed at a constant strain rate of $1x10^{-3}$ s^{-1}, approximately in the middle of the above range. All specimens were deformed to rupture and most of them were quenched immediately after fracture.

3.4.2 - Evaluation of hot ductility

The final diameter of the fractured sample was measured with an accuracy of $\pm$.1 mm using a projection microscope. The reduction of area (R of A) at fracture was defined in the following way:

$$R\,of\,A = \frac{A_0 - A_f}{A_0} = 100\,.\,(1 - D_f^2/D_0^2)\ \ (\%) \tag{3.2}$$

where D_0 (or A_0) and D_f (or A_f) are the initial and final diameter (or area) respectively. Reduction of area at fracture is a conventional measure of ductility [80] and has been used to define embrittlement in almost all the investigations of cracking mechanisms in cast products. One important reason for using the R of A is that this value does not rely on the specimen dimensions and/or geometry (as opposed to total elongation to fracture), which facilitates the comparison among different studies.

3.4.3 - Constant strain rate tensile testing program

The computer program to control the tensile test (presented in Appendix I) was written for this work in MTS-RT11 BASIC language. The main consideration was to test at a constant strain rate, since, as seen in the previous chapter, strain rate can affect the hot ductility behavior of steels.

In a tensile test, the true strain (ε) applied to a specimen deformed from an initial gauge length (L_0) to an instantaneous gauge length (L) is given by:

$$\varepsilon = \int_{L_0}^{L} \frac{dL}{L} = ln\,\frac{L}{L_0} \tag{3.3}$$

The true strain rate $\dot{\varepsilon}$, is defined by:

$$\dot{\varepsilon} = \frac{d\varepsilon}{dt} = \frac{dL}{L}\,\frac{1}{dt} \tag{3.4}$$

Since L increases continuously during the test, dL/dt must also be increased to maintain a constant strain rate. But dL/dt is the velocity of the lower grip (i.e. actuator). Therefore, in order to have a constant true strain rate, the actuator velocity must be increased during the test. This can be achieved by dividing the total test time into equal increments and then programming the actuator to move progressively longer distances over each subsequent increment of time.

In this case the total time estimated for each test (t) was calculated assuming that the fracture strain would not exceed the total strain programmed (ε_t). Thus:

$$t = \varepsilon_t/\dot{\varepsilon} \tag{3.5}$$

where $\dot{\varepsilon}$ is the required strain rate.

The strain ε_t was arbitrarily divided into 250 increments. Therefore at the I^{th} increment of time, the strain at that instant is

$$\varepsilon_I = \varepsilon_t.(I/250) \tag{3.6}$$

but, from Eq. (3.3),

$$\varepsilon_I = ln(L_I/L_0) \tag{3.7}$$

where L_I is the position of the actuator at the I^{th} increment.

Therefore,

$$L_I - L_0 = exp(\varepsilon_t.(I/250)) \tag{3.8}$$

and this value of L_I was used to vary the speed of the actuator to produce a constant strain rate.

After each experiment, the load and displacement information was recorded into a floppy disk and converted into load-elongation and true stress-strain curves. The data contained in the curves, such as elongation to fracture, peak stress,etc., as well as the shape of the curves, were used to evaluate the microstructural mechanisms which were operative during deformation (e.g. dynamic recrystallization, recovery, precipitation, etc.).

3.5 - FRACTOGRAPHY

At fracture, the bottom part of the specimen was quenched into cold water (see Section 3.3.2), whilst the upper part was allowed to cool to room temperature in argon, to prevent oxidation. Fractography was performed on some samples using the upper part of specimens with a JEOL T300 scanning electron microscope (SEM), operating at an accelerating voltage of 20 KV.

Specimens were prepared by discarding the head and shoulder to decrease the specimen height to approximately 8 mm. These were then mounted onto aluminum stubs. Decreasing the specimen height increases the working distance and effectively decreases the aperture angle in the SEM analysis [81], resulting in a high depth of field, which is essential in fracture surface examination. Fracture surfaces which indicated the presence of some oxidation were coated with a layer of evaporated carbon, with the aim of improving the resolution by increasing the electron conductivity of the surface.

Fractography was used to identify the type of fracture (brittle, ductile) and other characteristics such as the approximate dimple sizes and the presence of ferrite and precipitates on the austenite grain boundaries.

3.6 - METALLOGRAPHY AND ANALYSIS OF PRECIPITATES

The quenched samples were longitudinally sectioned, and the region adjacent to the fracture surface was mounted in bakelite. These were then polished in the normal manner from 240 to 600 grit silicon carbide, finishing through 6, 1 and .05 μm diamond paste.

The samples which were tested at temperatures corresponding to the duplex austenite-ferrite region were etched with 3% nital, thus delineating the austenite grain boundaries by ferrite, as well as revealing the ferrite. The volume fraction of the phases present were estimated either from the thickness of the ferrite layer or, for higher amounts of ferrite, by point counting using a 6x6 element grid and 15 different fields [82]. In the case of specimens tested in the single phase austenite region, etching was performed by immersion, for approximately 30 s, in a hot (80°C) solution of saturated aqueous picric acid containing 15 drops of concentrated hydrochloric and 3 drops of a wetting agent, sodium tricyclobenzene sulfonate ("Teepol 601"). The main objective in this case was to verify whether or not dynamic recrystallization had taken place. With both etching procedures, the type of fracture and the propagation of cracks could also be observed.

The samples were examined in a NEOPHOT 21 optical microscope and, for magnifications above 1000 X, scanning electron microscopy was used. For the latter, since bakelite is not electron conductive, a thin layer of graphite paste was painted from the sample to the metallic sample holder, to allow electron conduction away from the specimen. An energy dispersive x-ray spectrometer coupled to the SEM was used for chemical analysis of particles observed in the microstructure. To facilitate microanalysis, the accelerating voltage was reduced to 10 KV to diminish the excitation of the matrix iron atoms.

For the samples quenched after the solution treatment at 1350°C, the measurement of the austenite grain size was performed by the method of linear intercept as described in ASTM Standard E-112 [83].

In order to detect the presence of small precipitates, such as AlN, and to evaluate their morphology and distribution, carbon replicas were prepared from selected samples in a manner similar to that described by Ladd [84]. The samples, mounted in bakelite and polished as described above, were slightly etched in 3% nital and an evaporated carbon film was deposited on the specimen surface. The carbon coated surface was scribed with a scalpel blade to produce squares approximately 3x3 mm in size. These were then removed by etching through the carbon film with 8% nital and rinsing with ethanol. The films were then supported on copper grids.

The replicas were examined under a JEOL type 100CX transmission electron microscope (TEM), operating with an accelerating voltage of 80 KV. For chemical analysis of precipitates, energy dispersive x-ray spectrometry was used.

3.7 - DILATOMETRY TESTS

As noted previously, the austenite-to-ferrite phase transformation plays an important role in the hot ductility of steels. In order to determine the onset and the end of the non-equilibrium transformation during cooling (temperatures Ar_3 and Ar_1, respectively), dilatometric measurements were performed at Metals Technology Laboratories (MTL) of CANMET (Ottawa) on the four steels investigated, using a programmable MMC Quenching and Deformation Dilatometer. Cylindrical samples, measuring 6 mm (dia.) x 10 mm (length), were austenitized for 5 minutes and cooled at a constant rate of 1°C/s (in a vacuum or argon atmosphere), similar to the reference thermal cycle applied to the tensile specimens (Fig. 3.6(a)), but with continuous cooling and no deformation. To prevent damage of the equipment, the austenitization temperatures were reduced to 1300°C for the High Al and Ti treated steels and to 1250°C for the Low Al and High Mn steels, which are still above the dissolution temperature of AlN and the presumed grain coarsening temperature.

In addition to these measurements, non-deformed samples submitted to the reference thermal cycle were quenched (at the point at which deformation would have been initiated) from temperatures close to the Ar_3 indicated by dilatometry, for metallographic confirmation of the dilatometric determinations. The Ar_3 and the calculated equilibrium transformation temperatures (Ae_3, see section 4.1) were compared with the findings from the metallography of the non-deformed specimens as well as the tensile tested samples. Based on these data, the effect of strain on the austenite-to-ferrite transformation could be assessed.

CHAPTER 4

EXPERIMENTAL RESULTS

4.1 - AUSTENITE-FERRITE PHASE TRANSFORMATION

As mentioned previously, the ductility behavior of low carbon steels is significantly influenced by the austenite-to-ferrite phase transformation. Therefore, the temperatures that characterize the transformation were determined for the steels investigated. The non-equilibrium temperatures for the start (Ar_3) and finish (Ar_1) of transformation were determined by dilatometric measurements, as described in Section 3.7. The corresponding equilibrium transformation temperatures, the Ae_3 and Ae_1, were calculated using procedures available in the literature. These temperatures are compared below and will be correlated with the ductility behavior.

4.1.1 - Dilatometry (Ar_3 and Ar_1)

An example of a dilatometric curve (corresponding to the Low Al steel) is shown in Fig 4.1. Here, the ordinate and abscissa represent the specimen length and temperature, respectively. After the austenitizing heat treatment of 5 min at 1250°C, the sample is cooled down at a constant rate of 1 °C/s. In the austenite domain, the sample length decreases due to thermal contraction (the jump at 940 °C is simply a change in scale). At about 785 °C the curve deviates from linearity, indicating the onset of the phase transformation (Ar_3). Here, the sample length decrease is offset by expansion due to the presence of an increasing ferrite volume fraction. With further decreases in temperature, the sample contracts, and the point where the curve reassumes linearity indicates the completion of transformation (Ar_1), approximately 645 °C in the example shown in Fig. 4.1.

The Ar_3 and Ar_1 temperatures, together with the relevant test conditions, are listed in Table 4.1. The dilatometric measurement for each steel was repeated at least once (as shown in Table 4.1) due to some some scatter observed in the results. This scatter may be in part due to the coarse grain sizes resulting from the thermal cycle and/or to the fact that the dilatometer is not routinely used to work at such high reheat temperatures. The average of the Ar_3 and Ar_1 values determined for each steel was taken to be representative of the non-equilibrium transformation start and end temperatures, respectively, and are shown in Table 4.2.

4.1.2 - Equilibrium (Ae_3 and Ae_1)

The equilibrium transformation start temperature (Ae_3) was calculated for each steel using a computer program developed by Essadiqi [85], based on the work by Kirkaldy and Baganis [86], and are presented in Table 4.2 together with the Ar temperatures.

In the work of Kirkaldy and Baganis [86], an accurate thermodynamic determination of the Ae_3 in steels with additions of Mn, Si, Ni, Cr, Mo and Cu was performed. Some of these Ae_3 temperatures compared favorably with measured equilibrium transformation start temperatures from international compendia. It is concluded by Essadiqi [86] that the method of Kirkaldy and Baganis [86] can be considered to be accurate for total additions of the above elements of up to 7%. However, the model does not consider the influence of Ti and Al on the Ae_3 temperature. Being strong ferrite stabilizers [87], both these elements should raise the Ae_3, especially in the Ti steel, where the amount of Al and Ti in solid solution is significant. A frequently used alternative calculation available in the literature for determination of the Ae_3, is the expression determined by Andrews [88]. This is, however, shown in Appendix II not to apply for this work. For the determination of the equilibrium transformation end temperature (Ae_1), the Andrew's expression (given in Appendix II) is valid and therefore was used to generate the values listed in Table 4.2.

4.1.3 - Comparison between equilibrium and non-equilibrium transformation temperatures

The Ae_3 temperature is practically constant at about 860°C for the lower Mn steels, as can be seen in Table 4.2. For the High Mn grade it decreases to 842°C. The Ae_1 is around 720°C for all the steels investigated. Taking the Ar_3 determined for the Low Al steel as reference (783°C), increasing aluminum (High Al steel) raises the transformation start temperature by 20°C to 803°C. The addition of titanium together with the increased aluminum level (Ti treated steel) results in a further 17°C increase in the Ar_3 to 820°C. As mentioned before, this is due to the fact that

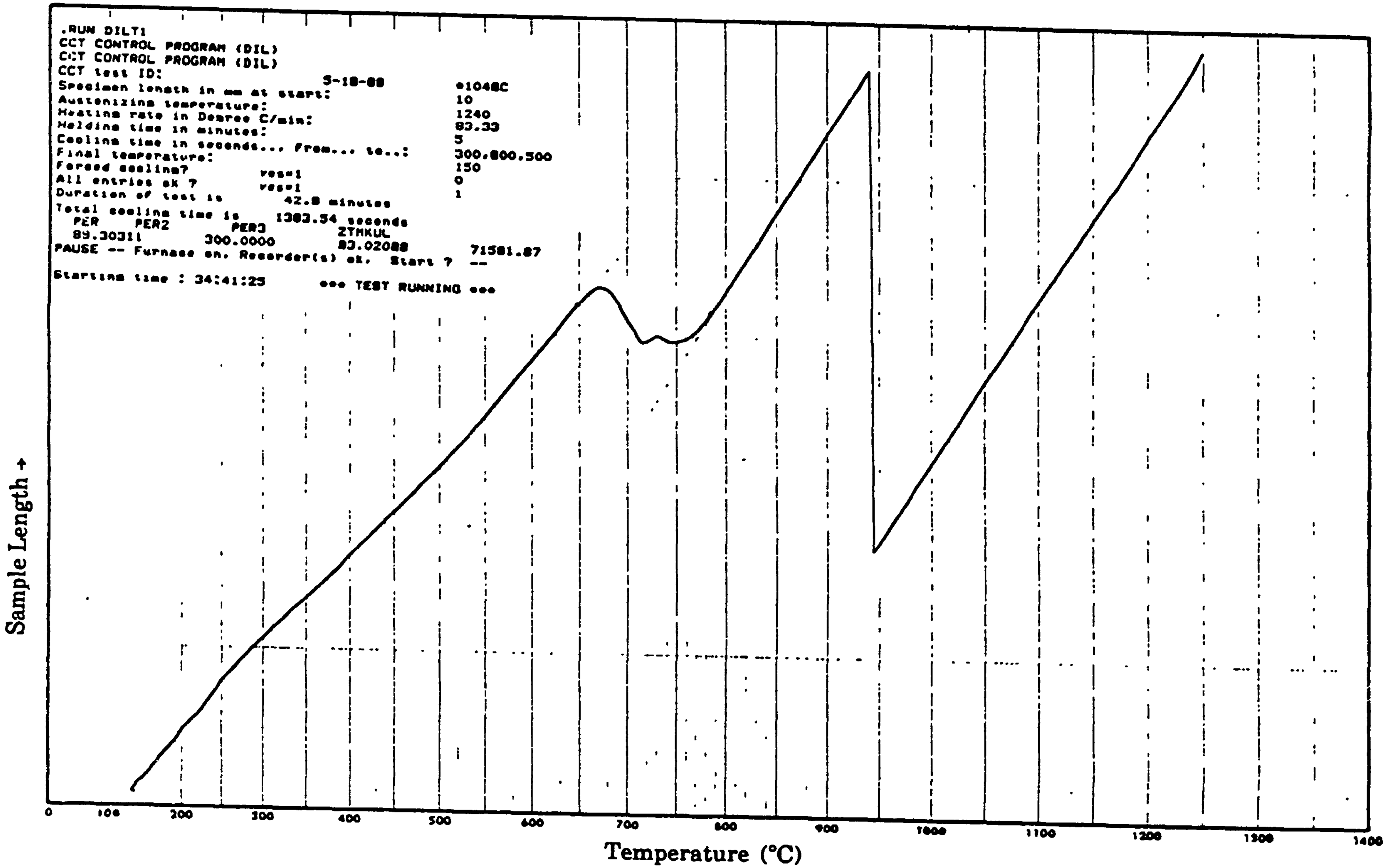

Fig. 4.1 - Dilatometric curve for the Low Al steel, reheated to 1250°C and continuously cooled to 100°C.

aluminum and titanium are ferrite stabilizing elements. Such behavior is not reflected in the Ae_3, because, as noted above, the calculations did not take these elements into consideration. The increased addition of Mn (High Mn steel), which is an austenite stabilizer, drops the Ar_3 by 48°C to 735°C; a significant but smaller drop (20 °C) in the Ae_3 is also noted.

From Table 4.2, the difference between the Ae_3 and Ar_3 temperatures (which is generally large for coarse grained material), decreases from 78 to 59 and finally to 43°C for the Low Al, High Al and Ti-treated steels, respectively, and increases to 107°C for the High Mn grade. This last observation is similar to the findings of Crowther and Mintz [36], who noted a difference of 96 °C between Ae_3 and Ar_3, in a steel with a chemical composition close to that of the High Mn steel.

The microstructures of non-deformed samples, submitted to the reference thermal cycle (Fig. 3.6(a)) and quenched from temperatures close to the Ar_3 measured by dilatometry, are shown in Fig. 4.2. Specimens were quenched after 5 minutes of temperature stabilization, which, in the tensile test, would be just prior to the start of deformation. Figure 4.2(a) shows the microstructure of the Low Al steel quenched from 800°C, a temperature 17°C higher than the measured Ar_3. No ferrite can be seen, although the austenite grain boundaries have been slightly delineated, perhaps indicating the presence of a very small amount of ferrite. The High Al steel, also quenched from 800 °C or 3 °C below the Ar_3, definitely indicates a thin layer of ferrite on some of the austenite grain boundaries (Fig 4.2(b)). Again, in the microstructure of the Ti-treated steel quenched from 830 °C or 10 °C above the Ar_3, shown in Fig 4.2(c), prior austenite boundaries are slightly delineated but no ferrite is observed. All these results are more or less in accord with the dilatometric measurements.

4.2 - TYPICAL TENSILE FLOW CURVES

The typical flow curves (true stress-true strain) observed in this work are presented in Fig. 4.3. The curves shown in this figure refer to the High Mn steel submitted to the reference thermal cycle, but the other grades show similar characteristics.

The full flow curves, from the beginning of straining up to fracture, exhibit three general deformation zones. Initially, the stress in the material rises rapidly and linearly to the applied strain, characterizing the elastic zone. The end of this region is marked by a decrease in the curve slope, although no yield point is observed.

Table 4.1 - Results of the austenite-to-ferrite non-equilibrium transformation temperatures (Ar_3 and Ar_1) determined by dilatometry.

Designation	Austenitizing temperature (°C)	Atmosphere	Ar_3 (°C)	Ar_1 (°C)
Low Al steel	1250	Vacuum	770	655
		Argon	795	635
			785	645
High Al steel	1300	Argon	800	650
			805	685
Ti treated steel	1300	Argon	830	660
			810	650
High Mn steel	1250	Vacuum	740	535
		Argon	730	520

Table 4.2 - Austenite-to-ferrite transformation temperatures for the steels investigated.

Designation	Ar_3 (°C)	Ar_1 (°C)	Ae_3 (°C)	Ae_1 (°C)
Low Al steel	783	645	861	719
High Al steel	803	668	862	719
Ti treated steel	820	655	863	721
High Mn steel	735	528	842	718

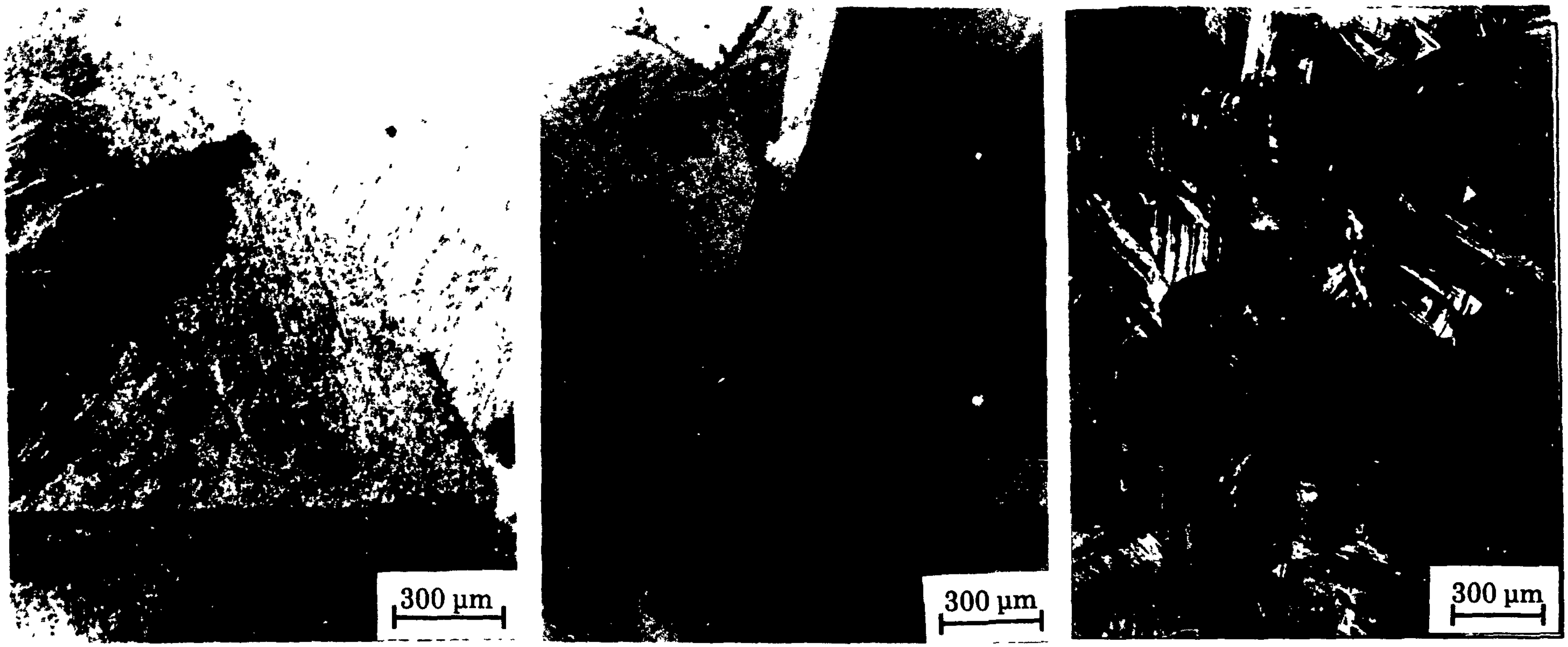

(a) (b) (c)

Fig. 4.2 - Microstructures of non-deformed samples quenched from temperatures close to the Ar3 (nital 3% etch). (a) Low Al steel - 800 °C. (b) High Al steel - 800 °C. (c) Ti treated Al steel - 830 °C.

The second stage of deformation is the plastic region which is characterized by work hardening, where the stress increases to a maximum and at the same time the slope of the curve (i.e., the strain hardening rate) decreases gradually. In this zone, the specimen gauge length increases and the diameter decreases uniformly throughout the gauge length. The second zone ends with strain localization at a point usually in the central region of the gauge length, resulting in necking.

The third and last deformation zone encompasses the beginning of necking and fracture. The constraints produced by the non deforming region outside the neck result in a state of triaxial stress in the necking region. Therefore the tensile flow curves shown in Fig. 4.3 are true stress-strain curves only up to the point of necking. In this work, no attempt has been made to account for necking in the stress/strain analysis. It is difficult to measure accurately the strain which corresponds to the onset of necking at hign temperatures. However this strain can be estimated by assuming that the diameter outside the necked region corresponds to the diameter at the onset of plastic instability. On each curve of Fig. 4.3, this estimated value of the strain at the point of necking is indicated by an arrow.

The ductility behavior is directly related to the shape of the flow curve, which is in turn controlled by microstructural changes occurring during deformation, as will be shown in detail in the next section. Figure 4.3(a) shows typical flow curves corresponding to specimens exhibiting high ductility in the single phase austenite region. In these curves, the stress reaches a maximum in the plastic region and then gradually decreases with continuing strain. This maximum is commonly called the "peak stress" and the corresponding strain is known as the "peak strain" Curves exhibiting single peak stress behavior, such as the ones given in Fig. 4.3(a), are indicative of dynamic recrystallization, and lead to austenite grain refinement [89]. It should be noted that, in the absence of necking (as in compression tests) the stress would attain a steady state value after the peak stress, i.e., deformation would continue at a constant stress.

The strain at which dynamic recrystallization begins is known as the "critical strain". For simplicity, the peak strain (ε_p) is often taken as the critical strain, although dynamic recrystallization actually begins at about 0.83 ε_p [90]. The 3 curves presented in Fig. 4.3(a) illustrate the influence of temperature on flow curves exhibiting dynamic recrystallization. Decreasing the temperature from 1000 to 900°C raises the strain hardening rate (slope of the curve), resulting in a higher peak

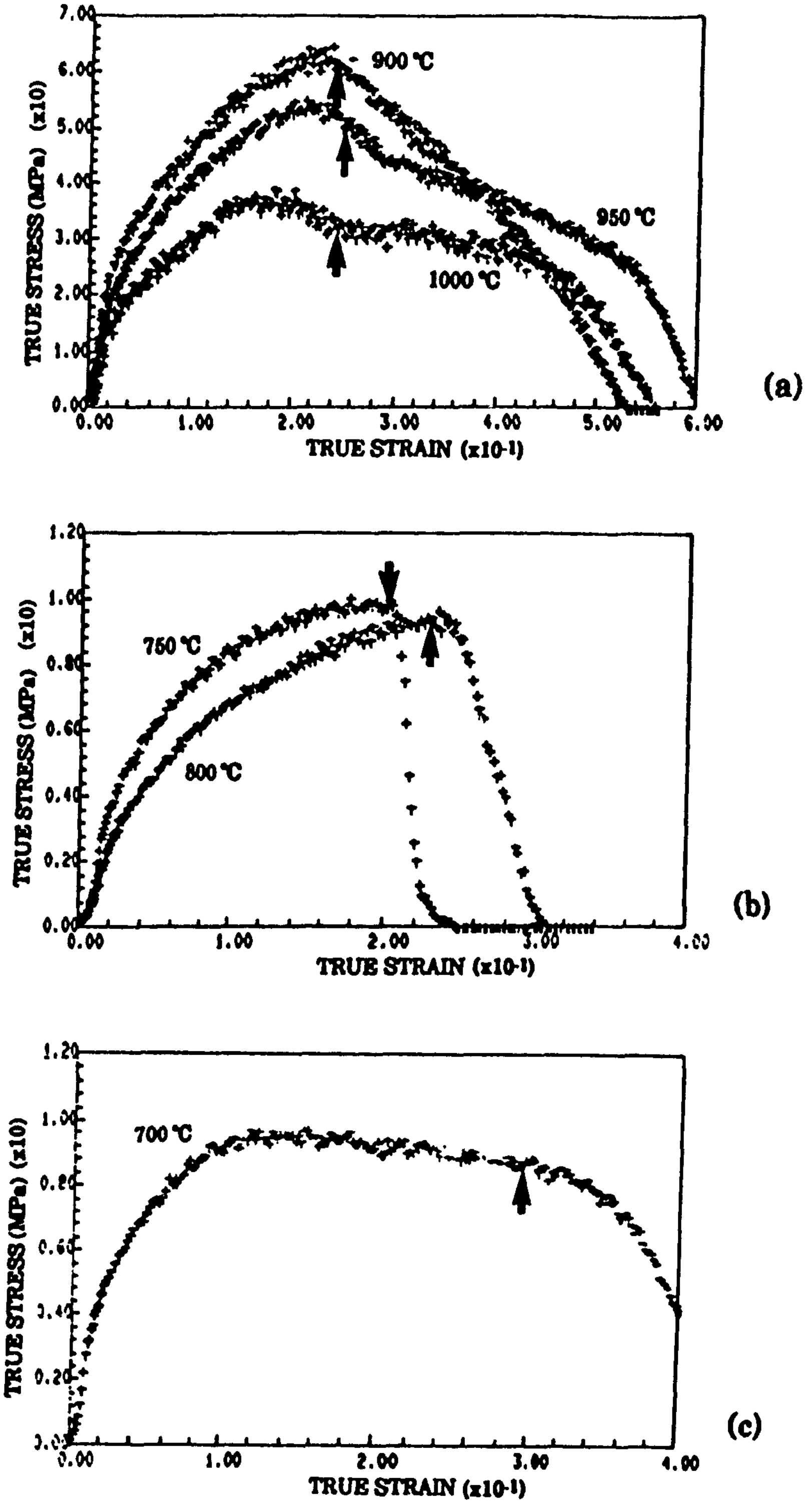

Fig. 4.3 - Typical flow curves (High Mn steel, reference cycle). (a) Good ductility in high temperature austenite; (b) Poor ductility in the duplex austenite-ferrite region; (c) Recovered ductility in the duplex region.

stress. For lower temperatures, dynamic recrystallization is more difficult to attain, i.e., ε_p increases. In these curves, the estimated strain at the onset of necking is found to be slightly greater than the peak strain.

Typical flow curves corresponding to low ductility specimens tested in the duplex austenite-ferrite ranges are shown in Fig. 4.3(b). Up to the peak stress, the behavior is similar to that of the curves described in Fig. 4.3(a), but the maximum stress is higher due to the lower temperatures of deformation (note the difference in scale for the stress-strain axes of Figs. 4.3(a) and 4.3(b)). After attaining the maximum stress, which approximately coincides with the estimated onset of necking, the stress drops abruptly to zero. Comparing the two curves in Fig. 4.3(b), the following characteristics are worth noting. At 750°C, work hardening is initially relatively rapid, but decreases somewhat towards the fracture strain. At 800°C the work hardening rate is initially lower compared to the low temperature test, but does not markedly decrease with continued deformation. Thus the stresses at strains close to fracture, i.e., the maximum stresses, are virtually coincident (about 100 MPa) for the two curves. Raising the test temperature from 750 to 800°C increases the strain to fracture, as would be expected.

At lower temperatures in the duplex austenite-ferrite range, the ferrite volume fraction is increased, and the characteristic flow curve is as shown in Fig. 4.3(c). Here, the work hardening rate gradually decreases until a plateau is reached, i.e., where the rate of work hardening is zero. This steady-state regime is characteristic of ferrite deformation and corresponds to dynamic recovery [89]. In this type of curve, it appears that necking occurs just prior to the decrease in stress, as expected.

Not all of the curves obtained in this work are represented in Fig. 4.3. These "atypical" curves will be described in the next section, together with the corresponding ductilities and microstructures.

4.3 - HOT DUCTILITY CURVES AND METALLOGRAPHY

As mentioned previously, the initial objective of this research was to analyse the brittle behavior of two continuously cast industrial grades. Therefore most of the results below relate to the High Al and Low Al steels (Table 3.1). The Ti treated grade was examined in order to ascertain whether a Ti addition could strongly improve the embrittlement susceptibility of the High Al steel. Finally the High Mn steel was used to generally indicate the effects of a marked change in the austenite-to-ferrite transformation temperature.

In the following, the hot ductility curves are shown as plots of the test temperatures against the reduction of area at fracture (R of A). Where a better understanding of the operating mechanisms is required, the metallography of the broken specimens and/or the corresponding flow curves are shown, together with comments on the ductility results. The results of the limited examination of replicas by TEM will also be included in this section.

4.3.1 - Microstructure prior to testing

The objective of the initial solution treatment at 1350°C (see Fig. 3.6), as mentioned in the previous chapter, was to ensure the complete dissolution of the AlN precipitates present, and to produce a similar coarse austenite grain size in all the steels (except the Ti-treated grade).

According to Eq. (3.1), all the Al and N will be in solution at temperatures higher than 1077, 1265 and 1099°C, for the Low Al, High Al and High Mn steels, respectively. In the Ti-treated steel, all the N is presumably combined with the titanium, and no AlN is precipitated. The following solubility equation for TiN was derived by Narita [91]

$$log\,(wt\%Ti)x(wt\%N) = (-15200/T_0) + 3\ 9 \tag{4.1}$$

where T_0 is the dissolution temperature in °K. Based on this equation, for the Ti and N levels present in this grade, the TiN particles will be completely dissolved only at very high temperatures (in liquid steel). At 1350°C, less than 3% of the TiN particles are dissolved. The percentage of MnS particles dissolved after the solution treatment was calculated using the following expressions developed by Turkdogan et al. [92]

$$K_S = \frac{[\%Mn]\,[\%S].f_S^{Mn}}{[A_{MnS}]} \tag{4.2}$$

where, f_S^{Mn} = activity coefficient of dissolved sulfur in the presence of manganese,

$[A_{MnS}]$ = activity of MnS, which is equal to 1, if there is more than 0.3% of Mn in solution.

The variation of the equilibrium constant with temperature is given by

$$\log K_S = (-9020/T) + 2.929 \tag{4.3}$$

and the dependence of f_S^{Mn} with temperature is given by

$$\log f_S^{Mn} = ((-215/T) + 0.097)\,(\%Mn) \tag{4.4}$$

As can be seen in Table 4.3, increasing the Mn level from about 0.4% (Low Al, High Al and Ti-treated steels) to 1.39% (High Mn grade) decreases the percentage volume fraction of MnS particles dissolved at 1350°C, from 79 to 22%.

Table 4.3 - Percentage of MnS dissolved and austenite grain size at 1350 °C.

Designation	MnS dissolved (%)	Austenite grain size (μm)
Low Al steel	79	450±20
High Al steel	79	460±20
Ti-treated steel	79	120±10
High Mn steel	22	420±20

The austenite grain sizes measured in samples quenched after 5 minutes holding at 1350°C are also presented in Table 4.3. The surface area examined of the samples used in this work measured 10x8 mm, which corresponded to more than 100 well defined grains. A coarse austenitic structure with a grain size of about 450±20μm was observed for the Low Al, High Al and High Mn steels. For the Ti-treated grade, a finer, more uniform austenite grain size was seen, measuring 120±10 μm. Based on the microstructures of the quenched specimens after rupture, to be presented in the next section, no significant change in grain size was apparent during cooling to the test temperature.

4.3.2 - Influence of chemical composition

In order to establish the effect of varying the chemical species (i.e. Al, Ti and Mn) and/or their concentration on the hot ductility behavior of the low carbon grades investigated, the results for the reference thermal cycle (Fig. 3.6.(a)) are compared below.

4.3.2.1 - Low aluminum steel

The ductility curve for the Low Al steel is shown in Fig. 4.4. At 950 and 1000°C the ductility is very high, close to 100%, and the flow curves indicate the occurence of dynamic recrystallization, i.e. a peak stress. For the 900 °C test, the R of A is slightly reduced to 90% and, as displayed in Fig. 4.5, no recrystallization can be inferred from the stress-strain curve. The corresponding microstructure is given in Fig. 4.6. Coarse non-recrystallized grains can be seen throughout the specimen, and close (approximately 2 mm) to the fracture surface (Fig. 4.6(a)). However, Fig 4.6.(b) indicates that the high deformation in the immediate vicinity of fracture has resulted in a fine recrystallized structure (all the subsequent micrographs are presented in the same way with respect to the test direction, i.e. the tensile axis is vertical and the fracture region corresponds to the upper part of the picture).

Decreasing the temperature to 850 °C results in a large fall in ductility to about 17% and intergranular fracture. A thin layer of ferrite (approximately 10 μm thick) and void formation in the prior austenite grain boundaries can be seen in Fig.4.7. The SEM micrograph, shown in Fig. 4.8(a), illustrates the martensite phase (quenched austenite) and an alignment of particles measuring 700 nm on average, as well as voids in the ferrite phase. The particles observed were identified as MnS, as shown in the energy dispersive spectrum (EDS), Fig. 4.8.(b).

At 800 °C the ductility is still very poor, about 16 %. Apart from increasing the ferrite thickness from 10 to approximately 20 μm, the microstructure and void characteristics are similar to the 850 °C specimen (Fig. 4.9). These 2 temperatures define the bottom of the ductility trough in this reference curve. On decreasing the test temperature to 750 °C, the ductility is regained to approximately 90%,

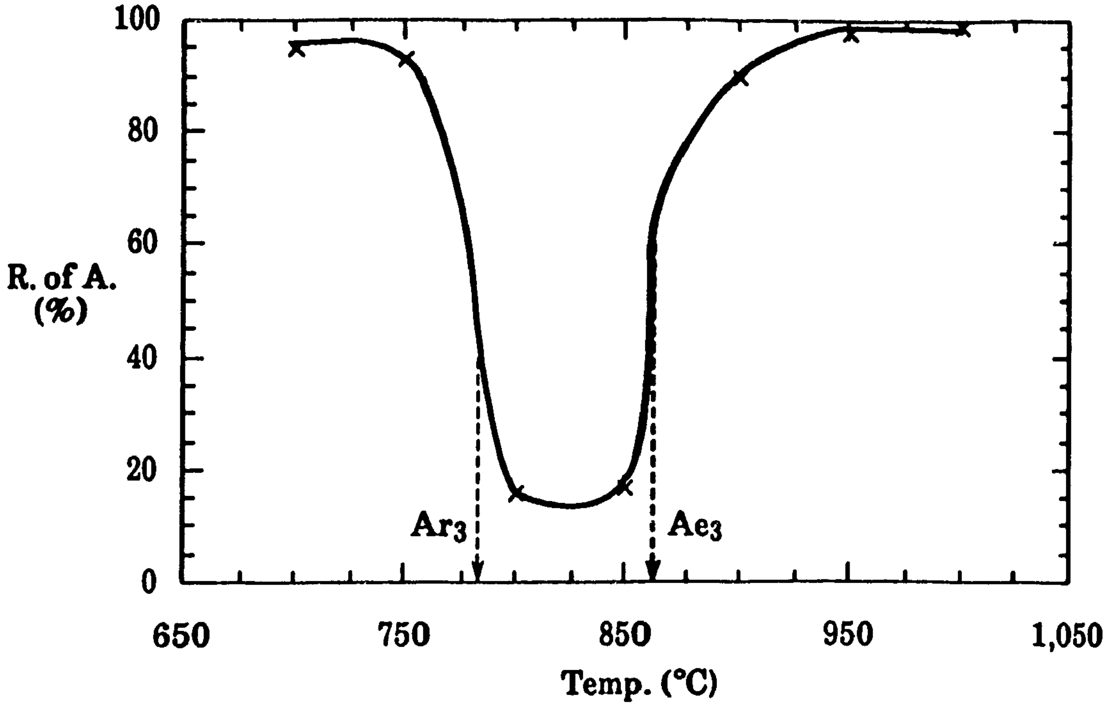

Fig. 4.4 - Ductility curve for Low Al steel (reference cycle).

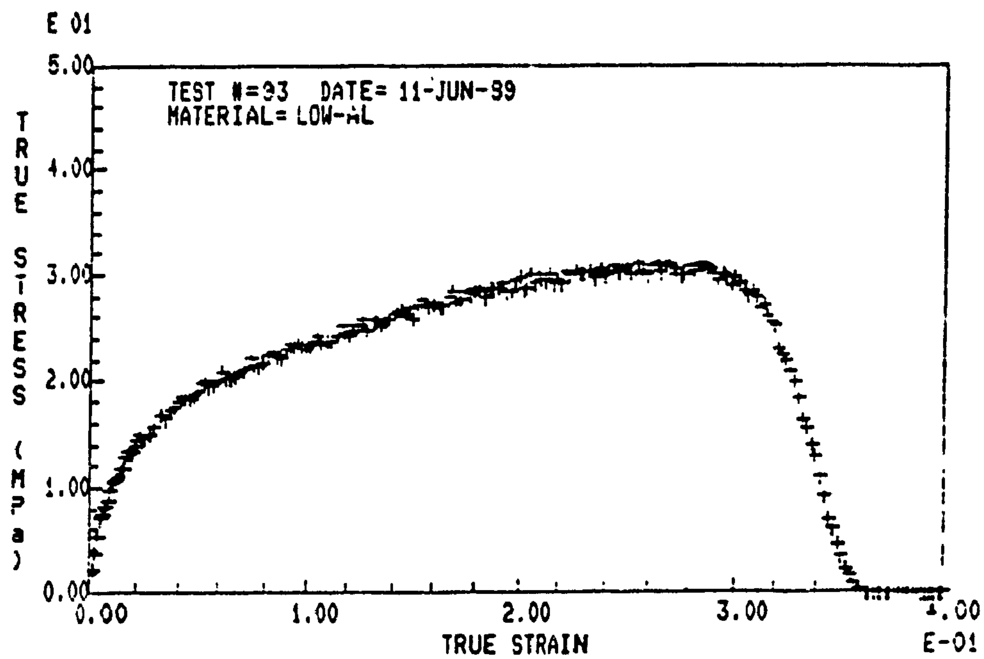

Fig. 4.5 - Flow curve for the Low Al steel tested at 900 °C (reference cycle).

≈2 mm from fracture

fracture surface

(a)

(b)

Fig. 4.6 - Microstructure of Low Al steel, tested at 900 °C using the reference cycle (picric etch):
(a) 2mm from fracture (coarse non-recrystallized structure);
(b) fracture tip (recrystallized structure).

Fig. 4.7 - Microstructure of Low Al steel, tested at 850°C using the reference cycle, showing voids formed within the 10 μm thick ferrite film nucleated at the austenite grain boundaries (3% nital etch).

(a)

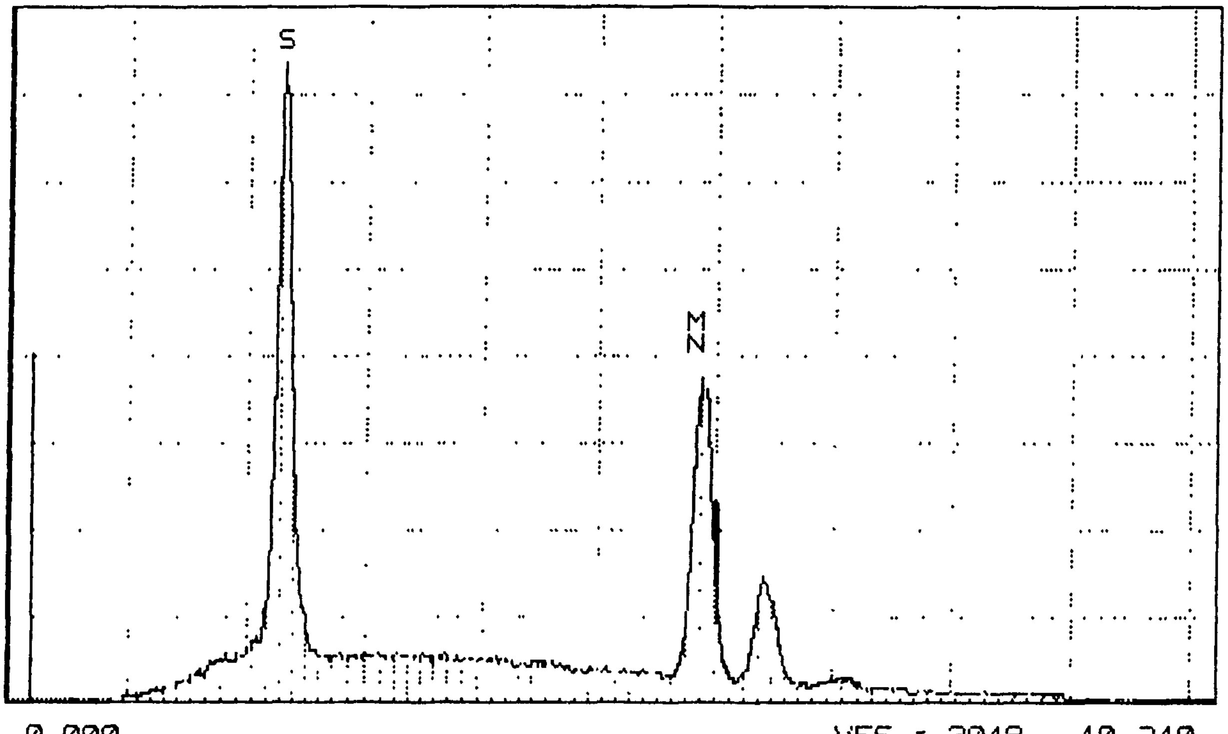

(b)

Fig. 4.8 - SEM analysis of Low Al steel tested at 850°C using the reference cycle: (a) MnS particles and voids aligned in the austenite grain boundary ferrite film; (b) energy dispersive spectrum of the particles shown in (a).

Fig. 4.9 - Microstructure of Low Al steel, tested at 800°C using the reference cycle, showing intergranular fracture associated with the 20 µm thick ferrite film at the austenite grain boundaries (3% nital etch).

Fig. 4.10 - Microstructure of Low Al steel, tested at 750°C using the reference cycle, showing large volume fraction of ferrite and ductile fracture (3% nital etch).

corresponding to an increased proportion of ferrite in the microstructure to about 55%, as can be seen in Fig 4.10. At 700 °C the R. of A. is even higher, about 95%. The ductility trough is thus located between the Ae_3 (861°C) and the Ar_3 (783°C) temperatures for this steel, as indicated in Fig. 4.4.

4.3.2.2 - High aluminum steel

The ductility curve for the High Al steel is presented in Fig. 4.11, together with the Low Al grade results for comparison. Essentially, for the same base composition, increasing the ASA from 0.026 to 0.085%, results in a slightly deeper trough, which is extended to higher temperatures in the austenite region.

At 950°C, although the ductility was almost completely recovered from the trough which extended from 800 to 900 °C, dynamic recrystallization was not clearly detected from the flow curve (Fig. 4.12). However, a refined prior austenite grain size was present in the sample quenched immediately after fracture, indicating that recrystallization had taken place at this temperature. At 900 °C, where the ductility is sharply decreased to 20%, the fracture mode is intergranular (Fig.4.13), the cracks propagating along the austenite grain boundaries. No grain boundary ferrite was observed. In the TEM replica analysis, two types of precipitates were observed, one coarser than the other. These were round particles typically about 160 nm in diameter which were identified as MnS (Fig. 4.14(a)), and AlN cubic/triangular particles, having an approximate size of 60 nm (Figs. 4.14(a) and 4.14(b)).

At 850 °C, where the R of A decreases to 12%, a non-homogeneous grain size is seen (Fig. 4.15), with long cracks found mainly around the coarse grains. A layer of ferrite, about 10 μm thick was observed at the austenite grain boundaries. MnS particles were also found in these boundaries.

The minimum ductility (R of A ≈ 10%) for the High Al steel occurs at 800 °C. The corresponding microstructure is similar to that at 850 °C (Fig. 4.15), but with a somewhat thicker ferrite film (approximately 30 μm) delineating the austenite grain boundaries.

At 750 and 700 °C, the ductility and microstructures are similar to those shown by the Low Al steel, i.e., the R of A is regained to approximately 90 %, corresponding to large ferrite volume fractions.

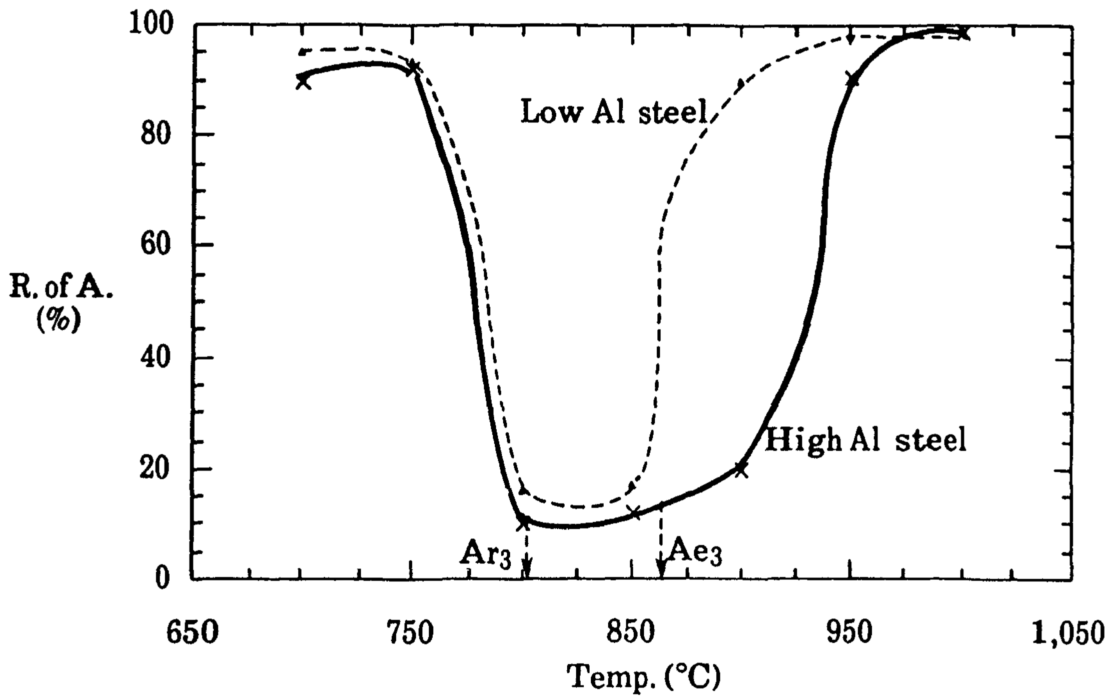

Fig. 4.11 - Influence of increasing Al on hot ductility (reference cycle).

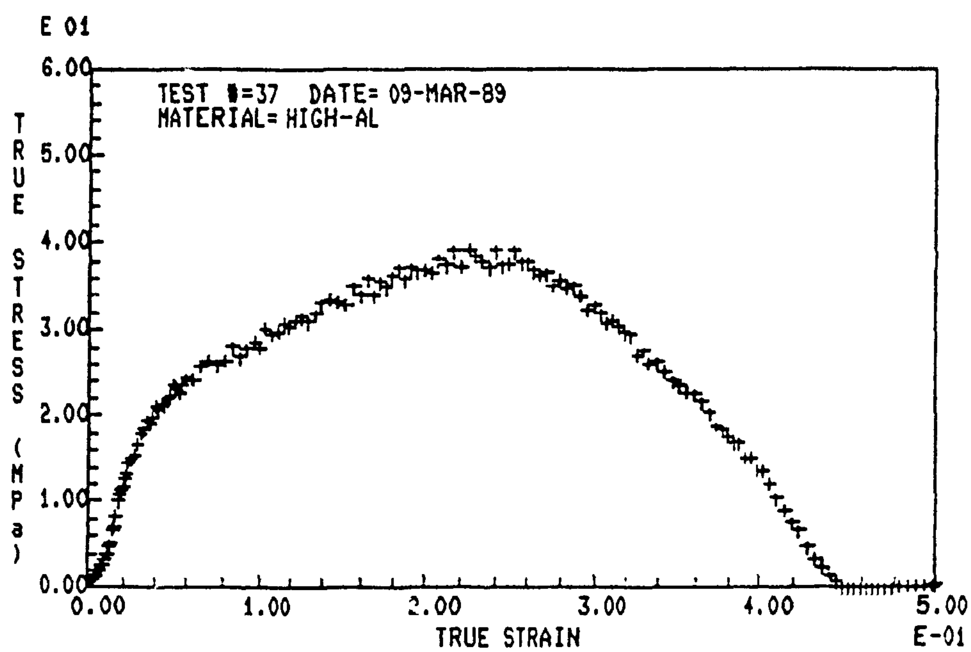

Fig. 4.12 - Flow curve for the High Al steel tested at 950 °C (reference cycle).

Fig. 4.13 - Microstructure of High Al steel, tested at 900°C using the reference cycle, showing wedge cracks at the austenite grain boundaries (picric etch).

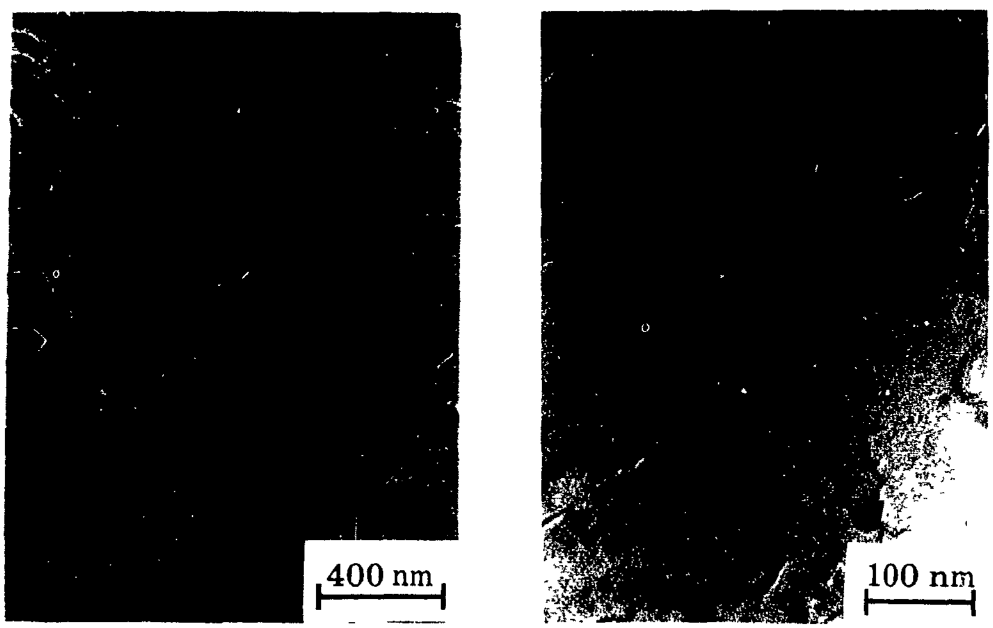

(a) (b)

Fig. 4.14 - TEM replica examination of High Al steel, tested at 900°C using the reference cycle: (a) MnS (round) and AlN (triangular); (b) AlN (cubic).

4.3.2.3 - Titanium treated steel

As mentioned previously, the difference between the Low Al and Ti treated steels used in this research is that, in the latter, the Al content is higher (similar to the High Al grade) and there is also an addition of 0.037% titanium. In order to examine the combined effect of these two alloying additions, the ductility curves for these two grades are compared in Fig 4.16. In the Ti steel, the ductility trough is more shallow, narrower and shifted to a higher temperature.

The microstructure at 900 °C, corresponding to a very high ductility ($\simeq$100% R of A), is shown in Fig. 4.17. Etching with picric acid reveals cracks scattered in the austenitic structure and aligned in direction of the test. The structure is completely recrystallized and the cracks are transgranular. All these observations are characteristic of ductile behavior.

At 850 °C (and down to 750°C), the ductility level was found to be around 92%, and the ferrite volume fraction was above 60 %, as can be inferred from Fig 4.18. An additional test was therefore introduced at 880 °C, in order to generate a thin layer of ferrite at the austenite grain boundaries. At this temperature, which is higher than the Ae_3 listed in Table 4.2, the ductility is decreased to 37%, and a fine ferrite film delineates the austenite grain boundaries, where several cracks can be observed (Fig. 4.19). The ferrite thickness is estimated to be 4 µm and the unrecrystallized austenite grain size is much finer (and elongated towards the test direction) when compared with the non-recrystallized structure for the other steels used in this work ($\simeq$450 µm).

4.3.2.4 - High manganese steel

The hot ductility results for the Low Al and High Mn steels are compared in Fig. 4.20. These grades differ essentially in the Mn level, which is increased from .39 to 1.39%, respectively (see Table 3.1). As shown in Table 4.2, and indicated in the respective ductility curves, increasing Mn drops the austenite-to-ferrite transformation temperature (Ar_3) by approximately 50°C, shifting the ductility trough in the same direction by the same amount. Note also that the trough of the

Fig. 4.15 - Microstructure of High Al steel tested at 850 °C using the reference cycle, showing non-homogeneous grain structure and crack propagating mainly around the coarse grain (3% nital etch).

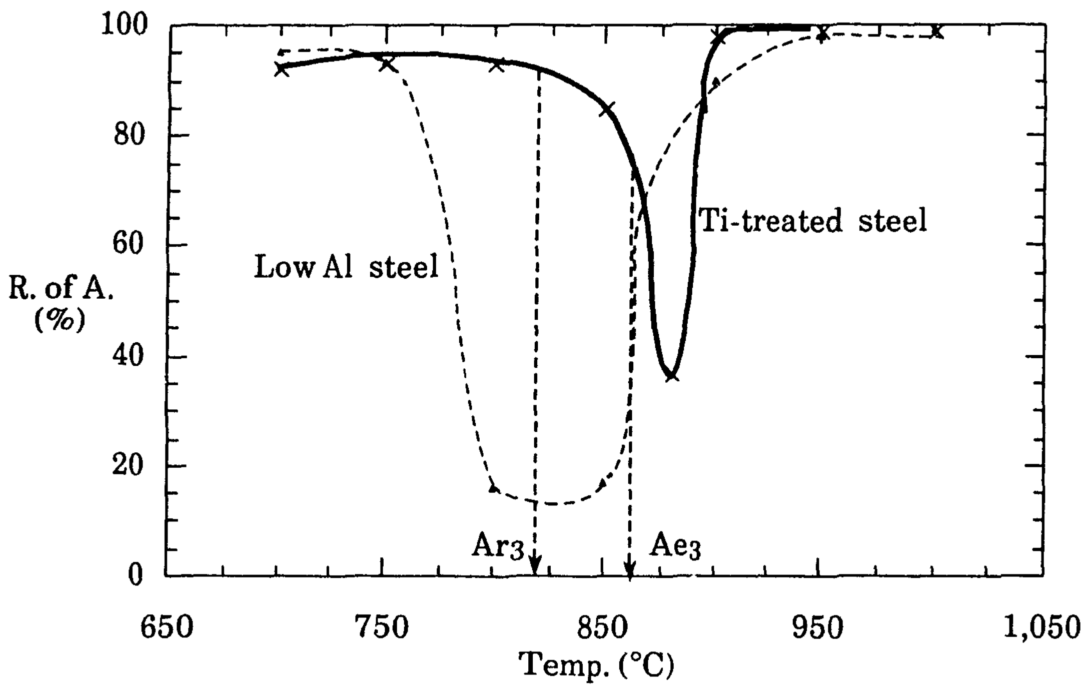

Fig. 4.16 - Influence of increasing Al together with Ti addition on hot ductility (reference cycle).

Fig. 4.17 - Microstructure of Ti treated steel at 900°C using the reference cycle, showing transgranular cracks scattered in the recrystallized austenite grains (picric etch).

Fig. 4.18 - Microstructure of Ti treated steel at 850°C using the reference cycle, showing a large volume fraction of ferrite (3% nital etch).

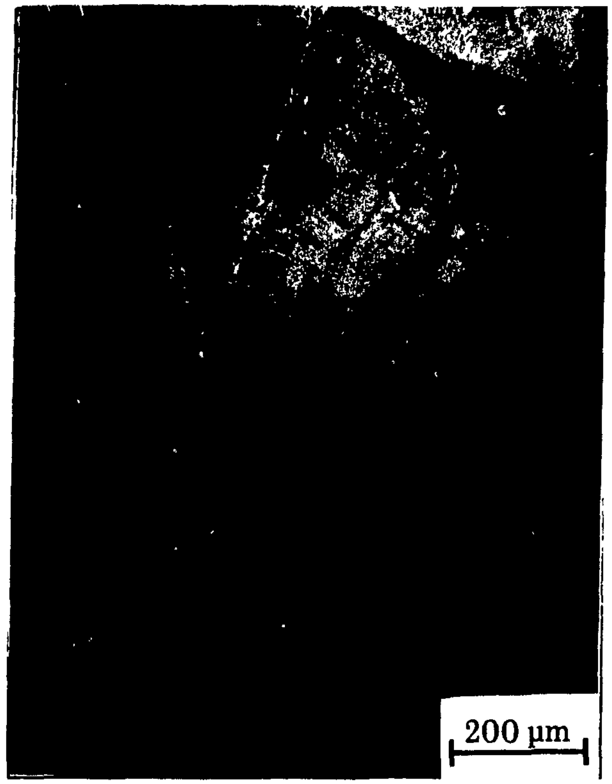

Fig. 4.19 - Microstructure of Ti steel tested at 880°C using the reference cycle, showing intergranular fracture propagating through the grain boundary ferrite film (3% nital etch).

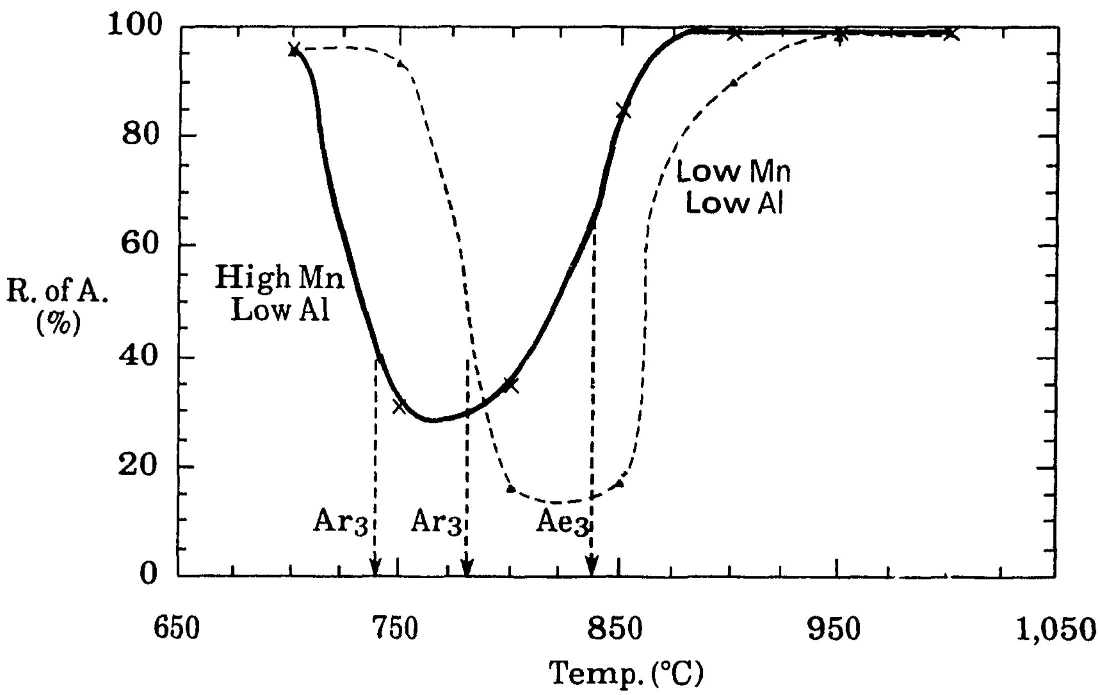

Fig. 4.20 - Influence of increasing Mn on the hot ductility (reference cycle).

High Mn steel is significantly shallower than that of the low Mn containing grade (Low Al steel).

For the High Mn steel at 850°C the R of A value is 85%. No indication of dynamic recrystallization can be inferred from the flow curve, but the microstructure (Fig. 4.21) exhibits signs of recrystallization via a grain refinement. This was not expected at such a low test temperature. Further decrease in the test temperature to 800°C resulted in the intergranular failure and a ductility of 35%. At high magnification, a very thin (<5 µm) and discontinuous ferrite film is observed at the austenite grain boundaries (Fig. 4.22). Metallographic examination of the samples corresponding to the trough in the High Mn curve, revealed very few MnS particles in the ferrite film. The lowest ductility is observed at 750°C, i.e, R of A=31%. Finally, at 700°C, the high ductility at this temperature was accompanied by a microstructure consisting of about 66% ferrite.

4.3.3 - Influence of thermal cycling

As mentioned previously, the process variables that can influence the hot ductility of a continuously cast slab during unbending are represented in the hot tensile test by the test temperature and strain rate. Since the slab thickness is constant and the casting speed does not change significantly during the operation, the strain rate at the straightening stage cannot vary much for a given continuous casting machine curvature (See Section 2.1.4). As seen in Chapter II, to observe any influence of the strain rate on hot ductility, a variation of about an order of magnitude is needed. Therefore, the main variable operating during unbending is the resultant temperature profile in the secondary cooling zone of the machine. As shown above, hot ductility is extremely sensitive to test temperature. Moreover, thermal cycling in the strand occurs in practice, and this has been shown to influence ductility via the precipitation and transformation processes. Thus, the influence of the thermal cycles described in Section 3.4.1 on the hot ductility of the Low Al and High Al steels are presented below.

4.3.3.1 - Low aluminum steel

The ductility curves for the Low Al steel, submitted to the various thermal cycles used in this work, are presented in Fig. 4.23. In Figs. 4.23(a) and 4.23(b), the

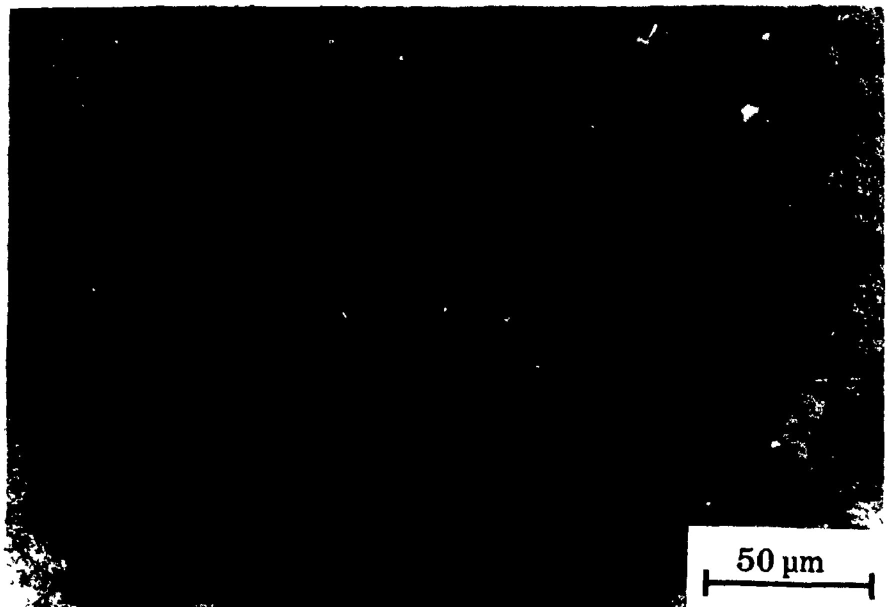

Fig. 4.21 - Microstructure of High Mn steel tested at 850°C using the reference cycle, showing recrystallized austenite grains (picric etch).

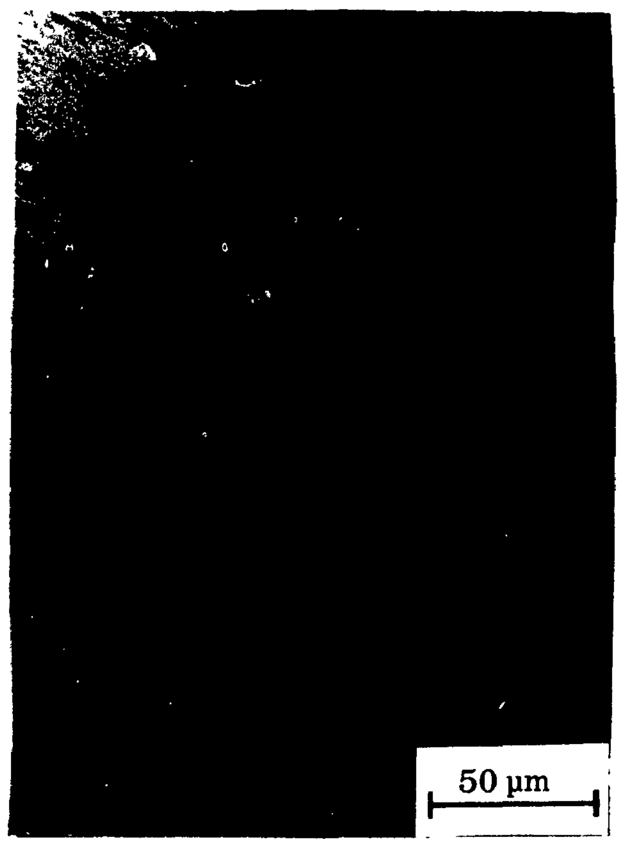

Fig. 4.22 - Microstructure of High Mn steel tested at 800°C using the reference cycle, showing intergranular cracks and a discontinuous ferrite film at the austenite grain boundaries (3% nital etch).

results for the one-step cycling are presented, with holding time at the undercooling temperature of 1 and 5 minutes, respectively. In Fig. 4.23(c) the ductility curve for the two-step cycling is displayed. The results represented in Fig. 4.23(d) correspond to a thermal cycle which is similar to the reference cycle, but with 1 hour holding at the test temperature, before deformation. In all four cases, the effects of these cycles are discussed with respect to the reference curve, which is included in all the diagrams for comparison.

The one step-1 min holding cycle (Fig. 4.23(a)) narrows the trough and shifts it to higher temperatures. The trough occurs at 850°C, with a R of A value of 14%, and the ductility recovers to 77% at 800°C. Incidentally, the micrograph at 950°C, corresponding to a ductility close to 100%, clearly illustrates the concept of voids formed at the initial austenite grain boundaries (Fig. 4.24) being isolated inside the newly recrystallized grains, and therefore being prevented from coalescing.

The one step-5 min holding cycle (Fig. 4.23(b)) shifts the trough to temperatures above the calculated Ae_3 but does not change the width. The ductility thus starts to drop at 950°C. The metallography at 900°C, corresponding to the bottom of the trough, reveals a coarse non recrystallized structure and void formation at the boundaries (Fig. 4.25). It is interesting to note that, in this micrograph, it appears that one of the boundaries (arrowed) was starting to migrate at the time of fracture. The results obtained from the TEM replica examination are given in Fig. 4.26, which show two typical sizes of precipitates, measuring on average 70 and 300 nm. Based on their morphologies, these particles appear to be AlN (rod shaped) and MnS (spherical), respectively. At 850°C the ductility improves to 55%, corresponding to a ferrite volume percentage of 40% , and is almost completely recovered below this temperature.

Comparing the reference and the two-step cycling curves (Fig. 4.23(c)), a widening of the trough to about 900°C is observed in the latter. The microstructure corresponding to this temperature, presented in Fig 4.27, indicates a partially recrystallized austenite grain structure. However, dynamic recrystallization cannot be detected from the flow curve. In Fig. 4.28, examination of replicas by TEM reveals some round precipitates with an average diameter of 40 nm, which because of their small size are likely to be AlN. At 850°C,the low ductility of 29% is associated with intergranular fracture. The amount of grain boundary ferrite is reduced ($\simeq$5μm thick film), compared to the microstructures of the specimens tested at this temperature using the other thermal cycles (micrograph not shown). The

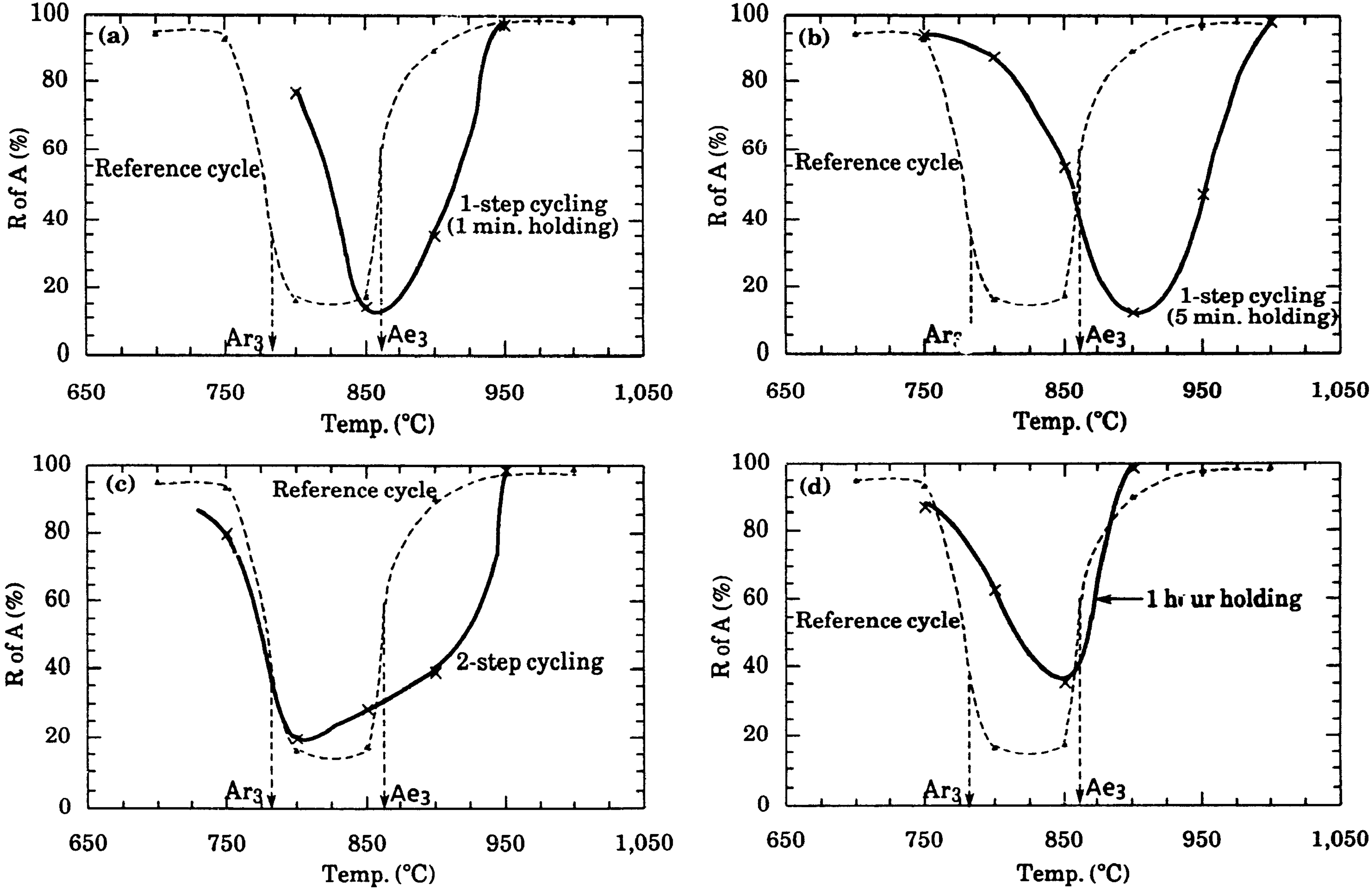

Fig. 4.23 - Influence of thermal cycle on hot ductility of the Low Al steel.
(a) one-step cycling (1 min. holding); (b) one-step cycling (5 min. holding);
(c) two-step cycling; (d)1 hour holding before deformation.

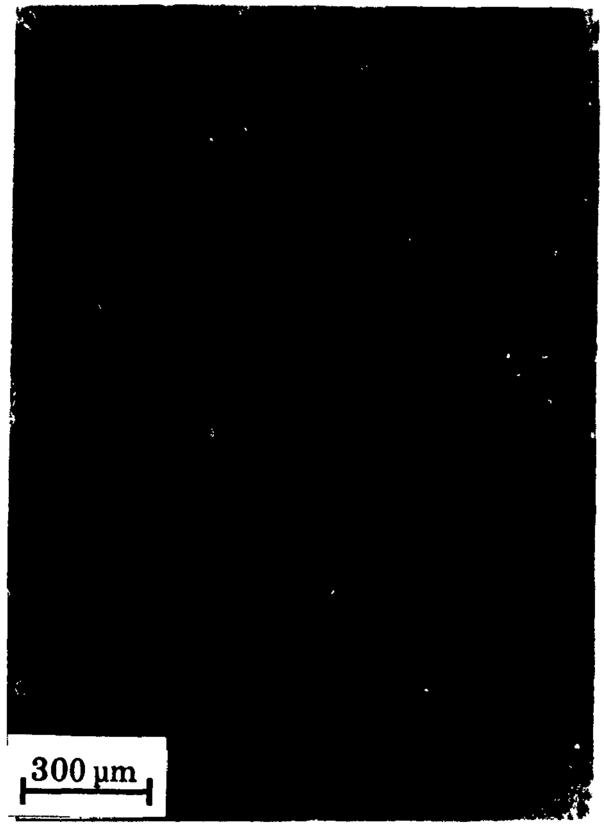

Fig. 4.24 - Microstructure of Low Al steel tested at 950°C (one-step cycling - 1 min. holding), showing voids isolated within recrystallized grains (picric etch)

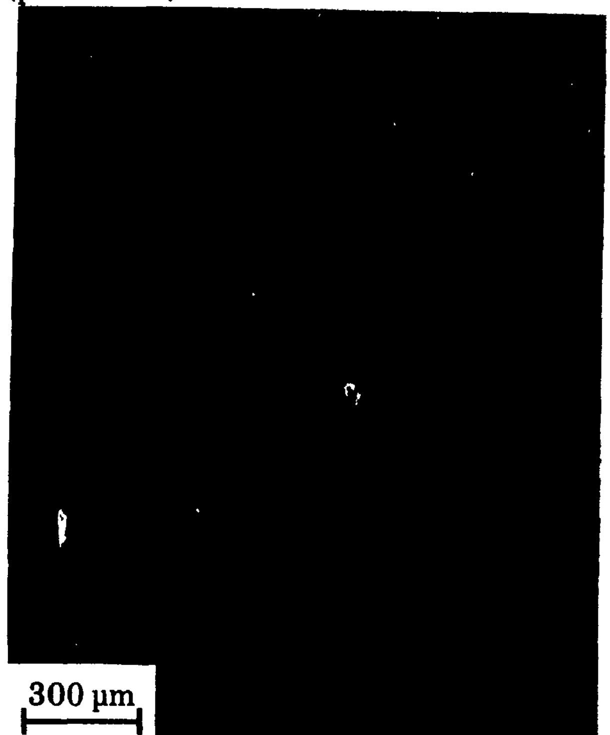

Fig. 4.25 - Microstructure of Low Al steel tested at 900°C (one-step cycling - 5 min. holding), showing indication of grain boundary migration at the time of fracture (picric etch).

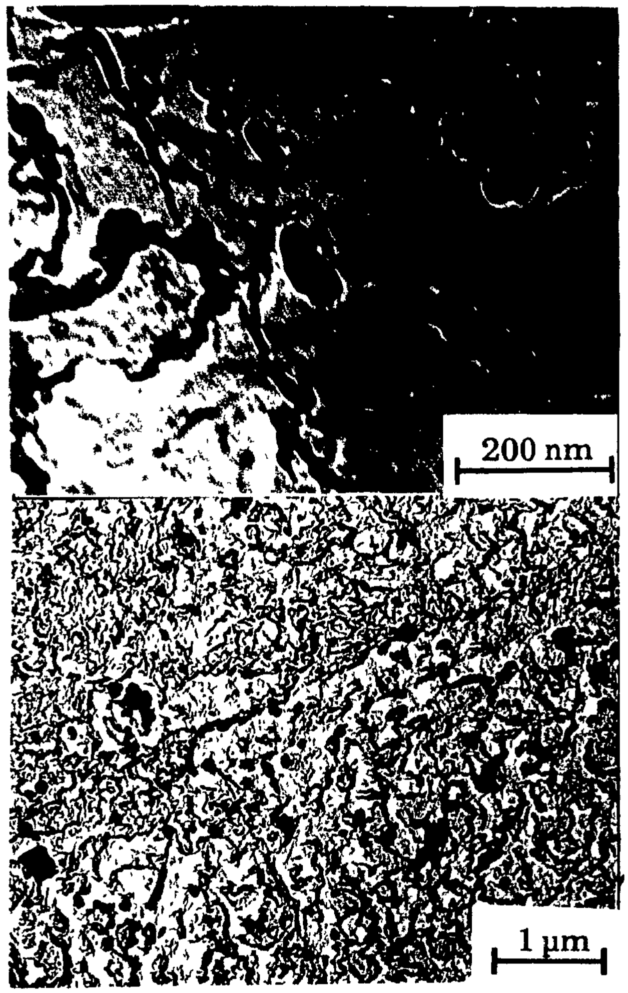

Fig. 4.26 - TEM replica analysis of Low Al steel tested at 900°C (one step cycling - 5 min holding), showing precipitates, some of which (rod shaped) appear to be AlN.

Fig. 4.27 - Microstructure of Low Al steel tested at 900°C (two-step cycling), showing partial recrystallization (picric etch)

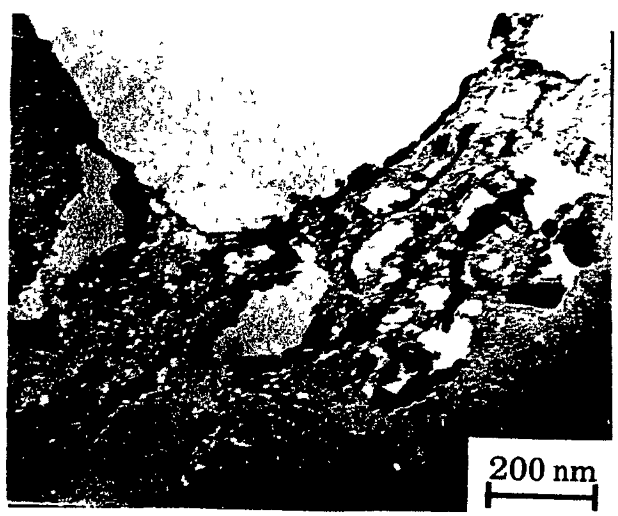

Fig. 4.28 - TEM replica analysis of Low Al steel tested at 900°C (two-step cycling), showing small precipitates (probably AlN).

microstructure at 800°C (where the lowest ductility occurs in this curve, i.e., R of A $\simeq$ 20%) is displayed in Fig. 4.29, and reveals a 20 μm ferrite layer and extensive void formation on the austenite grain boundaries. At the slightly lower temperature of 750°C the proportion of ferrite is markedly increased (over 80%), and this leads to an essentially recovered ductility.

A variant of the two-step cycling was performed at 800°C. This consisted of a multicycle thermal oscillation starting at 1100°C, with an amplitude of 100°C about the mean cooling rate of 1°C/s, and a period of 90s (resulting in four oscillations). The resultant ductility was 16%, which is quite similar to the R of A obtained for the reference cycle and two-step cycling conditions at 800°C. The corresponding microstructure (Fig. 4.30) shows extensive void formation and coalescence in the 20μm ferrite thickness formed at the austenite grain boundaries. The results of the SEM examination of this sample are given in Fig. 4.31. It can be seen that the voids are formed around particles (Fig. 4.31(a), and these were identified as MnS from the energy dispersive spectrum (Fig. 4.31(b)).

It is shown in Fig. 4.23(d) that, in the reference cycle, increasing the holding time from 5 minutes to 1 hour before testing results in a narrower and shallower trough. At 900°C, the austenitic structure is completely recrystallized and the ductility is high. On the other side of the trough, at 800°C, where ductility is again high, an increased ferrite volume percentage compared to the reference cycle sample, was observed.

4.3.3.2 - High aluminum steel

The one-step cycle with one minute holding at the undercooling treatment narrows the trough and shifts it completely to the austenite domain (Fig. 4.32(a)). The microstructure at 900°C, corresponding to the bottom of the trough in this curve (R of A = 15%) is illustrated in Fig. 4.33. Some ferrite has nucleated at the austenite grain boundaries, but the film is discontinuous. A further decrease in the test temperature to 850°C results in a ferrite volume percentage of 44%, and a partially recovered ductility of 58%.

Increasing the holding time at the undercooling temperature of the one step cycle from 1 to 5 minutes does not change the profile of the ductility curve, as can be observed in Figs. 4.32(a) and 4.32(b), respectively. The microstructure is also similar at all temperatures, except for a small increase in the ferrite volume percentage for

Fig. 4.29 - Microstructure of Low Al steel tested at 800°C (two-step cycling), showing extensive void formation within the grain boundary ferrite film (3% nital etch).

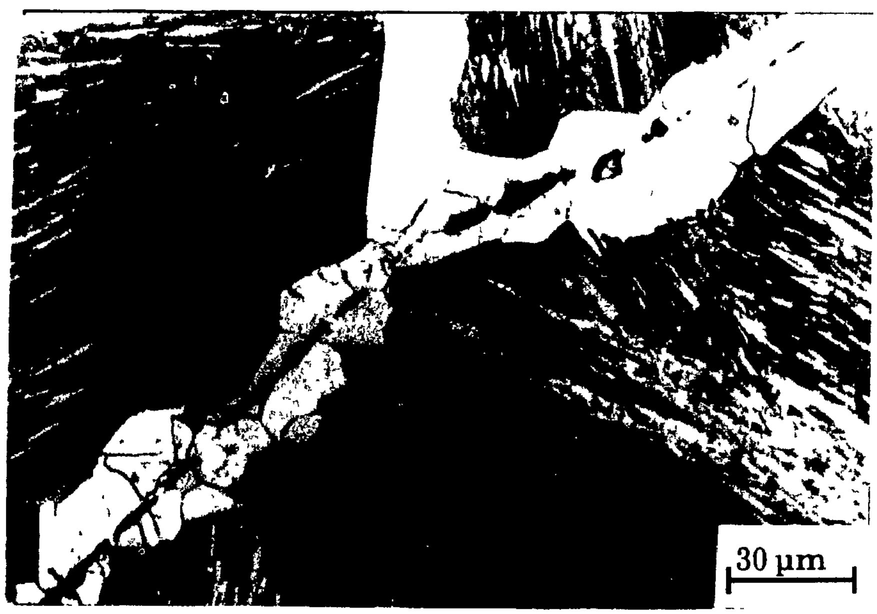

Fig. 4.30 - Microstructure of Low Al steel tested at 800°C (multi-step cycling), showing void coalescence within the grain boundary ferrite film (3% nital etch).

(a)

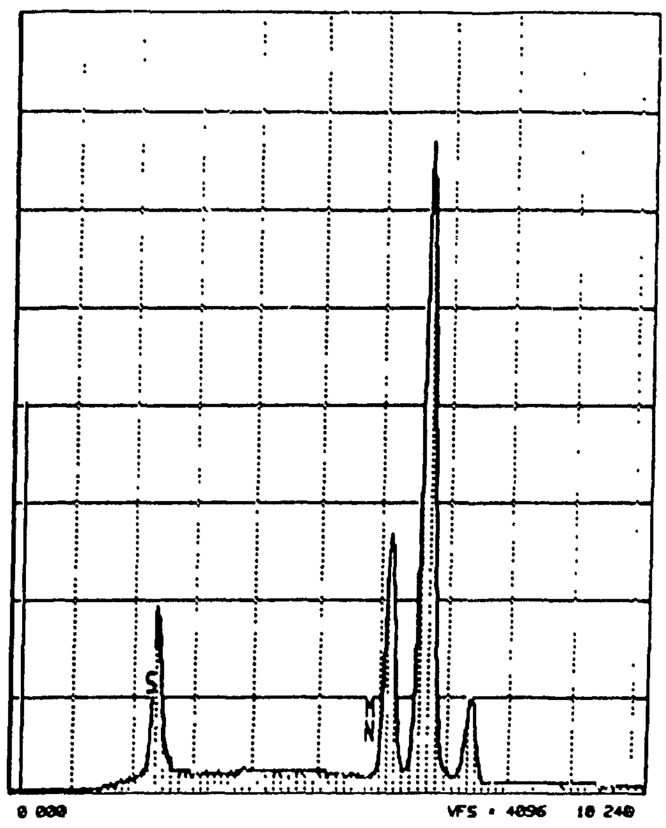

(b)

Fig. 4.31 - SEM analysis of Low Al steel tested at 800°C (multi-step cycling): (a) MnS particles aligned in the austenite grain boundary film; (b) energy dispersive spectrum of the particles shown in (a).

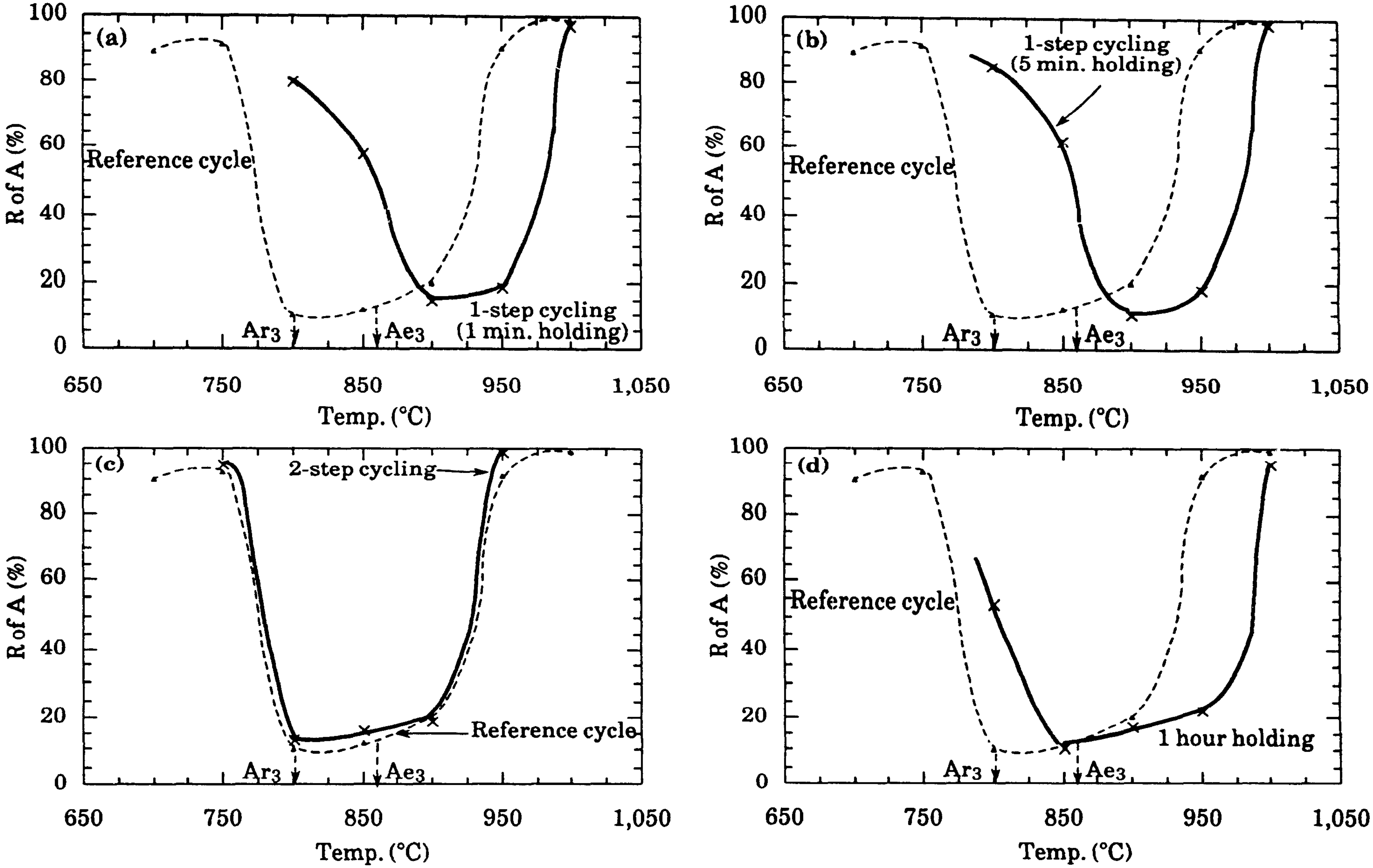

Fig. 4.32 - Influence of thermal cycle on hot ductility of the High Al steel.
(a) one-step cycling (1 min. holding); (b) one-step cycling (5 min. holding);
(c) two-step cycling; (d)1 hour holding before deformation.

the increased holding time variant. For example, in the 850°C test, the percentage of ferrite increases from 44 to 48% for 1 and 5 minutes holding at 750°C. The same behavior is found at the 800°C test temperature, where increasing the holding time increases the ferrite from 60 to 67%, leading to ductilities of 80 and 85%, respectively.

The reference and two-step cycling curves are practically coincident (Fig. 4.32(c)), but some microstructural differences are apparent. The following results refer to the two-step cycling. The ductility approaches 100% at 950°C and the microstructure is completely recrystallized close to the fracture surface. There is a weak indication of a peak stress in the flow curve (Fig. 4.34). Decreasing the test temperature to 900°C results in intergranular fracture and R of A value of 19%, which is basically the same as for the reference curve. At the slightly lower temperature of 850°C, the ductility decreases to 16% and at 800°C it has its lowest value (13%). The microstructures of the 800°C tests corresponding to the reference and two-step cycles are compared in Figs. 4.35 and 4.36, respectively. Both micrographs show intergranular cracks and a similar ferrite thickness of about 30 µm delineating the austenite grain boundaries. However, more sites for void nucleation can be observed in the case of the cycled test. In order to illustrate the void linkage process, higher magnification micrographs of the two step cycled specimen fractured at 800°C (Fig. 4.37) are presented. At 750°C the phase transformation is practically complete in the High Al steel as a result of undercooling down to 650°C during the cycling, and this leads to an R of A value of 95%.

In the reference cycle, increasing the holding time before the test from 5 min. to 1 hour, shifts the ductility trough about 50°C towards higher temperatures, as can be observed in Fig. 4.32(d). At 1000°C the ductility is very high and recrystallization has occurred during the test. Decreasing the test temperature to 950°C results in an R of A value of 22% and intergranular failure. The ductility still decreases to 17% at 900°C, similar to the 5 minutes hold variant, and grain boundary cracks are again observed. In Figs. 4.38(a), round and plate-like precipitates measuring approximately 200 nm are observed in the specimen tested at 900°C. The energy dispersive spectrum given in Fig. 4.38(b) indicates the presence of Al, Mn and S in the same precipitate. This probably suggest the concurrent precipitation of MnS and AlN (nitrogen cannot be detected by EDS). At 850°C the ductility is at a minimum (11%) for this curve and the corresponding microstructure reveals a 20 µm thick film of grain boundary ferrite. The ductility is regained to 54% at 800°C when large amounts of ferrite are again present.

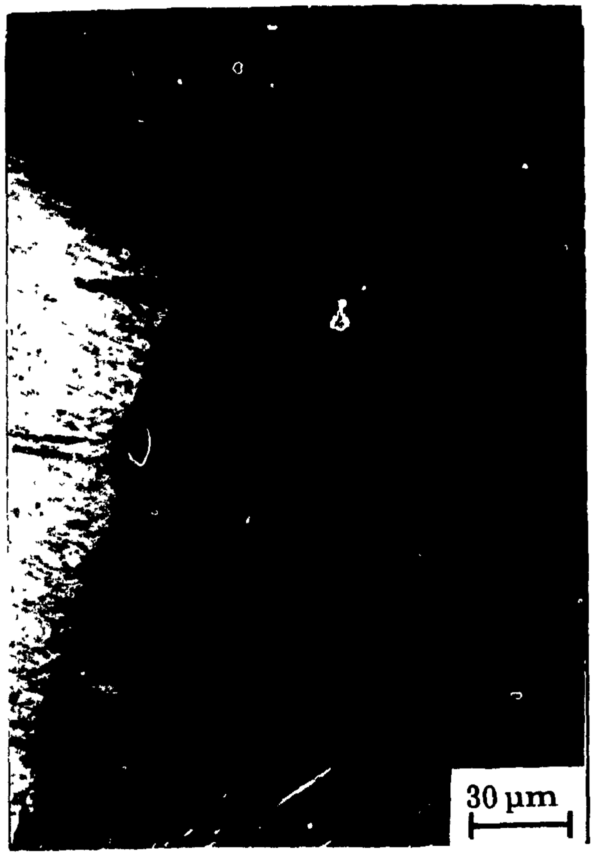

Fig. 4.33 - Microstructure of High Al steel tested at 900°C (one-step cycling - 1 min. holding), showing intergranular cracks associated with a discontinuous ferrite film at the austenite grain boundaries (picric etch).

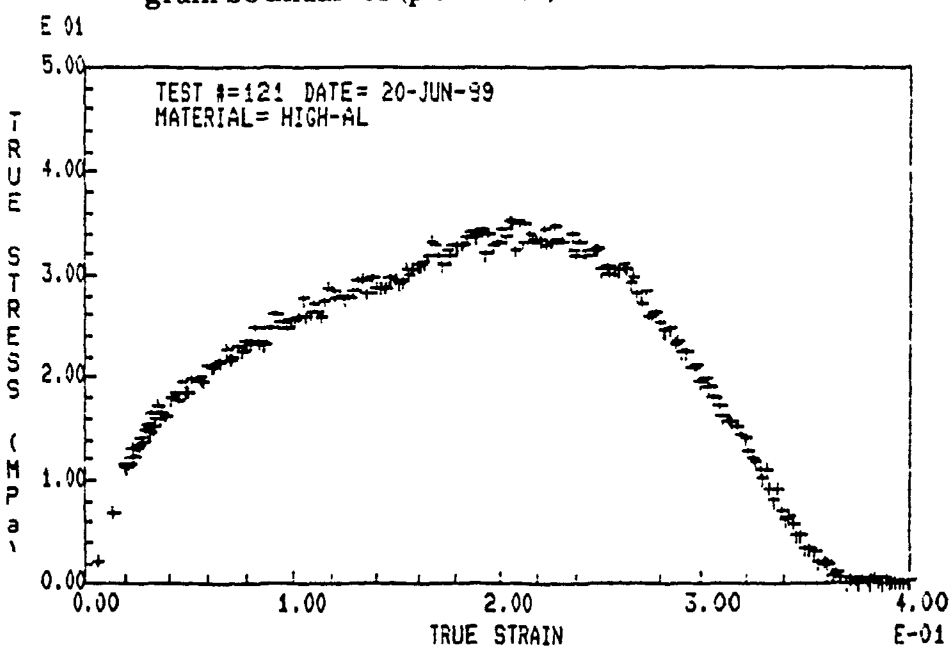

Fig. 4.34 - Flow curve of High Al steel tested at 950°C (two-step cycling).

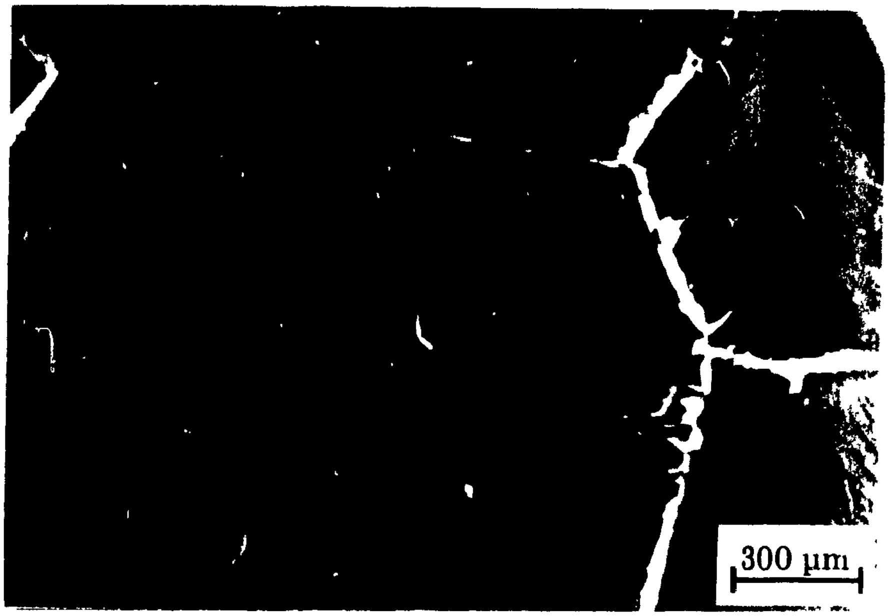

Fig. 4.35 - Microstructure of High Al steel tested at 800°C (reference cycle), showing intergranular fracture associated with the thin grain boundary ferrite film (3% nital etch).

Fig. 4.36 - Microstructure of High Al steel tested at 800°C (two-step cycling), showing extensive void formation and linkage at the grain boundary ferrite film (3% nital etch).

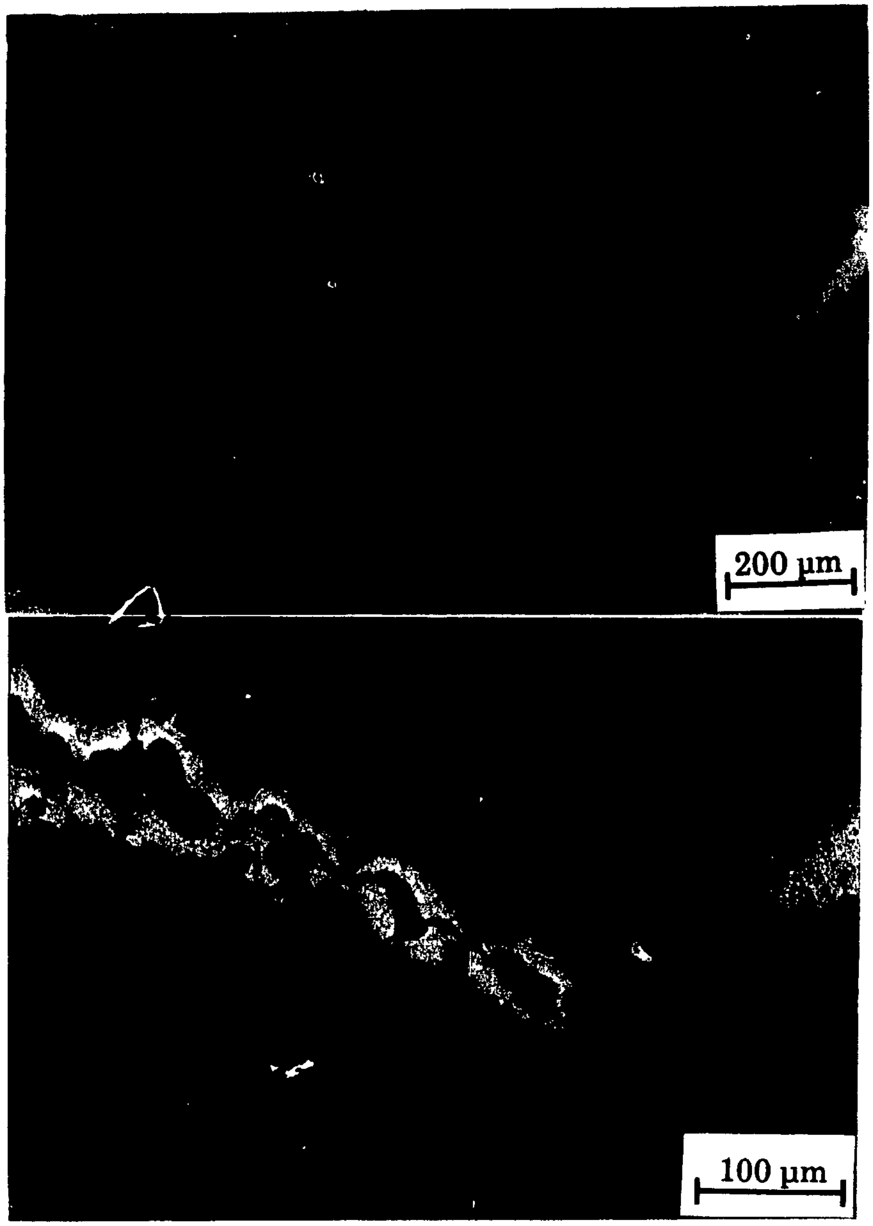

Fig. 4.37 - Same as Fig. 4.36 at higher magnification, illustrating void linkage.

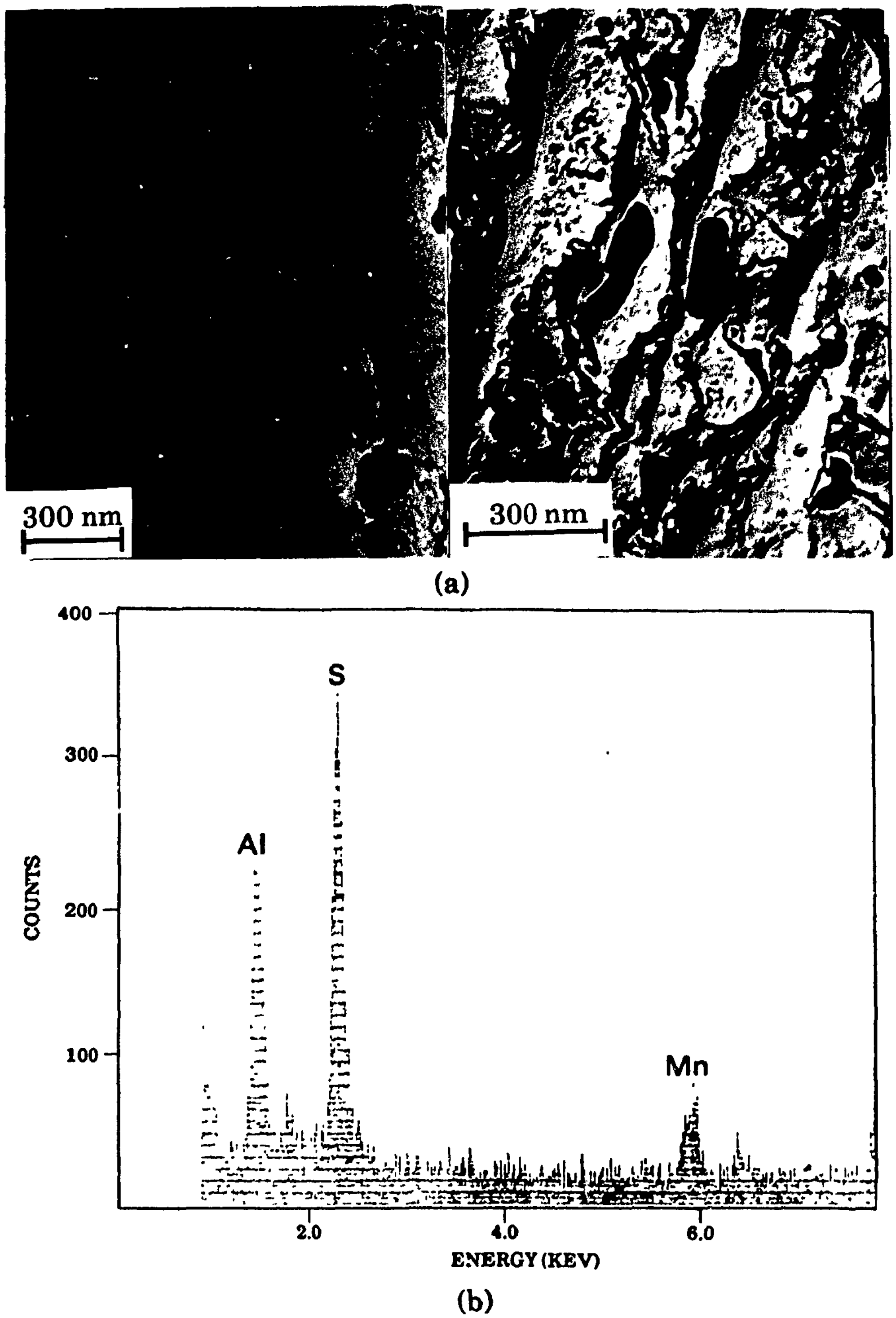

Fig. 4.38 - (a) TEM replica analysis of High Al steel tested at 900°C (1 hour holding before test), showing round and plate-like precipitates; (b) energy dispersive spectrum of particles shown in (a).

4.4 - FRACTOGRAPHY

The ductility behavior of the steels used in this investigation (and under the thermomechanical conditions presented in section 3.4) is directly reflected in the appearance of the fracture surface. The variation of fracture characteristics with ductility was found to be similar for all the steels investigated. Thus, in this section, only the fracture surfaces of the High Al steel specimens (submitted to the reference thermal cycle, unless otherwise stated) are described in detail, to avoid repetition. Fractographs of other grades are presented only when the fracture behavior differs from that of the High Al grade, or to emphasize a particular behavior.

The fracture surface at 950°C, shown in Fig. 4.39, is characteristic of the high temperature ductile rupture mode. Here, large voids (20~40 μm) can be observed, which appeared not to be associated with second-phase particles. This type of fracture, which has been reported by Crowther and Mintz [65] and observed by Wray [93] in γ-iron, is always associated with an R of A > 80%. The large voids are assumed to have developed from initially intergranular cracks which formed at an early stage of deformation [65]. As deformation proceeds, the original boundary crack is distorted into an elongated void, until final failure occurs by necking between the voids. However, after holding for one hour at 950°C before straining, intergranular fracture takes place, with a flat fracture facet of approximately 400μm (Fig. 4.40).

For the specimen tested at 900°C, corresponding to a drop in ductility in the reference cycle, intergranular fracture is observed (Fig. 4.41), with facet size of the order of 400 μm. The facet surfaces are predominantly flat and some dimples are observed at high magnifications at triple points. The dimples have probably formed around the particles observed in replica examination (Figs. 4.14(a) and 4.14(b). However, these particles (200nm) were too small to be detected. For this reason, the AlN particles, which are even smaller, were not observed in any sample examined at the SEM. The Low Al steel, tested at 900°C using the one-step cycling with 5 minutes holding at the undercooling treatment (R of A=12%), again resulted in a predominantly flat type fracture (Fig. 4.42), typical of grain boundary sliding [66]. The offset observed between the grains in Fig. 4.42 is probably an indication of grain boundary sliding.

Fig. 4.39 - Fracture surface of High Al steel tested at 950°C using the reference cycle (R of A = 91%), showing high temperature ductile rupture mode.

Fig. 4.40 - Same as 4.39, but with 1 hour holding before test (R of A = 22%), showing intergranular fracture and flat grain facets.

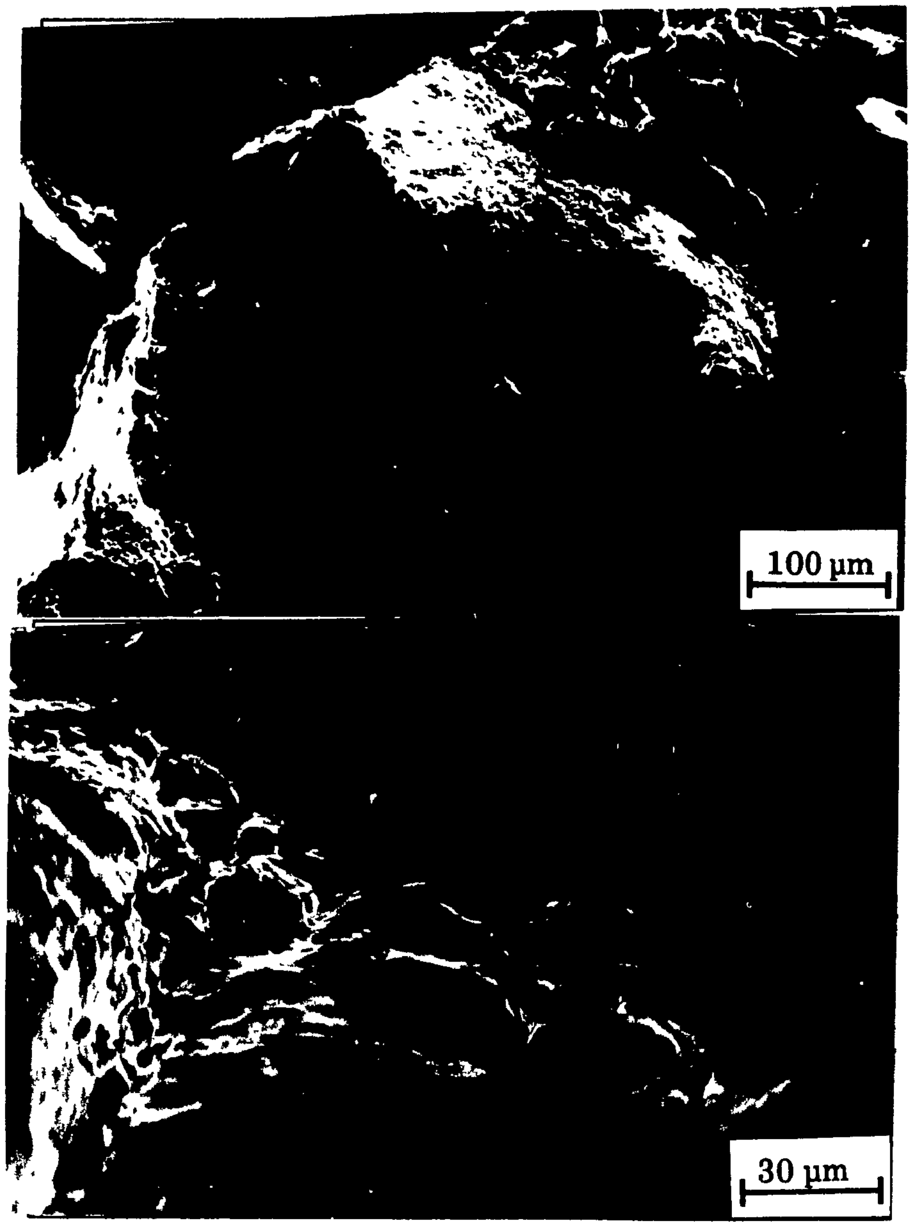

Fig. 4.41 - Fracture surface of High Al steel at different magnifications, tested at 900°C using the reference cycle (R of A = 20%), showing grain facets which are predominantly flat, and dimples at triple points.

Fig. 4.42 - Fracture surface of Low Al steel tested at 900°C using the one-step cycling - 5 min. holding (R of A = 12%), showing indication of grain boundary sliding in the single phase austenite.

Fig. 4.43 - Fracture surface of Ti treated steel tested at 880°C using the reference cycle (R of A = 37%), showing mixed intergranular fracture and ductile dimpled areas.

The fractography of the Ti treated steel tested at 880°C using the reference cycle, corresponding to the bottom of the ductility trough, shows mixed intergranular fracture and ductile dimpled areas (Fig. 4.43). The grain facets that are clearly visible measured on average 150 μm.

At 850°C, slightly below the Ae_3 temperature for the High Al steel, the fracture is again intergranular (R of A=12%). Ductile dimples were observed on some of the facets, but the majority were again largely flat and featureless (Fig. 4.44). An offset between the austenite grains is again observed.

Decreasing the test temperature to 800°C (R of A=10%), results in a fracture surface which is macroscopically intergranular but microscopically dimpled with shallow voids (Fig. 4.45). Such a fracture has been described as "intergranular ductile fracture" [13]. This is the apparent result of dimples forming in the thin ferrite film nucleated at the austenite grain boundaries [66]. The specimens submitted to the two-step cycling treatment (R of A = 13%) show similar features, where the facet surfaces are covered with ductile dimples (Fig. 4.46). However, the dimples are much more numerous when compared with the specimens tested using the reference cycle (Fig. 4.45). Spheroidal or elongated particles, measuring from 1 to 3 μm, were present at the bottom of the majority of the dimples, as shown in Fig 4.46. Some of these particles were analyzed and identified as MnS. The Low Al steel specimens submitted to the reference (R of A = 16%) and two-step cycles (R of A = 20%) exhibited similar fractographs to those obtained for the High Al steel. For example, for both thermal treatments, intergranular fracture in which the facets are covered with dimples were observed when ferrite films were present. A higher magnification again indicates that there are far fewer dimples in the reference cycle tested specimen (Fig. 4.47), as compared to the two-step cycled one (Fig. 4.48). Still higher magnification in the latter case shows non-metallic particles, measuring 1 to 3 μm, inside the dimples, these again being analyzed as MnS . Although the same relative tendency of increasing dimples is observed when changing the thermal treatment (from the reference cycle to two step cycling) for both Low Al and High Al steel, the latter shows many more dimples (Fig. 4.46) as compared to the former Fig. 4.48), when the two-step cycling treatment was used.

Fig. 4.44 - Fracture surface of High Al steel at different magnifications, tested at 850°C using the reference cycle (R of A = 12%), showing indication of grain boundary sliding in the duplex austenite-ferrite region.

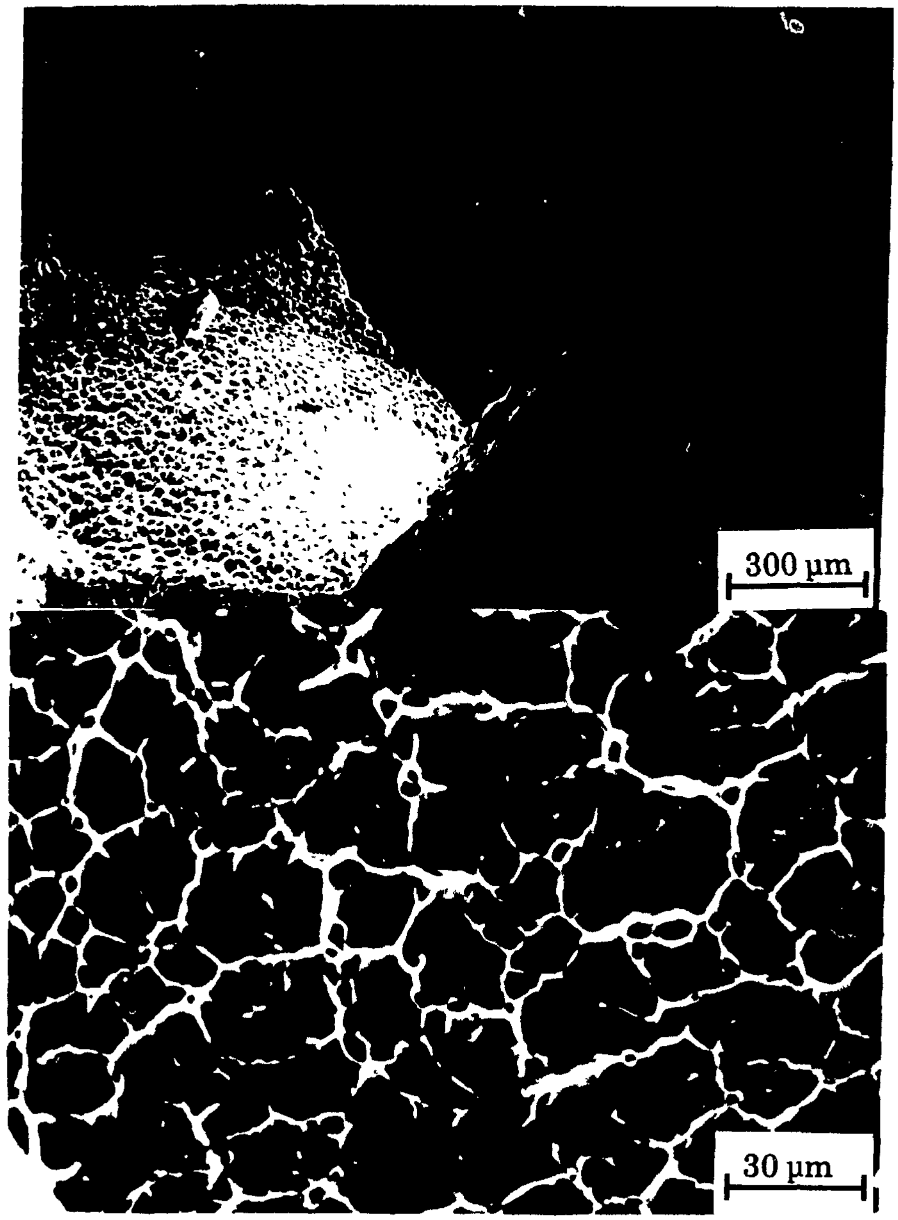

Fig. 4.45 - Fracture surface of High Al steel at different magnifications tested at 800°C using the reference cycle (R of A = 10%), showing intergranular ductile dimples.

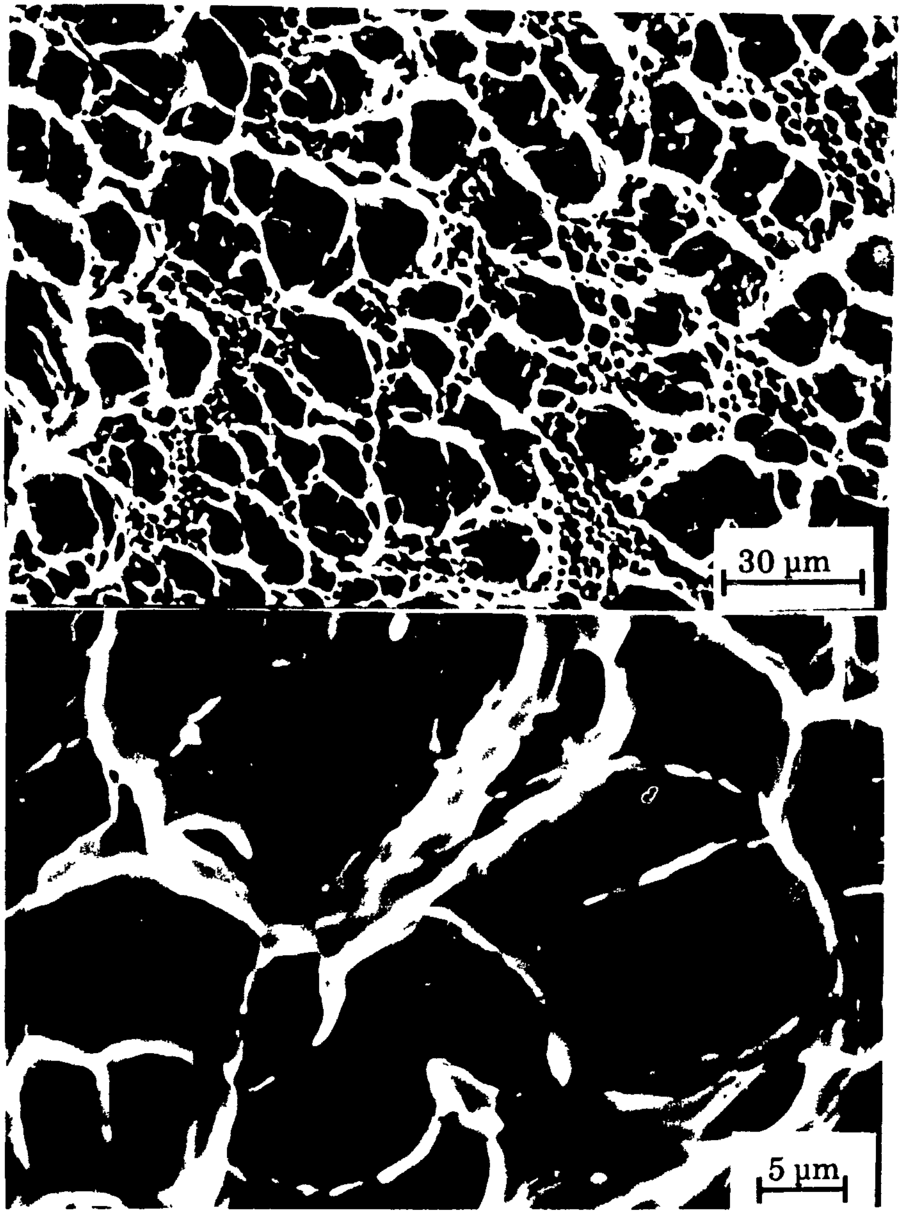

Fig. 4.46 - Fracture surface of High Al steel at different magnifications tested at 800°C using the two-step cycling (R of A = 13%), showing increased number o·' dimples associated with second phase particles.

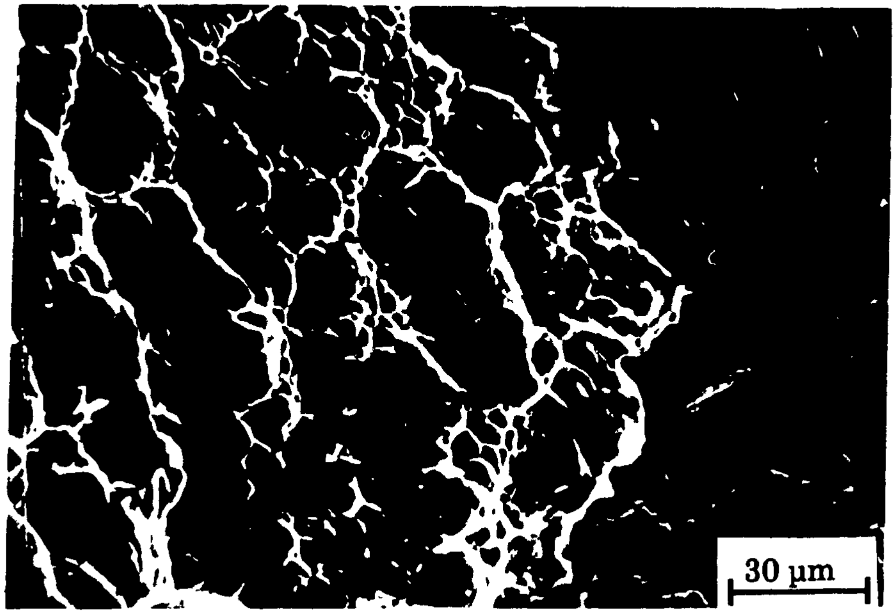

Fig. 4.47 - Fracture surface of Low Al steel tested at 800°C using the reference cycle (R of A = 16%), showing intergranular ductile fracture (few dimples).

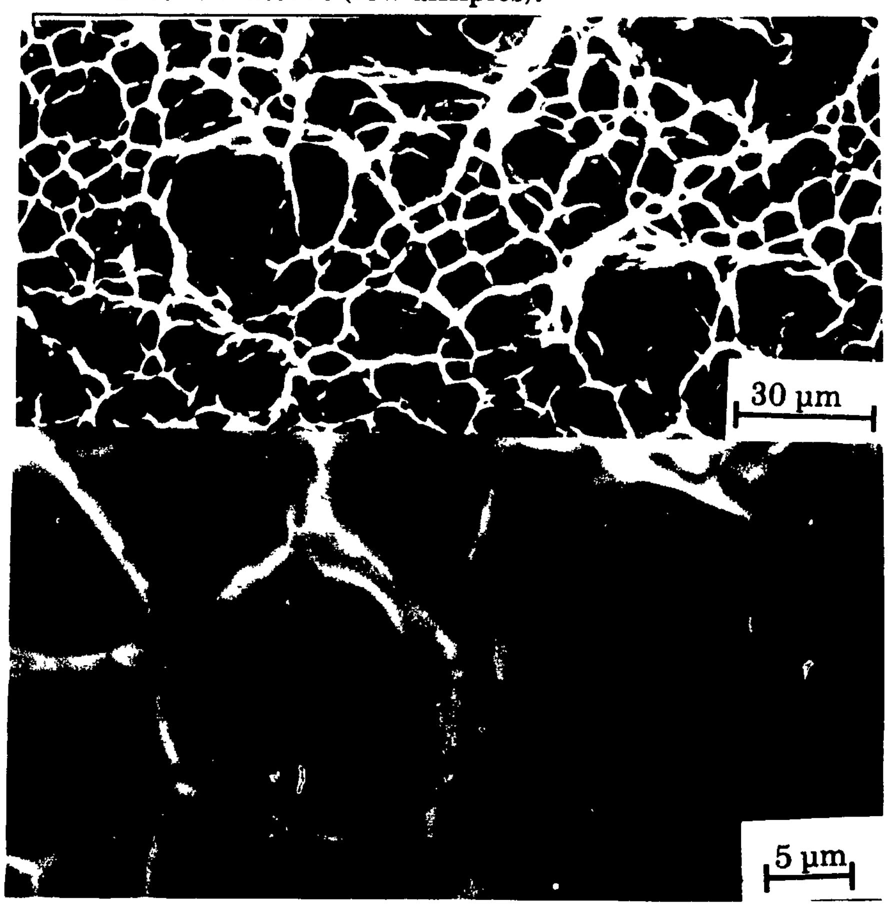

Fig. 4.48 - Fracture surface of Low Al steel tested at 800°C using the two-step cycling (R of A = 20%), showing increased number of dimples associated with second phase particles.

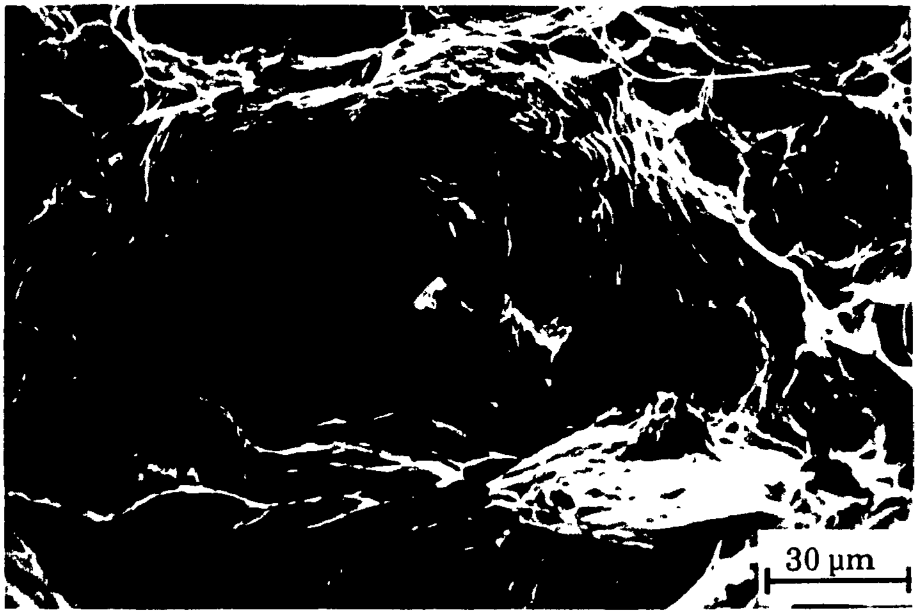

Fig. 4.49 - Fracture surface of High Al steel tested at 750°C using the reference cycle (R of A = 92%), showing ductile dimples associated with increased amount of ferrite.

At 750°C, corresponding to recovered ductility (92% for High Al steel), the fracture surface is essentially composed of ductile dimples, most of them with sizes varying between 5 to 10 μm (Fig. 4.49). It was also observed that the depth of the dimples increases the higher the volume percentage of grain boundary ferrite (at the low temperature end of the ductility trough), confirming the observations of Ouchi and Matsumoto [17].

CHAPTER 5

DISCUSSION

HOT DUCTILITY OF LOW CARBON STEELS IN THE TEMPERATURE RANGE 700-1000°C

5.1 - MECHANISMS OF EMBRITTLEMENT

As outlined in the literature survey, various mechanisms have been proposed to account for the loss in ductility in the low temperature austenite range and in the duplex austenite-ferrite region of C-Mn-Al steels [13,19,42], and these have been reviewed by Thomas et al. [20]. The embrittling mechanisms are summarized in the schematic diagram presented in Fig. 5.1, and have been found to apply in the material and test conditions used in this investigation.

The strain rate applied to the slabs during the straightening operation in continuous casting is at the upper strain rate limit of the creep range. Thus, in these embrittling mechanisms there is always a creep component via grain boundary sliding, which plays an important role in the intergranular failure condition, as described below, although this is not indicated in Fig. 5.1. The strain rate used in this work ($1x10^{-3}s^{-1}$) is adequate to produce both wedge shaped cracks and "r" type cavities, which are characteristic of grain boundary sliding, and both types have been observed in the present investigation. According to creep investigations [71,72] it is quite possible to have intergranular failure without the presence of particles at the boundaries, since wedge type cracks can form by grain boundary sliding alone. However, it is generally accepted [19,42,43] that the presence of precipitates will enhance grain boundary sliding.

<u>Intergranular failure in the austenite region</u>

At the reheating temperature of 1350°C that was used in this work, Al, Mn, S and N, can exist in solid solution in the C-Mn-Al steels. On cooling to the test temperature, these elements can precipitate out as AlN and MnS at the austenite grain boundaries, as represented in Fig. 5.1(a). If a tensile stress is applied to this microstructure, these particles will act as sources of stress concentration, producing small voids, which, at low strain rates, are extended by grain boundary sliding [19,42]. In addition to providing sites for void nucleation, small particles very close to each other can pin grain boundaries, impeding their movement and allowing void coalescence to more easily take place [42].

Intergranular failure in the austenite-plus ferrite region

In the early stages of the austenite-to-ferrite phase transformation, a thin layer of ferrite forms around the austenite grain boundaries, as represented in Fig. 5.1(b). At a given temperature in the two phase region, ferrite is always softer than austenite and therefore deforms preferentially, leading to stress concentration in the ferrite layer and early fracture. It will be shown in the next section that, this ferrite film can be formed at temperatures well above the measured Ar_3, and often close to the calculated Ae_3, due to stress concentration at the austenite grain boundaries producing strain induced ferrite. As the austenite-to-ferrite transformation progresses with decreasing temperatures, the ferrite layer thickens, the stress concentration is reduced and the ductility gradually recovers with increasing ferrite volume fraction.

In the duplex austenite-ferrite range, ferrite film nucleation frequently occurs concurrently with precipitation, as in Fig. 5.1(c), aggravating the problem of stress concentration and void nucleation.

In the following sections, the discussion will center first on the condition of minimum ductility (i.e. in the austenite-plus-ferrite region). This will be followed by an analysis of the factors influencing the recovery of hot ductility at the low temperature end of the trough. Finally, the possible mechanisms for the improved ductility at the high temperature side of the trough will be considered.

5.2 - DEFORMATION IN THE AUSTENITE-PLUS-FERRITE REGION

5.2.1 - Influence of ferrite film thickness, ferrite volume fraction and austenite grain size on ductility in the trough

It has been well established [13,17,19,39,52] that a ductility trough is observed during deformation in the duplex austenite-ferrite region. Suzuki [19] found that the ductility was at a minimum when the pockets of nucleating primary ferrite first linked into a continuous film at the austenite grain boundaries. In the present

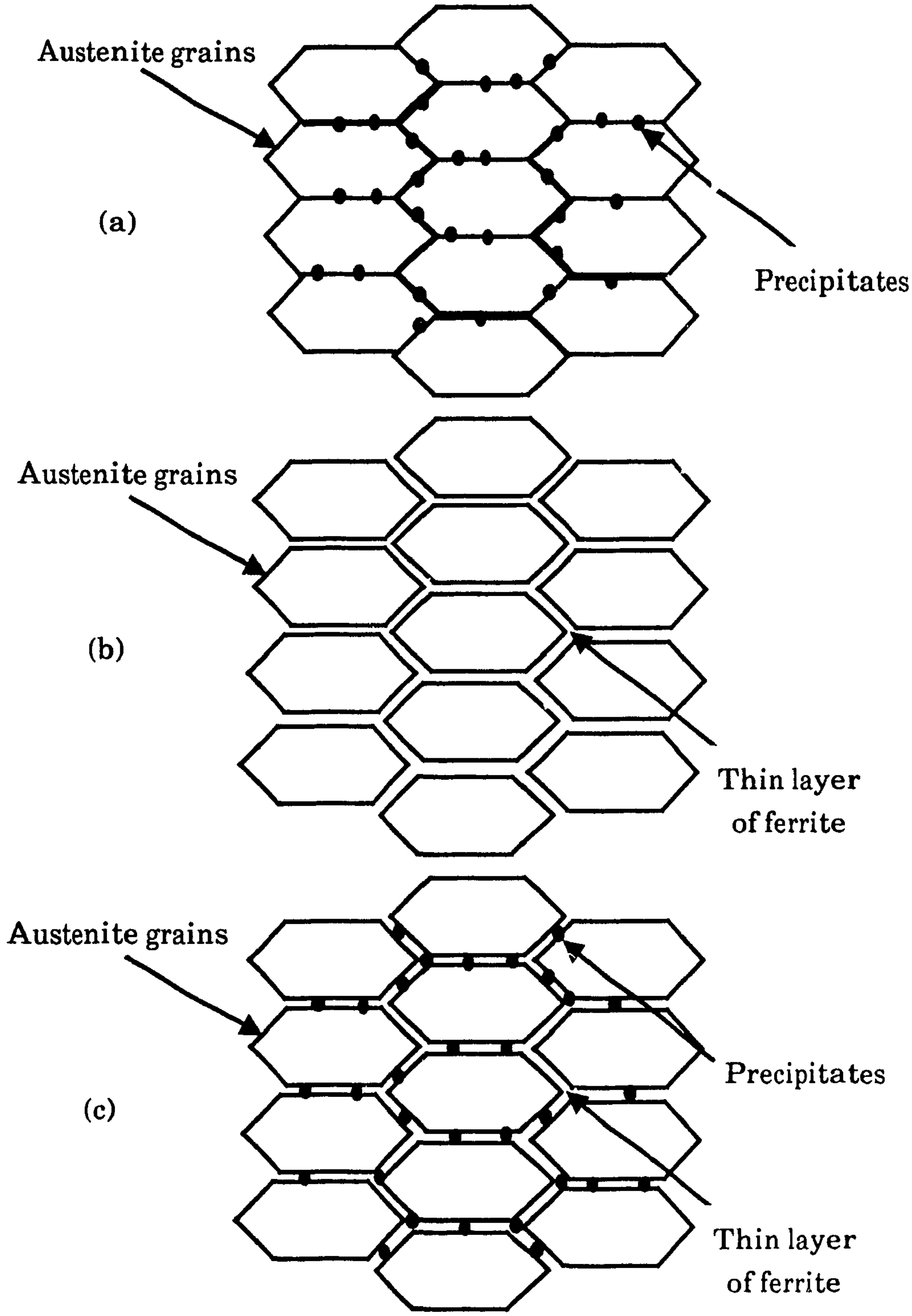

Fig. 5.1 - Mechanisms for embrittlement. Stress concentration on: (a) precipitates (single austenite range); (b) ferrite film (duplex austenite-ferrite range); (c) ferrite + precipitates.

investigation, a ductility trough was observed in all the steels examined and for all the different thermal treatments.

Gráf and Hornbogen [94] have developed a model describing the effect of the soft, precipitate free zone (PFZ) at the grain boundary of a precipitation hardened alloy, on the fracture behavior, which is analogous to a microstructure with a thin films of the softer ferrite phase at the grain boundaries. Maki et al. [37] have adapted their model to the latter, and obtained:

$$\varepsilon = \frac{d}{D_\gamma}\varepsilon_\alpha + \frac{D_\gamma - d}{D_\gamma}.\varepsilon_\gamma \tag{5.1}$$

where ε is the total strain applied to the specimen, ε_α and ε_γ are respectively the strain in the α and γ phases, d is the average thickness of the ferrite film formed along the austenite grain boundaries, and D_γ is the average austenite grain size. If the degree of inhomogeneity in deformation ($\varepsilon_\gamma/\varepsilon_\alpha$) is expressed by P, then Eq. 5.1 becomes

$$\varepsilon = \left[\frac{d}{D_\gamma} + P\left(1 - \frac{d}{D_\gamma}\right)\right]\varepsilon_\alpha \tag{5.2}$$

As mentioned previously, in the two-phase region the strain is concentrated in the α phase, thus $P<1$, i.e P is small for a large inhomogeneity. Assuming the specimen fractures when ε_α reaches a critical value $\varepsilon_{\alpha f}$ (strain of the α phase at fracture), the total strain to fracture is expressed by the following equation:

$$\varepsilon_f = \left[\frac{d}{D_\gamma} + P\left(1 - \frac{d}{D_\gamma}\right)\right]\varepsilon_{\alpha f} \tag{5.3}$$

Equation 5.3 indicates that the ductility decreases if:

(i) the thickness of ferrite, d, decreases,

(ii) the austenite grain size, D_γ, increases,

(iii) the strain inhomogeneity is larger (i.e. P decreases),

(iv) the ductility in α phase ($\varepsilon_{\alpha f}$) is itself smaller.

Though the description given here is only qualitative, it can be used to explain some of the results of this study. It can be seen from Eq. (5.3) that, if the thickness of the ferrite film is the same, then the coarser the austenite grain size, the lower will be the fracture strain. According to the model above, if the austenite grain size is large as is observed in this work for the Low Al and High Al steels (~450 μm), embrittlement in the two-phase region is more pronounced. The difference in grain size can thus explain the changes in the depth of the ductility trough, observed between the coarse grained Low Al and High Al steels (minimum RA $\simeq 12\%$, Fig. 4.11) and the grain refined (grain size ~120 μm) Ti treated steel (minimum RA $\simeq 37\%$, Fig. 4.16).

However, it is noticeable in the present investigation that in the trough itself, ductility remains approximately constant or decreases slightly with decrease in temperature whilst the ferrite film thickness increases. According to Eq. (5.3) this should improve ductility and certainly not impair it.

A summary of the influence of the ferrite volume percentage on the R of A values is shown in Fig. 5.2 for the coarse grained materials used in this investigation (Low Al, High Al and High Mn steels) for all thermal cycles. The ductility is at a minimum (about 20%) when the percentage of ferrite is less than 5%, which corresponds to a thin film of strain induced ferrite surrounding the austenite grain boundaries. Ductility is completely recovered when the proportion of ferrite is approximately 50%. Although this recovery is mainly due to a lowering of the stress concentration caused by an increased ferrite volume fraction, there is an additional probability that it is also related to the strength difference between austenite and ferrite phases, which decreases for lower temperatures [93].

5.2.2 - Influence of austenite-to-ferrite phase transformation on the position and width of the ductility trough

5.2.2.1 - Reference cycle

Table 5.1 lists the temperature range spanned by the trough for all the steels examined and tested according to the reference thermomechanical cycle (Figs 4.4, 4.11, 4.16 and 4.20 for the Low Al, High Al, Ti-treated and High Mn steels, respectively). For the purpose of this discussion, the trough width is defined by R of A values which are lower than 50%.

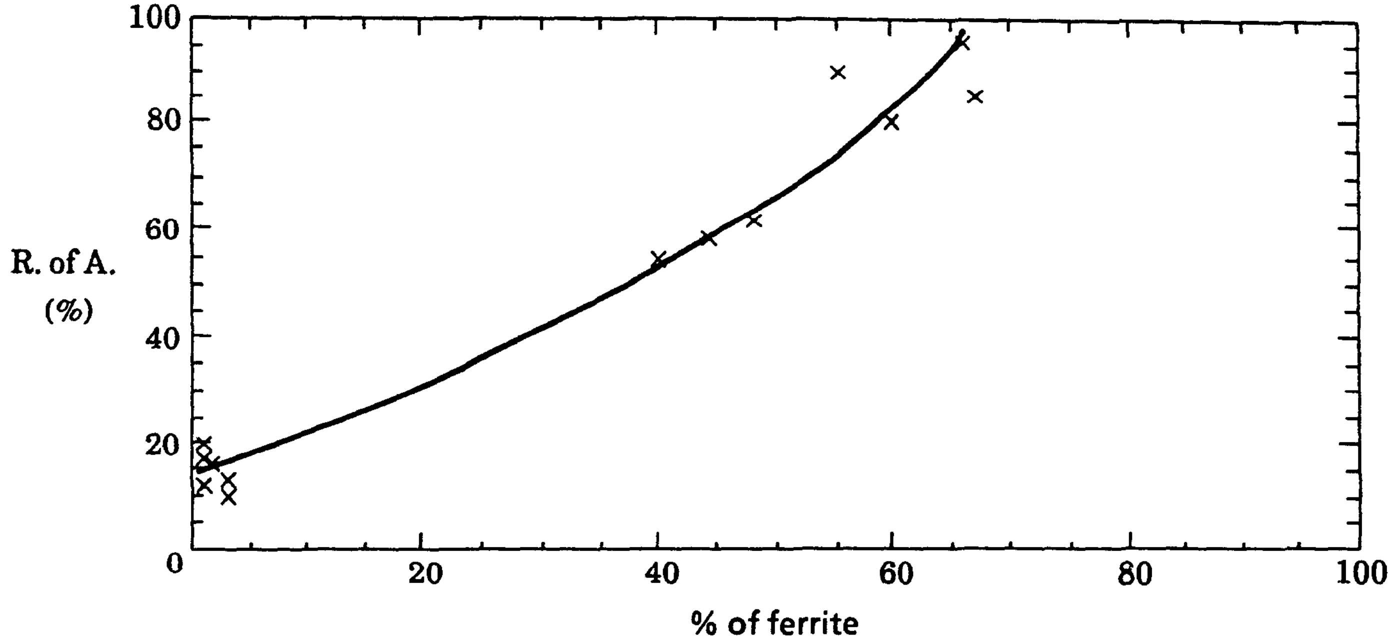

Fig. 5.2 - Influence of volume percent of ferrite on the hot ductility.

The austenite-to-ferrite transformation start temperatures, the Ar_3 values (measured by dilatometry in nondeformed samples), and the equilibrium Ae_3 (calculated) temperatures, are also listed in Table 5.1 and shown in all the figures.

For the Low Al and High Mn steels, it can be seen in Table 5.1 that the ductility troughs occur between the Ar_3 and Ae_3 temperatures. Because the difference between the Ar_3 and Ae_3 temperatures is large, the trough is accordingly wide. The Ti steel has a narrow trough which occurs close to the Ae_3. In these three grades no AlN precipitation was observed in austenite. For the High Al grade, the additional presence of AlN precipitation extends the trough to temperatures significantly higher than the Ae_3, as will be discussed in section 5.3.2, but recovery in ductility at the low temperature end of the trough again occurs close to the Ar_3 temperature. As already mentioned, one of the explanations for the drop in ductility at the high temperature end of the trough is the formation of a continuous thin film of ferrite around the austenite grain boundaries, once the temperature is low enough to allow transformation from austenite to ferrite to take place. Evidence for these thin films of ferrite was found in all the steels examined, and was always associated with poor ductility and intergranular failure. However, the first appearance of these thin films did not coincide with the Ar_3 temperature, but were more related to the Ae_3 temperature, indicating that the ferrite formed was deformation induced, as will be discussed later.

For the Low Al steel, a thin ferrite film (~10 μm thick) is observed at the austenite grain boundaries at 850°C (Fig. 4.7), a temperature just below the Ae_3, and is responsible for the ductility loss. At 800°C, which is still above the Ar_3 (783°C) for the Low Al steel, the ferrite film is increased to 20 μm (Fig. 4.8). For the High Al steel, grain boundary ferrite is also first observed at 850°C (Fig. 4.15) and the thickness increases from 10 to 30 μm as the temperature decreases to 800°C, this being practically coincident with the Ar_3 temperature. The small increase in the ferrite film thickness which occurs with decreasing temperature below the Ae_3 is probably due to an increase in the driving force for transformation, plus a higher strain energy (i.e. dislocation density), which will increase the ferrite nucleation rate [85].

The increased addition of Mn in the steel (High Mn grade) decreased the transformation temperatures. This causes the ductility trough to be shifted in the same direction (Fig. 4.20), as the ferrite is now nucleated at lower temperature. Similar behavior has been noted by Crowther and Mintz [36] when the C level was increased in steels with otherwise the same base composition (Mn content at 1.4%).

For the titanium treated steel, which exhibited the highest ductility of all the steels examined, the ductility trough at 880°C was again found to be due to strain induced ferrite forming at the austenite grain boundaries (Fig. 4.19). This embrittlement temperature is 60°C and 17°C above the Ar_3 and the calculated Ae_3 temperatures, respectively. Although deformation can induce the phase transformation, the upper limit for nucleating ferrite must be the equilibrium start transformation temperature. Here, the probable explanation for the appearance of ferrite at temperatures higher than the calculated Ae_3 is that the model used for the Ae_3 evaluation does not consider the influence of Ti and Al, both of which are strong ferrite formers [52] and therefore should raise the Ae_3. In this steel, the amount of these elements in solid solution is significant. No data concerning the influence of Ti and Al on the Ae_3 is available in the literature (except in Andrew's equation [88], which was not applicable in this study, as is discussed in Appendix II).

The observation of a thin film of strain induced ferrite in the fine grained titanium steel contradicts the work of Crowther and Mintz [66] who have suggested that deformation induced ferrite does not form in fine grain steels. The present findings indicate that not only does a strain induced transformation occur in fine grained steel, but, as will be shown in the next section, it occurs more readily in fine than in coarse grained material.

The temperatures at which the ductility is observed to recover for the Low Al and the High Al steels deformed in the austenite-ferrite duplex region (i.e. the low temperature end of the trough), under the various thermal cycles used in this investigation, are shown in Table 5.2 and also in Figs. 4.23 and 4.32. Here, recovery in ductility is considered to have occurred when the R of A values are greater than 50%. Ductility continues to improve for both steels as the temperature is reduced below the Ar_3 and this is due to the increased proportion of the ferrite phase, as seen in Fig. 4.10 for the Low Al grade. The above results suggest that as soon as the Ar_3 temperature is reached, a further drop in temperature leads to a rapid increase in ferrite, resulting in improved ductility. It should be recalled at this point that Ar_3 values referred to in this work pertain only to the reference cycle and have no direct association with the values in Table 5.2 for the other thermal cycles. Therefore, it may more generally be stated that ductility recovery is invariably associated with the appearance of the statically transformed ferrite (i.e. non strain induced), which is present at temperatures *prior* to testing.

In general, the above results correspond well to the findings of Crowther and Mintz [66], who demonstrated that the temperature at which strain induced transformation at grain boundaries could take place could be as high as the Ae_3, resulting in low R of A values. Similarly, they have shown that ductility is recovered at temperatures close but below the Ar_3, due to a large amount of static nucleated ferrite (30% before deformation, in their findings).

5.2.2.2 - Other thermal treatments

<u>One-step cycling</u>

All the cycling treatments used in this work involve undercooling. This undercooling often introduces precipitation, which, as will be discussed later, affects the high temperature side of the ductility trough. However, this undercooling also very much influences the temperature at which the ductility recovers at the low temperature side of the trough. Since, in the one-step cycling treatment, a holding treatment is given at 100°C below the test temperature, statically transformed ferrite will be introduced, prior to straining, at a much higher test temperature ($\simeq$100°C) than in the reference cycle. It should be noted that once this ferrite is introduced at the lower holding temperature, it will persist at least up to test temperatures as high as the Ae_3 and possibly higher.

The shift in the position of the recovery temperature (at the low temperature end of the trough) for the one-step cycle treatments compared to the reference cycle can be seen from Table 5.2 to be generally 100°C, as might be expected. However, holding time at the lower temperature is also likely to be important in controlling the amount of ferrite produced. In the reference cycle, hold times were 5 minutes, whilst in the one-step cycling treatments hold times at the lower temperature were 1 and 5 minutes. Thus, whilst a shift of 100°C in recovery temperature would be expected for the one-step cycle, given a 5 min. hold, the shorter time (1 min.) hold might be expected to produce less ferrite. Hence, for the Low Al steel the ductility recovery temperature rises from 750°C (reference cycle) to 800 (one step cycling - 1 minute holding) i.e. only 50 °C. For this steel, it can be seen in Table 5.2 that the ductility recovers at still higher temperatures with increasing holding time from 1 to 5 minutes in the undercooling stage, the longer the holding period, presumably allowing more austenite-to-ferrite transformation to occur For the High Al grade, the ductility recovers at 850°C for the one-step cycling treatment, irrespective of the holding time at the undercooling stage. This is due to the fact that amount of ferrite on increasing the holding time at 750°C increased only slightly from 44 to 48%. This difference in behavior between the Low Al and High Al steels can be explained by their different Ar_3 temperatures. For the one-step cycling test at 850°C, the specimen is held at 750°C before deformation, which is approximately 30°C and 50°C below the Ar_3 temperatures for the Low Al and High Al steels, respectively. The austenite-to-ferrite transformation is characterized by site saturation, which results in a logarithmic type curve for the amount of ferrite transformed with time [95]. Since the undercooling at 750°C with respect to the Ar_3 temperature is higher for the High Al steel as compared to the Low Al grade, the amount of ferrite statically transformed is more strongly time dependent for the Low Al steel.

Two-step cycling

For both the Low and High Al steels, the two-step cycling does not change the temperature at which the ductility recovers at the low temperature side of the trough, as compared to the reference cycle curve (Figs. 4.23(c) and 4.32(c), for the Low Al and High Al steels, respectively). This is because, in addition to the fact that there is no hold period at the undercooling stage, most of the extra amount of ferrite nucleated by cycling at lower temperatures is likely to be transformed to austenite when reheated to 100°C above the test temperature, immediately before deformation.

Increasing the holding time in the reference cycle

Increasing the holding time from five minutes to one hour before deformation for the Low and High Al steels, again increases the ductility recovery temperatures (at the low temperature end of the trough), because statically transformed ferrite will be formed at higher temperatures. This is also seen in Table 5.2 as well as in Fig. 4.23(d) and 4.32(d), for the Low Al and High Al steels, respectively. It is worth noting that holding for 5 minutes at 100°C below the test temperatures nucleates more ferrite (and consequently recovers ductility more readily) than a 1 hour hold at the test temperature.

Table 5.1 - Comparison between temperatures at which ductility trough occurs and the start of the austenite-to-ferrite transformation (reference cycle).

Designation	Ductility trough temperatures (°C)	First appearance of ferrite (°C)	Transformation temps. (°C)	
			Ar_3	Ae_3
Low Al steel	800 to 850	850	783	861
High Al steel	800 to 900	850	803	862
Ti treated steel	880	880	820	863
High Mn steel	750 to 800	800	735	842

Table 5.2 - Recovered ductility temperatures during deformation in the austenite-plus-ferrite region.

Designation	Temperature of recovered ductility (°C)	
	Low Al steel	High Al steel
reference cycle	750	750
one-step cycling (1 min. holding)	800	850
one-step cycling (5 min. holding)	850	850
two-step cycling	750	750
one hour holding (variant of ref. cycle)	800	800

5.2.3 - The formation of strain induced ferrite and its influence on hot ductility

The results from this work clearly demonstrate that the hot ductility in the steels deformed in the duplex austenite-plus-ferrite region is intimately related with the strain induced ferrite. At equilibrium, the austenite-to-ferrite phase transformation is affected only by thermodynamic considerations, which are in turn determined by the steel chemical composition and temperature. At temperatures lower than the Ae_3, ferrite is the thermodynamically stable phase, but, due to the kinetics of the transformation process, a certain amount of time (incubation period) is required for the ferrite to form. The incubation time decreases for lower temperatures, due to an increased driving force (i.e. supersaturation) for the transformation to occur. Therefore, at temperatures close to but below the Ae_3, the period of incubation for ferrite is long, and a short holding time is not long enough for the unstable austenite to transform to proeutectoid ferrite. On continuous cooling from a high temperature (single phase austenite region), the transformation to ferrite thus starts at a much lower temperature, the Ar_3, which is in turn affected by the cooling rate and austenite grain size. In this work, the Ar_3 temperature in the undeformed condition was measured by dilatometry for all the steels investigated (Table 5.1) and the validity of these temperatures was obtained from the metallographic examination of quenched samples submitted to the same heat treatment.

The application of deformation on unstable austenite accelerates the austenite-to-ferrite phase transformation kinetics [37,85]. In this way, the formation of proeutectoid ferrite can start at a much higher temperature, tending towards the Ae_3 [66]. The ferrite which is formed during the deformation is called dynamically nucleated [37,85] or strain induced ferrite [66], and is to be distinguished from the statically nucleated ferrite which is formed under no load condition simply by isothermal holding at a constant temperature below the Ae_3.

Whether or not the ferrite is strain induced or statically transformed influences the morphology, distribution and quantity of the ferrite [37,60]. Several investigators [37,60,66] have observed that the morphology and distribution of statically transformed proeutectoid ferrite depends on the austenite grain size. For a small grain size (100 μm), relatively isolated globular ferrite grains are produced on the austenite grain boundaries. For a large grain size (350 μm) a thin ferrite film is produced along the austenite grain boundaries (c.f. Fig. 4.2(b) in this investigation). However, Maki et al. [37] have observed that strain induced ferrite exhibited a thin film like network along the austenite grain boundaries, irrespective of the austenite grain size. This latter observation has been confirmed in the present work in grain sizes of 120 μm (Ti treated steel) and $\approx$450 μm (Low Al, High Al and High Mn grades).

Strain induced ferrite characteristics have been shown to be affected by strain rate [85,96] and prior austenite grain size [37]. The influence of these parameters is analysed below.

Strain rate

Although strain rate was not varied in the present investigation, it is important to know how strain rate influences the formation of strain induced ferrite to more fully understand the present results. Maki et al. [96] have found that no ferrite was formed at temperatures higher than the Ar_3 by deforming the austenite at a strain rate of $9s^{-1}$, whereas at a lower strain rate of $2x10^{-2}s^{-1}$, a thin film of strain induced ferrite was observed. Essadiqi and Jonas [85,97] have also observed the presence of strain induced ferrite at a very low strain rate. In their work, a fine grained Mo steel, deformed at 800°C at a strain rate of $7.4x10^{-4}s^{-1}$ gave an $\approx$5% ferrite volume percentage, after a true strain of $\approx$0.016. Notably, this strain and strain rate correspond approximately to those occurring at the slab surface during the straightening operation in continuous casting. Therefore it can be inferred that deformation induced ferrite can occur during straightening. Since the grain size is much coarser in the cast slab, according to Eq. (5.3) this small amount of ferrite (forming a continuous film) can be very deleterious to the material ductility, and cause grain boundary embrittlement, resulting in transverse cracking.

It has been shown [37,85] that the volume fraction of strain induced ferrite (which is produced at temperatures up to the Ae_3) increases as the strain rate is lowered. Thus, it can be reasonably assumed that at the low strain rate of $1x10^{-3}s^{-1}$ used in this work, the austenite-to-ferrite transformation at the boundaries approaches the equilibrium condition.

Coarse grain austenite

Deformation induced ferrite forms readily, in the temperature range Ae_3, to Ar_3 in the form of thin bands and its volume fraction is always very small. The volume fraction is observed to increase slightly as the temperature falls from the Ae_3 to the Ar_3 due primarily to the greater driving force for transformation, as already explained. Below the Ar_3, although it is a straightforward matter to estimate the total volume fraction of ferrite, it is difficult to differentiate between the statically transformed and the deformation induced ferrite. However, note that the difference between the Ae_3 and Ae_1 is similar to the difference between the Ar_3 and Ar_1 for the Low Al and High Al steels (i.e. the Δ values are small in Table 5.3). For these two steels, it is therefore reasonable to assume that a given decrease in temperature below the Ae_3 is equivalent to the *same* decrease below the Ar_3, with respect to the volume fraction of statically transformed ferrite. Unfortunately, the Δ value is greater for the Ti-treated and High Mn grades (-23 and -83°C, respectively). The reason for high value of Δ in the latter is not clear, particularly in view of the findings of Crowther and Mintz [36], who observed a low Δ value in a similar high Mn containing steel. In light of this, the Ar_1 temperature for the High Mn grade in the present investigation does appear questionable. In the case of the Ti treated steel, however, the difference of 23°C could represent the effect of Al plus Ti in solid solution on raising the Ae_3 temperature, which was not considered in the model used for the Ae_3 temperature calculation. In this case the Ae_3 temperature for the Ti treated grade would be 886°C. In view of these possible discrepancies, it is not unreasonable to assume that the *actual* Δ values are small.

The volume fraction of statically produced ferrite can be estimated for equilibrium conditions using a computer program written by Essadiqi [85] based on the thermodynamic model developed by Kirkaldy and Baganis [86]. The proportion of ferrite in equilibrium with decreasing temperature below the Ae_3, using Essadiqi's program for the steels used in this investigation, is presented in Table 5.4.

The results for the Low Al, High Al and Ti treated steels are very similar (due to the practically coincident calculated Ae_3) and are presented together. At a temperature 31°C below the Ae_3, 830°C, the volume fraction of ferrite in equilibrium for the Low Al steel is 51%. For a similar fall in temperature below the Ar_3 (33°C), practically the same amount of ferrite (~55%) was observed in the microstructure of the Low Al steel tested at 750°C, using the reference thermal cycle (Fig. 4.10). This indicates that the amount of deformation ferrite is probably small at these temperatures, in accordance with the small amounts of strain induced ferrite observed between the Ae_3 and Ar_3.

Fine grain austenite

For the fine grained Ti steel, thin films of deformation induced ferrite were also formed, but only a very narrow ductility trough was observed (Fig. 4.19). Crowther and Mintz [66] have also found narrow troughs for steels tested with a grain size range that encompasses the 120 μm austenite grain size observed for the Ti steel. As mentioned before, it is believed that the Ae_3 temperature for this steel would be around 890°C. Below 880°C the ductility improved dramatically, even though only deformation induced ferrite can be present ($Ar_3 = 820°C$). In contrast to the coarse grained situation, a very high volume percentage of strain induced ferrite was observed in samples quenched after fracture at 850°C ($\simeq$ 60% ferrite). This high volume fraction of ferrite would be expected to give the observed high ductility. Note that, the calculated amount of ferrite present in the Ti steel at equilibrium at 850°C (i.e. 40°C below the *estimated* Ae_3 of 890°C) is also in the region of 60% ferrite, i.e. the introduction of strain appears to increase the Ar_3 substantially back to the level of the Ae_3.

It therefore appears that it is much more difficult to form deformation induced ferrite in a coarse grained structure than in one with a fine grain size. Moreover, the rate of strain induced transformation is so rapid in the fine grained Ti steel that embrittlement due to a ferrite film occurs only over a very narrow temperature range.

5.2.4 - The role of second phase particles on the duplex austenite-ferrite region

The ductility loss in the austenite-plus-ferrite mixture depends largely on two factors. The first, which was discussed in the previous section, is the volume fraction of the phases present. The second factor is the form and number of inclusions and precipitates present at the austenite grain boundaries [13,37,93], shown schematically in Fig 5.1(c). Apart from the grain size effect discussed in the last section, it is expected that the fracture strain of the α phase ($\varepsilon_{\alpha f}$) is affected mainly by

Table 5.3 - Differences between the Ae and Ar temperatures.

Designation	$Ae_3 - Ae_1 = \Delta Ae$ (°C)	$Ar_3 - Ar_1 = \Delta Ar$ (°C)	$\Delta = \Delta Ae - \Delta Ar$ (°C)
Low Al steel	142	138	4
High Al steel	143	135	8
Ti treated steel	142	165	-23
High Mn steel	124	207	-83

Table 5.4 - Ferrite volume percentage in equilibrium for the steels investigated.

Designation	Temperature (°C)					
	850	840	830	820	810	800
Low Al, High Al and Ti treated steels ($Ae_3 \simeq 862$°C)	26%	41%	51%	59%	66%	71%
High Mn steel ($Ae_3 = 842$°C)	-	-	23%	36%	47%	55%

the characteristics of the precipitates, which act as void initiation sites [37]. Fractographic studies have indicated that the intergranular ductile fracture observed in the duplex region, can occur by coalescence of microvoids, nucleated at grain boundary precipitates such as AlN or MnS, as the result of stress concentration in the ferrite film [13,37].

Yamanaka et al. [13] have developed a model to predict the strain to fracture (ε_f) of a steel deformed in the two phase region, obtaining the following expression:

$$\varepsilon_f = (k\ \frac{1-f}{f}).(V_\alpha + P\ V_\gamma) \tag{5.4}$$

where,
k = constant, which is 0.0023 for pure iron and 0.0214 for alumina doped iron,
f = volume fraction of the second phase particles,
V_α and V_γ = volume fractions of the ferrite and austenite phases, respectively,
P is the strain inhomogeneity as defined for Eq. (5.3).

According to Eq. (5.4), the strain to fracture decreases if:

(i) the volume fraction of second phase particles increases;

(ii) the ferrite volume fraction increases;

(iii) the strain inhomogeneity between the two phases present is larger (i.e. P decreases).

<u>Comparison between the and High Mn and Low Al steels (reference cycle)</u>

In the present work, one effect of second phase particles on hot ductility in the duplex austenite-ferrite region is illustrated in Fig. 4.20, where the ductility trough in the High Mn steel is not as deep as for the low Mn containing grade (Low Al steel). The explanation for this behavior probably originates at the initial solution treatment at 1350°C. For the Low Al steel, approximately 80% of the sulfur, which is combined as MnS particles and dispersed in the matrix in the room temperature structure, is dissolved at 1350°C, as indicated in Table 4.3. Thus, it can reprecipitate as MnS in the grain boundary ferrite film, on cooling to the test temperature, as observed in the SEM examination (Fig. 4.8 (a)).

On the other hand, for the High Mn grade, only about 20 % of the MnS was dissolved by reheating to 1350°C because the high Mn concentration increased the Mn solubility temperature by 190°C. Therefore, in the High Mn grade, less MnS is available to reprecipitate in a fine form at the boundaries. Based on the respective solubilities of MnS, the amount of MnS that reprecipitates in these two grades can be quantified in the following manner.

The volume percent of second phase particles in the iron matrix can be calculated by [12]:

$$Volume\,percent = \left[\frac{\rho_{Fe}}{\rho_{XY}} \frac{M_{XY}}{M_X} \right] \left[\%X \right] = A \left[\%X \right] \tag{5.5}$$

where,

ρ is the density and M the molecular mass,

XY is the precipitate general formula,

[%X] is the concentration of precipitated element in mass percent.

The term A in Eq. (5.5) is given in the literature for the MnS [98]. Therefore Eq. (5.5) can be read as:

$$Volume\,percent\,of\,MnS = 5.318. \left[\%S \right] \tag{5.6}$$

It can be determined, using Eqs. (4.2) to (4.4) presented in the previous chapter, that the amount of S dissolved at the solution treatment at 1350°C is 0.0063% for the Low Al steel and 0.002% for the High Mn grade. This amount of S is then available to reprecipitate as MnS at the austenite grain boundaries. The maximum volume percentage of MnS at the grain boundary ferrite film of the Low Al and High Mn steels, calculated by Eq (5.6), is presented in Table 5.5.

Table 5.5 - Maximum volume percentage (V_p) of MnS particles available for precipitation in the grain boundary ferrite film

Designation	V_p of MnS	Ductility at 800°C (Reference cycle)
High Mn steel	$1.06x10^{-2}$	35%
Low Al steel	$3.35x10^{-2}$	16%

Thus, there is over three times the volume fraction of precipitation in the Low Al steel. Furthermore, it has been shown by Lankford [9] that, for a given temperature below the MnS solubility line, the degree of supercooling increases with increasing Mn, and this favors MnS precipitation in the matrix (i.e., homogeneous nucleation). Consequently, there will be a lower particle density at the austenite grain boundaries for the High Mn steel. Therefore, the difference in the depth of the troughs between the high and low Mn containing steels represents the additional effect of a greater volume fraction of grain boundary particles in the low Mn containing steel.

Grain boundary embrittlement could thus be reduced by increasing the Mn content of the steel, but the amount required may be impractically large. In any case, despite the fact the the trough is shallower for the High Mn steel, the minimum observed R of A for this grade is still about 30%. Leslie [98] suggests that, it would be possible to eliminate this kind of embrittlement (which is termed overheating) by replacing the MnS by a more stable sulphide, by additions of calcium, rare earths or titanium, and reducing the S content in the steel.

Comparison between the Low Al and High Al steels

In all the conditions for which an increased amount of precipitation in the austenite-plus-ferrite region was expected, the result was an increased apparent number of sites for void nucleation. This is clearly illustrated in this work, for several tests performed at 800°C, in the following instances:

1- Increasing the Al content:

fractography has indicated that the number of dimples in the High Al steel (Fig. 4.45) is much more numerous than for the Low Al grade (Fig. 4.47).

2- Introduction of thermal oscillation in the Low Al steel:

increased number of voids is observed in the two-step cycled specimen (Fig. 4.29), as compared to the one submitted to the reference cycle (Fig. 4.9). This is confirmed by fractography (Figs. 4.47 and 4.48).

3- Introduction of thermal oscillation in the High Al steel

the characteristics are identical to those of the Low Al grade described above.

All the above conditions lead to a higher supersaturation at the same temperature, either by thermal cycling or by increasing the Al content, therefore increasing the AlN and/or MnS precipitation. As mentioned in the previous chapter, the AlN particles are usually too small (<100nm) to be detected in the SEM. However, the extensive presence of MnS inclusions was observed in the two-step cycled specimens, both for the Low Al steel (Fig. 4.8) and the High Al grade (Fig. 4.46). Wray [93] has shown that excess oxygen is removed with higher aluminum contents and therefore, relatively massive sulphide inclusions replace the more dispersed oxysulfides. Fracture is favored at these sulfides in the heavily strained ferrite regions. He also notes that the aluminum in solution (and this would be greater in the High Al steel) strengthens the austenite matrix, increasing the strength differential between the matrix and the ferrite film, consequently increasing the stress concentration in the ferrite.

Although increased precipitation was detected in the above cases, it is interesting to note that this did not influence the depth of the ductility trough at 800°C, as can be seen in Figs. 4.11, 4.23(c) and 4.32(c), for the cases 1 to 3 above, respectively. This is presumably because the ductility at 800°C, in all these tests, was already very poor (R of A<20%).

5.3 - DEFORMATION IN THE SINGLE AUSTENITE REGION

In the austenite region, ductility can also be poor and intergranular failures occur when fine precipitation takes place at the austenite grain boundaries, as schematically shown in Fig. 5.1(a) Ductility recovers in austenite when the temperature is high enough for dynamic recrystallization to be sufficiently developed to isolate grain boundary cracks, preventing them from joining up. Thus, the characteristics of the embrittlement according to the mechanism presented above in Fig. 5.1(a) will be largely the result of a competition between dynamic recrystallization and precipitation.

5.3.1 - Effect of grain boundary precipitation on embrittlement

For the steels investigated, three types of precipitates can be present in the austenite, i.e. TiN, MnS and AlN. As mentioned before, TiN is usually coarse and distributed throughout the matrix, and in this condition is not deleterious to ductility. The role played by the MnS at the grain boundaries of single phase austenite is not clear. Because these precipitates are coarser, they are unlikely to be important in the pinning process, although they will encourage void formation [11]. In contrast, the fine AlN precipitation has been shown by many investigators to be instrumental in giving low ductility intergranular failures.

In the case of high Al and/or high N steels (such as the High Al steel) it is likely that AlN precipitates are formed at the austenite grain boundaries, pinning them and encouraging grain boundary sliding. The Ti treated grade, despite the very high Al content (Al=0.095%) exhibited excellent ductility in the whole austenite region (Fig. 4.16). It has been shown that when the titanium/nitrogen ratio in the steel is greater than stoichiometry (Ti/N>3.4), most of the free N is removed from solution as TiN. Thus, with sufficiently high titanium, the precipitation of AlN (a sluggish reaction) can be eliminated, even in slow cooled castings [38].

In the High Mn grade, AlN precipitation is a possibility. However, tensile tests of this same grade at several strain rates performed by Guillet [25], and analysis of the flow stress variations, suggested that no precipitation was occurring in the austenite region. Michel and Jonas [57] have argued that solute elements such as Mn, increase the solubility of carbonitrides, and render them less likely to precipitate. They also pointed out that the marked differences in the kinetics of precipitation of AlN observed in the literature may be ascribed to differences in Mn levels, rapid precipitation being associated with low Mn contents. Mintz and co-workers [11] have suggested that for steels having 1.4% Mn (i.e. the High Mn grade), the (Al)x(N) solubility product must approach 2.5 to 3 x 10^{-4} for precipitation to occur. This is two times higher than the solubility product given in Table 3.1 for the High Mn steel. Vodopivec [99], for example, used a low Mn level (0.36%) in his Al containing steel, and consequently the precipitation rate for AlN was markedly increased.

The hot deformation of austenite supersaturated with aluminum and nitrogen results in a complex interaction between dynamic and static recovery and recrystallisation, and dynamic and static precipitation of AlN. The kinetics of precipitation during hot deformation depend on the strain rate [57], the temperature of deformation [57,54,100,101] and steel analysis [55]. It is generally acknowledged that the hot deformation of Al-killed steels results in a marked increase in the kinetics of precipitation of AlN. Michel and Jonas [57], using the "peak stress" method found that, during hot torsional deformation of a series of Fe-Al-N steels, the kinetics of the dynamic precipitation of AlN were more than an order of magnitude faster than the corresponding static precipitation rates. Vodopivec [54,99] has similarly reported an increased rate of nucleation of AlN during deformation (dynamic precipitation), but no alteration in the rate of precipitation in the subsequent unloaded state. It was suggested [54] that the onset of recrystallisation during or immediately following the deformation would, by eliminating dislocation substructures, reduce the subsequent precipitation rate to that typical of undeformed austenite.

Hence, based on the above, the lower manganese steels, i.e. the Low Al and High Al steels used in this investigation (%Mn$\simeq$0.40) are more prone to the detrimental effect of AlN precipitation at the austenite grain boundaries.

5.3.1.1 - Precipitation in reference tests

The static precipitation of AlN is very slow in austenite [14], but if it occurs prior to test, it is very detrimental to the ductility because AlN preferentially nucleates on the grain boundaries as fine particles [61]. The probability of AlN nucleation is favored by increasing the degree of supersaturation of Al and N in the austenite matrix, thereby increasing the driving force for precipitation.

As can be seen in Table 5.6, for the Low Al and High Al grades, the ductility trough (i.e. R of A values < 50%) extends to higher temperatures, when the thermomechanical treatments are favorable for AlN precipitation. For example, using the reference thermal cycle, raising the ASA content in the steels, extends the embrittlement to the austenite region (Fig. 4.11), confirming other studies [16,45,46]. In fact AlN particles were observed in the High Al steel specimen tested at 900°C (Fig. 4.12), such precipitation giving rise to extensive intergranular and wedge type cracks (Fig. 4.13). Increasing the holding time before test to 1 hour for the Low Al steel failed to promote embrittlement at 900°C (Fig. 4.23(d), and the corresponding structure was completely recrystallized. This suggests that no AlN precipitation took place under these conditions. However, in contrast, the 1 hour holding treatment for the High Al steel extended the trough to 950°C (Fig. 4.32(d)). The increased time at the test temperature coarsened the AlN particles for the High Al grade, making them more clearly visible, as shown in Figs. 4.38(a)-(c), for the test at 900°C. This tends to suggest that the particles are precipitating prior to test rather than during the test.

Table 5.6 - Ductility trough in the austenite region for the Low Al and High Al steels.

Designation	Ductility trough temperatures in austenite (°C)	
	Low Al steel	High Al steel
reference cycle	trough in $\gamma + \alpha$ region	900
one-step cycling (1 min. holding)	900	900-950
one-step cycling (5 min. holding)	900-950	900-950
two-step cycling	900	900
one hour holding (variant of ref. cycle)	trough in $\gamma + \alpha$ region	900-950

The above results confirm the studies of Crowther et al. [49], who compared the precipitation and ductility behavior of a low Al (Al = 0.017%, N = 0.006%) and a high Al (Al = 0.068% and N = 0.006%) steel. For the former, they found that even after 6 hours holding before testing at 850°C (the austenite region for this particular steel) no AlN precipitation occurred nor was there any evidence for AlN being precipitated dynamically during the test. For the high Al containing steel, they observed improved ductility when no holding time was given before testing, but when a very short holding treatment of <2 min. was given prior to deformation, enough AlN precipitation occurred and was accompanied by a deterioration of ductility. Their results also suggest that there was no evidence for dynamic precipitation of AlN, but static precipitation at the austenite grain boundaries was effective in reducing hot ductility.

5.3.1.2 - Precipitation in cycling tests

It can be inferred from Table 5.6 (and Figs. 4.23 and 4.32) that the one-step cycling treatment is much more effective in promoting precipitation than long holding times before test. For example, for the Low Al steel tested at 900°C in the one-step cycling treatment, a 1 min. hold at 800°C was sufficient to result in embrittlement (Fig. 4.23(a)). Increasing the holding time at the undercooling stage to 5 minutes probably increased grain boundary precipitation, expanding the trough to 950°C (Fig 4.23(b).

For the High Al steel, the one step cycling treatment extended the trough to 950°C, irrespective of whether the holding time was 1 or 5 minutes (Figs. 4.32(a) and 4.32(b)). In this steel, the (ASA)x(N) product is high (Table 3.1) and the probability of extensive AlN precipitation is increased, even for a 1 min. hold at the undercooling stage. It is worthy of note that at 900°C, a very small amount of ferrite was observed at the austenite grain boundaries due to the undercooling to 800°C (very close to the Ar_3 temperature for this grade) as shown in Fig. 4.33. This small amount of statically nucleated ferrite may have contributed significantly to AlN precipitation. Since the ductility for the High Al steel tested at 900°C using the reference cycle was poor, a low R of A value was also expected for the test at 1000°C using the one step cycling (because the specimen was held for 5min at 900°C prior to raising to the test temperature), due to a similar amount of static precipitation. Instead, the ductility was high, probably due to an increased grain boundary mobility at 1000°C, facilitating dynamic recrystallization.

The two-step cycling treatment did not exert such a strong influence in terms of significantly increasing the range of embrittlement in austenite, as compared to one-step cycling. It appears that in the latter, the hold period at the undercooling stage, for times even as short as 1 minute, promotes enough precipitation to lead to embrittlement. However, the two-step cycling at least extends the embrittlement to the austenite region of the Low Al steel, as shown in Fig. 4.23(c). The partially recrystallized structure shown in Fig. 4.27 is probably the result of AlN pinning the grain boundaries, and contributes to embrittlement. For the High Al grade, where AlN nucleation is already significant at 900°C (according to the ductility curve of the reference cycle), two step cycling did not increase precipitation sufficiently to change the shape of the ductility curve (Fig. 4.32(d)). It is interesting to note that, for the two step cycling treatment, which is closer to the industrial thermal cycle experienced by a slab during casting, the embrittlement in the austenite region occurs in the same temperature range for the Low Al and High Al steels (Table 5.6).

5.3.2 - Effect of dynamic recrystallization on ductility recovery

If recrystallization can occur during the deformation, the cracks associated with void linkage from precipitates are trapped inside the new grains. Thus, the stress concentration at the boundaries is reduced and the ductility is high. This is clearly illustrated in the microstructure presented in Fig 4.24, for the Low Al steel tested at 950°C under the one-step cycling (1 min. holding) treatment, in which a high R of A value was obtained. Here, the undercooling treatment at 850°C has not promoted ferrite nucleation (at this temperature only strain induced ferrite could form, as discussed in Section 5.2.2), but some grain boundary precipitation may have taken place, although apparently not extensive enough to impede grain boundary migration and prevent dynamic recrystallization. Alternatively, as described in section 2.2.8, the grain refining effect of dynamic recystallization could also be the reason for improved ductility [16,60].

Whatever the mechanism, in this work, high ductility in austenite correlates strongly with the occurrence of dynamic recrystallization, as shown in Table 5.7. This is based on the observation of the microstructure of the specimens quenched immediately after fracture, since dynamic recrystallization frequently could not be readily identified from the flow curve, especially in low temperature austenite. However, when the conditions for AlN grain boundary precipitation were not favorable, dynamic recrystallization in austenite was always observed in the specimens quenched after rupture, even if the flow curves failed to indicate that recrystallization had occurred. For example, the Low Al specimen tested at 900°C using the reference cycle gave no indication of dynamic recrystallization from the flow curve (Fig. 4.5). However, the test had resulted in a high R of A value, suggesting that dynamic recrystallization had occurred. Examination of the gauge length suggested that this recrystallization was apparently confined to the very narrow necked region. This was probably the reason why no indication of recrystallization was observed on the flow curves.

As shown in Table 5.7, for this investigation, the lowest temperature in austenite corresponding to high R of A values was always associated with the minimum temperature for dynamic recrystallization to occur. The findings presented in this table are for the reference cycle tests only, although a correspondence between dynamic recrystallization and high ductility in austenite was noted for all thermal cycles applied. For the steels where precipitation of fine grain boundary particles is less likely (Ti treated and High Mn grades) the embrittlement occurred only in the duplex austenite-plus-ferrite region, where no recrystallization was observed. Even at relatively low temperatures in austenite, such as 850°C for the High Mn grade, a recrystallized structure was observed (Fig. 4.21), corresponding to improved ductility. For the Ti steel tested at 900°C, corresponding to the temperature at which the recovery in ductility was noted at the high temperature side of the trough, although extensive cracking was observed (Fig. 4.17) the cracks were transgranular and situated in a recrystallized austenite, resulting in good ductility. This is in accord with the studies of Funnell and Davies [42], who indicate that the improved ductility obtained in high [Al].[N] steels with addition of Ti, is associated with a reduction in grain boundary pinning.

Also included in Table 5.7 are the results from other investigations showing the temperature range where ductility recovers on the austenite side of the trough, compared to the lowest temperature where dynamic recrystallization is observed. In all these examinations it can be seen that, although the minimum temperature at which dynamic recrystallization is observed is close to the temperature at which ductility recovers, it is often higher. One possible reason for this is that in these investigations [49,102], evidence for dynamic recrystallization was based on the

Table 5.7 - Relationship between the temperature range of high ductility in austenite and dynamic recrystallization start temperature in austenite.

Steel	Strain rate (s^{-1})	Ae_3 temperature (°C)	Other details	Temp of high ductility in austenite (°C)	Dynamic Recryst. minimum temperature (°C)	Reference
C-Mn-Al	3×10^{-3}	?	no holding time before test	850-1000	900	49
C-Mn-Al	3×10^{-3}	?	15 min holding before test	900-1000	900	49
C-Mn-Al	1.5×10^{-4}	850	commercial cast	950-1100	975	102
C-Mn-Nb-Al	1.5×10^{-4}	856	commercial cast	1050-1100	1075	102
C-Mn	1.5×10^{-4}	$\simeq$820	lab. cast	all temp. (even below Ae_3)	775	102
C-Mn-Nb	1.5×10^{-4}	$\simeq$820	lab. cast	900-1000	1075	102
Low Al	1×10^{-3}	861	reference cycle	900-1000	950* 900**	present work
High Al	1×10^{-3}	862	reference cycle	950-1000	1000* 950**	present work
Ti treated	1×10^{-3}	863	reference cycle	900-1000	950* 900**	present work
High Mn	1×10^{-3}	842	reference cycle	850-1000	900* 850**	present work

* based on the flow curve shape; **based on optical metallography.

tensile curves, not on metallographic observations. It is worth noting that Wilcox and Honeycombe [102] found that for a C-Mn steel, the austenite continued to recrystallize dynamically even when a small amount of ferrite was present in the microstructure (below the Ae_3). This was sufficient to counter the embrittling effect of the ferrite, leading to a high ductility. They attributed the occurrence of dynamic recrystallization in that experiment to the low strain rate employed ($1.5x10^{-4}s^{-1}$). This is about one order of magnitude slower than the $1x10^{-3}s^{-1}$ used in the present investigation, where a trough was always associated with both the onset of austenite-to-ferrite phase transformation, as well as the absence of recrystallization. As mentioned in Section 4.2, lower strain rates reduce the critical strain for dynamic recrystallization, making it easier for dynamic recrystallization to take place.

It may be concluded that, when dynamic recrystallization is well established, the ductility is always high in laboratory tensile tests. In the case of continuous casting, in which a very coarse grain size is present, making the critical strain for dynamic recrystallization very high, dynamic recrystallization cannot play a role in preventing the formation of transverse cracks, because the unbending strains the slab is subjected to are very small ($\varepsilon \simeq .02$). The reduction in the incidence of transverse cracking, observed commercially, on raising the straightening temperature, is then possibly due to a reduction in the degree of precipitation at the austenite grain boundaries.

5.4 - CONTRIBUTION OF GRAIN BOUNDARY SLIDING TO EMBRITTLEMENT

As discussed above, if the grain boundaries are pinned by the precipitates and dynamic recrystallization cannot occur, the stress concentration around the precipitates will cause extensive void formation and linkage, favoring early fracture. The Low Al steel tested at the temperature of 900°C using the one-step cycling (5 min. holding), illustrates this situation. Although ferrite nucleation is still not possible, undercooling to 800°C is sufficient to encourage marked AlN precipitation. When deformed at 900°C, grain boundary migration (Fig. 4.25) is probably impeded. The grain boundary voids (shown in the upper part of Fig. 4.25) are caused by stress concentration at the AlN precipitates observed in this sample (Figs. 4.26(a) and 4.26(b). Under these circumstances, grain boundary sliding is extensive, as is evident by the offset between two adjacent grains in the fractographs (Fig. 4.42).

Funnell and Davies [42] have shown that, when grain boundary migration is relatively easy, superior ductility is observed. Their results also suggest that the retardation of grain boundary migration by AlN makes it easier for grain boundary cavities to grow by grain boundary sliding.

Ouchi and Matsumoto [17] have calculated the contribution of the grain boundary sliding strain (ε_{gb}) on the total strain (ε_t) applied during the tensile test for a 0.054% Nb containing steel, deformed at 900°C (single phase austenite). They determined that for a strain rate of $\simeq 10^{-3}s^{-1}$, the ratio $\varepsilon_{gb}/\varepsilon_t$ was $\simeq 0.28$. Increase in the strain rate decreased $\varepsilon_{gb}/\varepsilon_t$, although grain boundary sliding, which is mainly characteristic of creep rupture, was observed at strain rates as high as $10^{-1}s^{-1}$. However, the value $\varepsilon_{gb}/\varepsilon_t$ was insensitive to variations in the Nb content and also insensitive to changes in test temperature in the range of 900°C to 1100°C, despite the fact that the level of a precipitating forming element and temperature is known to have a strong influence on ductility. Based on this, they concluded that, although grain boundary sliding appear to be a necessary condition for initiation of a grain boundary crack, it is not the factor directly responsible for the embrittlement.

The common microstructural aspects which indicate the occurrence of grain boundary sliding are the presence of wedge and "r" type cracks [11], flat grain facets [66] and displacement of adjacent grains in the fracture surface. Apart from the example given above, considerable evidence for grain boundary sliding was observed in the present investigation. In the single austenite region, grain facets which were predominantly flat were observed in all fracture surfaces of low ductility specimens (Figs. 4.40~4.42). Wedge type cracks can be seen in Fig. 4.13, corresponding to the High Al steel tested at 900°C, using the reference cycle. In the two phase region, when a thin film of strain induced ferrite was nucleated at the austenite grain boundaries, displacement of grain facets is illustrated in Fig. 4.44, for the High Al grade tested at 850°C (reference cycle). The optical metallography of this same sample also reveals the presence of wedge cracks (Fig. 4.15).

Grain boundary sliding has been shown to be a common factor related to embrittlement in the single phase austenite and in the duplex range (in addition to the presence of grain boundary precipitates and the influence of grain size). The presence of grain boundary sliding throughout the temperature range of low ductility may explain why no marked singularity is observed in the depth of the ductility trough, for steels and test conditions which result in brittle behavior in austenite and in the austenite-plus-ferrite region (Figs. 4.23 and 4.32).

5.5.- SOME OBSERVATIONS ON THE PLASTIC BEHAVIOR AT ELEVATED TEMPERATURES

Because of the serious commercial problem of transverse cracking, interest in mechanical property data has been confined mainly to ductility rather than to strength. The actual plastic behavior as defined by yield strength, ultimate tensile strength, work hardening, etc, has been largely ignored. However, as shown in Section 5.2.1, knowledge of the plastic behavior (e.g. P in Eq. 5.3) is necessary in order to comprehensively define the conditions of embrittlement. Such an undertaking is beyond the scope of this work. However some aspects of the flow behavior are presented below, which underline the issues of the previous discussion.

Figure 5 3 shows the variation of maximum stress (peak) with temperature for the Low Al, High Al and Ti-treated steels (steels with the same Mn level), corresponding to the reference thermal cycle. At 900°C and higher, where only austenite is present, the maximum stress increases with decreasing temperature. The higher rate of stress increase observed for the Ti steel with decreasing temperature can probably be related to the greater amount of Al in solution in this grade compared to the others [93], together with the finer grain size. The first indication of strain induced ferrite formation in these steels (880°C for the Ti treated steel and 850°C for the Low Al and High Al grades) coincides with either a decrease in the peak stress, as observed for the High Al and Ti treated steels, or a levelling of the peak stress, as for the Low Al grade. These discontinuities in the curves are due to the introduction of the weaker ferrite phase, and have been revealed in other investigations [39,93]. At lower temperatures, the softening due to the higher volume fraction of ferrite becomes more significant and the stress decreases, as can be seen in the curve for the Ti steel. For the Low Al and High Al steels in the temperature range of 850-800°C, where a thin film of strain induced ferrite was observed, only a small variation occurs in the maximum stress. At lower temperatures, with increased ferrite volume fraction, the flow stress increases rapidly, due mainly to the ferrite strain hardening.

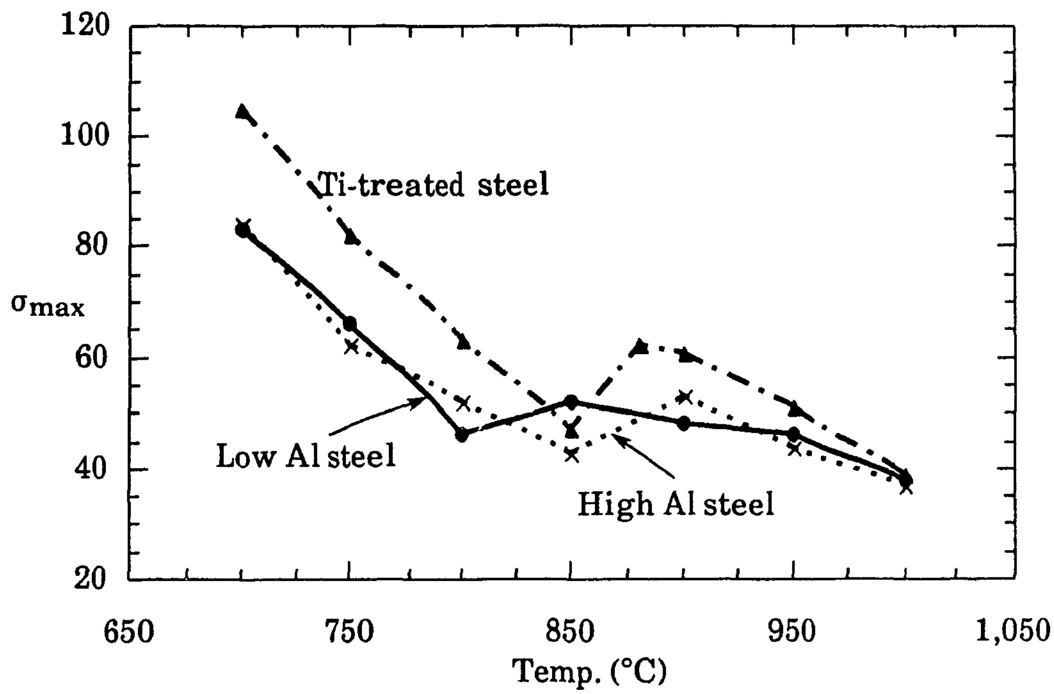

Fig. 5.3 - Variation of maximum stress with test temperature (reference cycle).

CHAPTER 6

CONCLUSIONS

During the straightening or unbending operation of continuous casting, tensile stresses are developed at the surface of the solidified strand. If the hot ductility of the steel is poor, the fracture strain is exceeded and transverse cracks appear.

In this work, the hot ductility at conditions approaching the straightening operation was evaluated by tensile testing at temperatures between 700 and 1000°C for three low carbon steels of varying Al and Mn contents and one low carbon/high aluminum steel with a titanium addition. The specimens were solution treated at 1350°C and cooled either directly to the test temperature or with different patterns of temperature oscillation about a mean cooling rate, the latter more closely simulating the industrial conditions. Test were performed at a constant strain rate of $10^{-3}s^{-1}$, and specimens were quenched immediately after fracture, thus allowing the high temperature structure to be correlated with hot ductility. Based on this work, the following main conclusions can be drawn:

1 - The four steels investigated displayed a ductility trough which could be associated with the onset of the austenite-to-ferrite phase transformation, i.e., when thin films ($\approx$10 µm) of ferrite form at the austenite grain boundaries. The concentration of stress in this relatively weak ferrite film promotes grain boundary embrittlement.

2 - The ferrite film has been shown to be strain induced, i.e., it is formed during deformation in the region just below the calculated equilibrium austenite-to-ferrite transformation start temperature (Ae_3) and at temperatures higher than the undeformed non-equilibrium Ar_3 determined by dilatometry.

3 - For the C-Mn-Al steels with coarse austenite grain size ($\approx$450 µm), in the absence of AlN precipitation at the austenite grain boundaries, the trough width has been shown to extend from the Ar_3 to the Ae_3 temperature. The observed increase in the film thickness over this temperature range, from approximately 10 to 20 µm is believed to be due to an increase in driving force for the transformation to occur.

4 - Increasing the Mn content in C-Mn-Al steels from $\approx$0.40 to 1.39% results in a shallower trough, which is shifted to lower temperatures. This effect was shown to

be due to the decrease in the amount of grain boundary MnS inclusions and to a decrease in the austenite-to-ferrite transformation temperature, respectively.

5 - Increasing the Al content and/or the application of thermal oscillation in low Mn containing steels, increases the amount of precipitation of AlN and possibly MnS in the ferrite film, as evidenced from an increased number of dimples on the fracture surface. However, this does not result in further decrease on ductility, probably because the R of A values are already below the 20% level.

6 - The addition of Ti results in a trough, which is shifted to a higher temperatures. This arises because Ti is a ferrite stabilizer and raises the transformation temperature. Furthermore, the TiN particles are not dissolved during the solution treatment, resulting in a finer grain size structure ($\approx$ 120 μm), which also increases the transformation temperature.

7 - Increasing the percentage of ferrite distributes the applied stress over a larger volume of ferrite and consequently improves ductility. Furthermore, at lower temperatures, the strength difference between ferrite and austenite is decreased, decreasing the strain experienced in the ferrite. It has been shown that recovery of ductility is practically completed when the proportion of ferrite is higher than 40%.

8 - For the coarse grained C-Mn-Al steels, recovery in ductility is observed only after statically formed ferrite is produced, either at temperatures below the Ar_3 or by using thermal treatments that emphasize ferrite formation.

9 - In the case of the Ti steel, recovery of ductility occurs more readily, because the finer grain size encourages strain induced ferrite to be produced in large quantities, approaching equilibrium levels. Therefore, the ductility is improved at higher temperatures, close to the Ae_3, resulting in a shallower trough.

10 - The ductility trough is extended to the single phase austenite region when fine AlN particles are precipitated at the austenite grain boundaries. These particles act as stress concentrators and pin grain boundaries, thus allowing void formation and coalescence to take place, resulting in intergranular cracks.

11 - Grain boundary embrittlement occurs in the austenite region when the Al content is increased from 0.026 to 0.085% in the C-Mn-Al steels. Similarly, poor ductility is observed even in the low Al containing grade, when thermal cycling across the austenite-to-ferrite phase transformation is applied to the test specimens

before deformation in the austenite region. These findings can be of commercial relevance with respect to preventing transverse cracks in slabs.

12 - The Ti addition does not promote embrittlement in the austenite region. This is attributed to the formation of coarse TiN particles distributed through the matrix, as opposed to the detrimental fine grain boundary precipitation of AlN.

13 - When austenite recrystallization occurs during deformation, the stress concentration at the grain boundaries is reduced and the ductility is high, because the cracks associated with void linkage are trapped within the new recrystallized grains. However, in case of the continuous casting process, dynamic recrystallization cannot be considered a mechanism for ductility recovery, since the strain to which the slabs are submitted during straightening are much smaller than the critical strain for dynamic recrystallization.

14 - Grain boundary sliding was shown to have contributed to the embrittlement in both the single phase austenite and the duplex austenite-ferrite region.

REFERENCES

1. C. A. Taylor, Metall. Trans. B, 6B, (1975), p. 359.
2. R. Scholey, "Process Technology Proceedings of the 5th Int'l Iron and Steel Congress", 6, April 6-8, (1986), Washington-DC, USA, p. 5.
3. D. Jaffrey, I. Dover and L. Hamilton, Metals Forum, 7 , (1984), p. 67.
4. J. K. Brimacombe and I. V. Samarasekera, "Fundamental Analysis of the Continuous Casting Process", In: Thermomechanical Processing of Steel, The Centre for Metall. Process Engineering, Univ. of British Columbia, Vancouver, BC, September (1989), p. 1.
5. H. Vom Ende and G. Vogt, J. Iron Steel Inst., 210, (1972), p. 889.
6. R. Alberny, Rev. Métall. - CIT, 7, (1980), p. 581.
7. A. Etienne and W.R. Irving, Proc. of the 1985 International Conference on Continuous Casting, "Continuous Casting 85", October 1985, The Institute of Metals, London, England, p. 11.
8. J. K. Brimacombe and K. Sorimachi, Metall. Trans. B, 8B, (1977), p. 489.
9. W. T. Lankford Jr., Met. Trans., 3, (1972), p.1331.
10. L. Schmidt and Å. Josefsson, Scand. J. Metall., 3, (1974), p. 193.
11. B. Mintz, S. Yue and J. J. Jonas, to be submitted to International Materials Reviews, 1990.
12. E. T. Turkdogan, "Steelmaking Conf. Proceedings, Pittsburgh, USA, 70, (1987), p. 399.
13. K. Yamanaka, F. Terasaki, H. Ohtani, M. Oda and M. Yamashima, Trans. Iron Steel Inst. Jpn., 20, (1980), p. 810.
14. B. Mintz and J. M. Arrowsmith, Met. Technol., 1, (1979), p. 24.
15. N. E. Hannerz, Trans. Iron Steel Inst. Jpn., 25, (1985), p.156.
16. G. Bernard, J. P. Birat, B. Conseil and J. C. Humbert, Métall., 7, (1978), p. 467.
17. C. Ouchi and K. Matsumoto, Trans. Iron Steel Inst. Jpn., 22, (1982), p.181.
18. T. H. Coleman and J. R. Wilcox, Mater. Sci. Technol., 1, (1985), p. 80.
19. H. G. Suzuki, S. Nishimura, and S. Yamaguchi, Trans. Iron Steel Inst. Jpn., 22, (1982), p. 48.

20. B. G. Thomas, J. K. Brimacombe and I. V. Samarasekera, ISS Transactions, 7, (1987), p. 7.

21. H. G. Suzuki, S. Nishimura, and S. Yamaguchi, "Proc. of the International Symposium on Physical Simulation of Welding, Hot Forming and Continuous Casting", May 2-4, (1988), Ottawa, Canada, in press.

22. P. J. Wray, Metall. Trans. A, 7A, (1976), p. 1621.

23. F. Weinberg, Metall. Trans. B, 10B, (1979), p. 219.

24. F. Weinberg, Metals Forum, 4, (1981), p. 102.

25. A. M. Guillet, Ph.D. thesis, McGill University, (1990), Montreal.

26. H. Fuji, T. Ohashi and T. Hiromoto, Trans. Iron Steel Inst. Jpn., 18, (1978), p. 510.

27. C. J. Adams, "Proc. of the Nation. Basic Open Hearth Conf.", The Metallurgical Society, 54, (1971), p. 290.

28. A. Josefsson, J. Koeneman and G. Langerberg, J. Iron Steel Inst., 3, (1959), p. 240.

29. T. Matsumiya, M. Ito, H. Kajioka, S. Yamaguchi and Y. Nakamura, Trans. Iron Steel Inst. Jpn., 26, (1986), p. 540.

30. C. Nagasaki, A. Aizawa and J. Kihara, Trans. Iron Steel Inst. Jpn., 27, (1987), p.512.

31. R. P. Messmer and C. L. Briant, Acta Metall., 30, (1982), p. 457.

32. M. Tacikowski, G. A. Osinkolu and A Kobylanski, Acta Metall., 36, 1988, p. 995.

33. G. A. Osinkolu, M. Tacikowski and A. Kobylanski, Mater. Sci. Technol., 1, (1985), p. 520.

34. P. Yi and A. Kobylanski, "Proc. of the International Symposium on Physical Simulation of Welding, Hot Forming and Continuous Casting", May 2-4, (1988), Ottawa, Canada, in press.

35. P. J. Wray, Metall. Trans. A, 15A, (1984), p. 2059.

36. D. N. Crowther and B. Mintz, Mater. Sci. Technol., 2, (1986), p. 671.

37. T. Maki, T. Nagamichi, N. Abe and I. Tamura, Tetsu-to-Hagane, 71, (1985), p. 1367.

38. F. G. Wilson and T. Gladman, Int'l Materials Review, 33, (1988), p. 221.

39. H. G. Suzuki, S. Nishimura, J. Imamura and Y. Nakamura, Trans. Iron Steel Inst. Jpn., 24, (1984), p. 169.

40. Y. Maehara and Y. Ohmori, Mater. Sci. Eng., 62, (1984), p. 109.

41. R. E. Reed Hill, "Physical Metallurgy Principles", 2nd Ed., D. Van Nostrand, New York, N. Y., (1973), p. 374.

42. G. D. Funnell and R. J. Davies, Met. Technol., 9, (1978), p. 151.

43. G. D. Funnell, "Proc. of Hot Working and Forming Processes Conference", Sheffield, England, July (1979), The Metals Society, London, 1980, p.104.

44. G. Bernard, Rev. Métall., 77, (1980), p. 307.

45. B. Chamont, P. Chemelle, and H. Biausser, "Proc. of the International Symposium on Physical Simulation of Welding, Hot Forming and Continuous Casting", May 2-4, (1988), Ottawa, Canada, in press.

46. S. Hasebe, Tetsu-to-Hagane Overseas, 3, (1963), p. 200.

47. H. Watanabe, Y. E. Smith and R Pehkle, "The Hot Deformation of the Austenite", Ed. J. B. Ballance, The Metallurgical Society of AIME, (1977), p. 140.

48. W. C. Leslie, R. L. Rickett, C. L. Dotson, C. S. Walton, Trans. Am. Soc. Met., 46, (1954), p. 1470.

49. D. N. Crowther, Z. Mohamed and B. Mintz, Metall. Trans. A, 18A, (1987), p. 1929.

50. B. Mintz, J. R. Wilcox and J. M. Arrowsmith, "Proc. Risø Int'l Conf. on Recrystallization and Grain Growth of Multiphase and Particle Containing Materials", Risø National Lab., Denmark, (1980), p. 303.

51. B. Mintz and J. M. Arrowsmith, "Proc of Hot Working and Forming Processes Conference", Sheffield, England, July (1979), The Metals Society, London, 1980, p.99.

52. L. Ericson, Scand. J. Metall., 6, (1977), p. 116.

53. H. G. Suzuki et al., "100th ISIJ Meeting", October 1980, #S803.

54. F. Vodopivec, J. Iron Steel Inst., 211, (1973), p. 664.

55. I. Weiss and J. J. Jonas, Metall. Trans. A, 10A, (1979), p. 831.

56. M. G. Akben, I. Weiss and J. J. Jonas, Acta Metall., 29, (1981), p. 111.

57. J. P. Michel and J.J. Jonas, Acta Metall., 29, 1981, p. 513.

58. J. R. Wilcox and R. W. K. Honeycombe, Mater. Sci. Technol., 3, (1987), p. 849.

59. Y. Maehara, K. Yasumoto, H. Tomono and Y. Ohmori, Trans. Iron Steel Inst. Jpn., 27, (1987), p. 222.

60. D. P. Rizio, R. B. Oldland and D. W. Borland, " Proc. of the Internat. Conf. on Physical Metallurgy of Thermomechanical Process. of Steels and Other Metals (Thermec 88), June 6-10, (1988), Tokyo, Japan, The Iron and Steel Institute of Japan, p. 178.

61. J. R. Wilcox and R. W. K. Honeycombe, "Proc of Hot Working and Forming Processes Conference", Sheffield, England, July (1979), The Metals Society, London, 1980, p.108.

62. T. Nozaki, J. Matsumo, K. Murata, and H. Ooi, Trans. Iron Steel Inst. Jpn., 18, (1978), p. 330.

63. B. Mintz, J. M. Stewart and D. N. Crowther, Trans. Iron Steel Inst. Jpn., 27, (1987), p.959.

64. C. Offerman, C. Å. Dacker and E. Enstrom, Scand. J. Metall., 10, (1981), p. 115.

65. D. N. Crowther and B. Mintz, Mater. Sci. Technol., 2, (1986), p. 1099.

66. D. N. Crowther and B. Mintz, Mater. Sci. Technol., 2, (1986), p. 951.

67. Y. Maehara, K. Yasumoto, Y. Sugitani and K Gunji, Trans. Iron Steel Inst. Jpn., 25, (1985), p.1045.

68. K. A. Bywater and T. Gladman, Met. Technol., 3, (1976), p. 358.

69. L. A. Norstrom and B. Johansson, Scand. J. Metall., 11, (1982), p. 139.

70. A. Gittins and W. J. Tegart,, Metals Forum, 4, (1981), p. 57.

71. G. F. Vander Voort, in "Metals Handbook", ASM International, Vol. 12, Fractography, 9th Ed, (1987), p. 91.

72. F. Garofalo, In: "Ductility", Seminar of the American Society for Metals, October 14 and 15, 1967, (1968), p. 87.

73. H. C. Chang and N. J. Grant, Trans. Metall. Soc. AIME, 206, (1956), p. 1241.

74. B. Mintz, J. J. Jonas and S. Yue, "Recrystallization'90 Conference, Wollogong, Australia, January (1990), in press.

75. ASTM Standard E 8M-85, p. 146.

76. J. Z. Briggs and R. Q. Barr, High Temp.-High Press., 3, (1971), p. 363.

77. R. W. Burman, J. Met., 29, (1977), p. 12.

78. M. Tacikowski, Ph.D. thesis, École des Mines de St Etienne, (1986), St Etienne, France.

79. E. A. Simielli, Ph.D. thesis, McGill University, Montreal, to be submitted in 1990.

80. G. E. Dieter, "Workability Testing Techniques", American Society for Metals, (1984), p. 21.

81. M. T. Postek, K. S. Howard, A. H. Johnson and K. L. McMichael, "Scanning Electron Microscopy, A Student Handbook", Ed. by M. T. Postek and Ladd Research Industries, Inc., Burlington, Vt, USA, (1980), p. 13.

82. G. F. Vander Voort, "Applied Metallography", Van Nostrand Reinhold Company Inc., New York, N. Y., (1986), p.89.

83. ASTM Standard E 112-85, p. 277.

84. M. W. Ladd, "The Electron Microscope Handbook", Ladd Research Industries, Inc., (1973), Burlington, Vt, USA, p.20.

85. E. Essadiqi, Ph.D. thesis, McGill University, (1986), Montreal.

86. J. S. Kirkaldy and E. A. Baganis, Metall. Trans. A, 9A, (1978), p. 495.

87. C. J. Smithells, "Metals Reference Handbook", Vol. I, 5th Ed., Butterworth, Boston, USA, (1976), p. 364.

88. K.W. Andrews, J. Iron Steel Inst., 227, (1965), p. 721.

89. H. J. McQueen and J. J. Jonas, "Treatise on Materials Science and Technology", Vol. 6, Academic Press, New York, USA, (1975), p. 393.

90. C. Rossard, "Microstructure and Design of Alloys", Vol. II, Inst. Metals and Iron Steel Inst., London, England, (1974), p. 175.

91. K. Narita, Trans. Iron Steel Inst. Jpn., 15, (1975), p. 145.

92. E. T. Turkdogan, S. Ignotowicz and J. Pearson, J. Iron Steel Inst., 180, (1955), p. 349.

93. P. J. Wray, Met. Technol., 12, (1981), p. 466.

94. M. Gráf and E. Hornbogen, Acta Metall., 25, (1977), p. 883.

95. D. A. Porter and K. E. Easterling, "Phase Transformation in Metals and Alloys", Van Nostrand Reinhold Co., New York, USA, (1981), p. 288.

96. T. Maki, I. Tamura, T. Nagamichi and N. Abe, Trans. Iron Steel Inst. Jpn., 24, (1984), p. B-131.

97. E. Essadiqi and J. J. Jonas, Metall. Trans. A, 19A, (1988), p. 417.

98. W. C. Leslie, ISS Trans., 2, (1983), p. 1.

99. F. Vodopivec, Met. Technol., 1, (1974), p. 151.

100. E. L. Brown and A. J. DeArdo, "Thermomechanical Processing of Microalloyed Austenite", Ed. A. J. DeArdo et al., Warrendale PA, USA, Metallurgical Society of AIME, (1982), p. 319.

101. P. P. Ianc and N. I. Dragan, "Thermomechanical Processing of Microalloyed Austenite", Ed. A. J. DeArdo et al., Warrendale PA, USA, Metallurgical Society of AIME, (1982), p. 361.

102. J. R. Wilcox and R. W. K. Honeycombe, Met. Technol., 11, (1984), p. 217.

APPENDIX I

LISTING OF PROGRAM FOR EXECUTING TENSILE TEST AT CONSTANT TRUE STRAIN RATE

```
10 REM ------------------------------------------------
20 REM CONTINUOUS CONSTANT TRUE STRAIN RATE TENSION TEST
30 REM ------------------------------------------------
40 ERASE
50 DIM X(250,2),Y(1100,2)
60 PRINT "DATE="; \ INPUT D$
70 PRINT "TEST IDENTIFICATION="; \ INPUT N$
80 PRINT  \ PRINT "MATERIAL="; \ INPUT M$
90 PRINT  \ PRINT "THERMAL TREATMENT (TEMP,HOLDING TIME)="; \ INPUT T1$,H1$
100 PRINT  \ PRINT "TEST CONDITIONS(TEMP,HOLDING TIME)="; \ INPUT T9$,H9$
110 PRINT  \ PRINT "INITIAL LENGTH(mm)="; \ INPUT L0
120 PRINT  \ PRINT "INITIAL DIAMETER(MM)="; \ INPUT D0 \ A0=PI*(D0)^2/4
130 PRINT  \ PRINT "TRUE STRAIN AND STRAIN RATE="; \ INPUT S,S1
140 PRINT  \ PRINT "STROKE RANGE(MM)="; \ INPUT S0
150 PRINT  \ PRINT "LOAD RANGE(KIP)="; \ INPUT L5 \ L9=L5*4.4482*1000
160 PRINT "PRESS RETURN TO START THE TEST"; \ INPUT G$
170 PRINT "STARTING THE AUTOMATIC POSITIONING OF THE PISTON"
180 FGARB(1,"R", TIME 100,.2)
190 ADIMMED(1,A)
200 FGGO
210 IF A>5.00000E-03 THEN GO TO 230
220 GO TO 190
230 FGSTOP
240 S9=A*L9/A0
250 ETIME \ SLEEP(1)
260 ADIMMED(3,B)
270 T5=S/S1
280 FOR I=1 TO 250
```

```
290 L1=L0*EXP(S*I/250)
300 X(I,0)=(L1-L0)/S0+B
310 NEXT I
320 CKTIME(1,.1)
330 R1=10 \ R2=20
340 ADTIMED(1,Y,,3,R1,1)
350 ADTIMED(2,Y,,3,R2,1)
360 FGARB(1,"R", TIME T5/250, ARRAY X)
370 PRINT  \ PRINT "ENTER 'RUN' TO BEGIN TEST"; \ INPUT Y$
380 IF Y$<>"RUN" THEN 370
390 PRINT "RUNNING"
400 ADINIT \ ADGO(1) \ FGGO
410 IF Y>20 THEN GO TO 430
420 GO TO 410
430 ADSTOP(1) \ ADGO(2)
440 FGSTATUS(1,W) \ IF W<>0 THEN GO TO 440
450 FGSTOP \ ADSTOP(2)
460 REM - RETURNING THE PISTON TO ZERO POSITION
470 FGIMMED(1,"R", TIME 10,0)
480 REM
490 ERASE
500 PRINT  \ PRINT "DATE: "; \ PRINT D$
510 PRINT  \ PRINT "TEST#="; \ PRINT N$;
520 PRINT "                                MATERIAL="; \ PRINT M$
530 PRINT  \ PRINT "SPECIMEN GAGE LENGTH="; \ PRINT L0; \ PRINT "mm"
540 PRINT "SPECIMEN DIAMETER="; \ PRINT D0; \ PRINT "mm"
550 PRINT  \ PRINT "LOAD RANGE="; \ PRINT L9; \ PRINT "N"
560 PRINT "STROKE RANGE="; \ PRINT S0; \ PRINT "mm"
570 PRINT  \ PRINT "ENTERED MAXIMUM STRAIN PROGRAMMED="; \ PRINT S
580 PRINT "STRAIN RATE="; \ PRINT S1; \ PRINT "(1/s)"
590 PRINT "THERMAL TREATMENT (TEMP,HOLDING TIME)="; \ PRINT T1$;"-";H1$
600 PRINT "TEST TEMPERATURE="; \ PRINT T9$
610 PRINT "HOLDING TIME AT TEST TEMPERATURE="; \ PRINT H9$
620 PRINT  \ PRINT "THE INITIAL STRESS ON THE SAMPLE IS:"; \ PRINT S3; \ PRINT "
630 PRINT  \ PRINT "PISTON INITIAL POSITION(B)="; \ PRINT B; \ PRINT "(FRACTION)"
640 PRINT  \ PRINT "NUMBER OF DATA ACQUIRED="; \ PRINT C
650 PRINT "RATE OF DATA ACQUISITION (FIRST 20 DATA)="; \ PRINT 1/(R1*.1);
660 PRINT "(DATA/SEC)"
670 PRINT "RATE OF DATA ACQUISITION (N>20)="; \ PRINT 1/(R2*.1);
```

```
680 PRINT "(DATA/SEC)"
690 W=SYS(4)
700 ERASE
710 PRINT "DO YOU WANT TO SAVE THE DATA"; \ INPUT G$
720 IF G$="N" THEN GO TO 760
730 OPEN "DU1:T"&N$ FOR OUTPUT AS FILE #1
740 FOUT(1,Y(1,1),,0,F)
750 CLOSE #1
760 PRINT "DO YOU WANT TO SEE THE DATA"; \ INPUT G$
770 IF G$="N" THEN GO TO 920
780 ERASE
790 OPEN "DU1:T"&N$ FOR INPUT AS FILE #1
800 FINP(1,Y(1,1),,0,F) \ CLOSE #1
810 PRINT "STEP";TAB(9);"LOAD";TAB(20);"DISPLACEMENT";TAB(37);"TRUE STRESS";
820 PRINT TAB(58);"TRUE"
830 PRINT TAB(9);"(N)";TAB(24);"(mm)";TAB(40);"(MPa)";TAB(57);"STRAIN" \ PRINT
840 FOR I=1 TO Y STEP 20
850 D=(ELEVEL(Y(I,1))-B)*S0
860 Z=L0+D
870 L=(ELEVEL(Y(I,2)))*L9
880 T=L/(A0*L0/Z)
890 PRINT I;TAB(7);L;TAB(22);D;TAB(39);T;TAB(56);LOG(Z/L0)
900 NEXT I
910 W=SYS(4)
920 PRINT \ PRINT "DO YOU WANT TO SEE THE GRAPHICS"; \ INPUT F$
930 IF F$="N" THEN GO TO 1440
940 OPEN "DU1:T"&N$ FOR INPUT AS FILE #1
950 FINP(1,Y(1,1),,0,F) \ CLOSE #1
960 PHYL(1,5,95,0,39)
970 PRINT \ PRINT "ENTER THE LOAD LIMIT(KN)"; \ INPUT K
980 PRINT \ PRINT "ENTER THE LOAD INTERVAL"; \ INPUT K1
990 PRINT \ PRINT "ENTER THE ELONGATION LIMIT(mm)"; \ INPUT E
1000 PRINT \ PRINT "ENTER THE ELONGATION INTERVAL"; \ INPUT E1
1010 ERASE
1020 SCALE(1,0,0,E,0,K)
1030 INVEC(1) \ PLOT(1,0,0)
1040 PLOT(1,0,K)
1050 PLOT(1,E,K)
1060 PLOT(1,E,0)
```

```
1070 PLOT(1,0,0)
1080 LABEL(1,"ELONGATION(mm)","LOAD(KN)",E1,K1,1)
1090 LABEL(1,"","",E1/5,K1/5,3)
1100 COMM(1,"TEST #=",.09*E,K*.95) \ COMM(1,N$,.2*E,K*.95)
1110 COMM(1,"DATE=",.27*E,K*.95) \ COMM(1,D$,.36*E,K*.95)
1120 COMM(1,"MATERIAL=",.09*E,K*.9) \ COMM(1,M$,.24*E,K*.9)
1130 FOR I=1 TO Y
1140 D=(ELEVEL(Y(I,1))-B)*S0
1150 L=(ELEVEL(Y(I,2)))*L9/1000
1160 IF D>E THEN GO TO 1190
1170 MARK(1,4,D,L)
1180 NEXT I
1190 W=SYS(4)
1200 ERASE
1210 PRINT  \ PRINT "ENTER THE TRUE STRESS LIMIT (MPa)"; \ INPUT T1
1220 PRINT  \ PRINT "ENTER THE TRUE STRESS INTERVAL"; \ INPUT T2
1230 PRINT  \ PRINT "ENTER THE TRUE STRAIN LIMIT"; \ INPUT S4
1240 PRINT  \ PRINT "ENTER THE TRUE STRAIN INTERVAL"; \ INPUT S5
1250 ERASE
1260 SCALE(1,0,0,S4,0,T1)
1270 INVEC(1) \ PLOT(1,0,0)
1280 PLOT(1,0,T1)
1290 PLOT(1,S4,T1)
1300 PLOT(1,S4,0)
1310 PLOT(1,0,0)
1320 LABEL(1,"TRUE STRAIN","TRUE STRESS (MPa)",S5,T2,1)
1330 LABEL(1,"","",S5/5,T2/5,3)
1340 COMM(1,"TEST #=",.09*S4,T1*.95) \ COMM(1,N$,.2*S4,T1*.95)
1350 COMM(1,"DATE=",.27*S4,T1*.95) \ COMM(1,D$,.36*S4,T1*.95)
1360 COMM(1,"MATERIAL=",.09*S4,T1*.9) \ COMM(1,M$,.24*S4,T1*.9)
1370 FOR I=1 TO Y
1380 D=(ELEVEL(Y(I,1))-B)*S0
1390 Z=L0+D
1400 T=(ELEVEL(Y(I,2)))*L9/(A0*L0/Z)
1410 MARK(1,4,LOG(Z/L0),T)
1420 IF LOG(Z/L0)>S4 THEN GO TO 1440
1430 NEXT I
1440 W=SYS(4)
1450 ERASE
1460 END
```

APPENDIX II

LIMITATIONS OF THE EQUATIONS OF ANDREWS IN THE DETERMINATION OF THE AUSTENITE-TO-FERRITE EQUILIBRIUM TRANSFORMATION TEMPERATURE

In the literature, the equilibrium temperatures for the start (Ae_3) and end (Ae_1) of transformation are frequently calculated by the following empirical expressions determined by Andrews [88]:

$$Ae_3(°C) = 910 - 25Mn - 11Cr - 20Cu + 60Si + 60Mo + 40W + 100V + 700P + 3 - (+250Al + 120As + 400Ti) \qquad (II.1)$$

$$Ae_1(°C) = 723 - 10.7Mn - 16.9Ni + 29.1Si + 16.9Cr + 290As + 6.38W \qquad (II.2)$$

with concentrations expressed in wt%. In his original publication, Andrews did not include the effects of C and Ni in equation (II.1). Instead, the influence of these 2 elements was tabulated. However, using this table for the chemical composition of the steels examined in the present work, the effects of C and Ni can be included in equation (II.1) as the terms (-480C) and (-48Ni), respectively.

As can be seen in the Ae_3 expression the effect of titanium and aluminum is to *lower* the Ae_3. This appears to be a typographic error because it directly contradicts the basic metallurgical fact that these 2 elements are strong ferrite stabilizers, and therefore should *raise* the Ae_3. In other words, Andrews' approach does not appear to apply to steels relatively high in Al and Ti. In fact, Andrews himself considers that the influence of the elements within parenthesis in Eq.(II.1) are "particularly doubtful". Thus, in steels with low Ti and Al concentrations, it is probably advisable to omit these terms. However, the following calculation indicates that the levels of Ti and Al used in this work are *not* negligible.

Since the available nitrogen in a steel combines preferentially with titanium (as compared with aluminum), it may be assumed that, for the Ti treated grade used in this investigation, all the added Al (Al = 0.095%, see Table 3.1) is in solid solution.

Assuming that the titanium nitride composition is TiN, the amount of Ti that remains in solid solution for this grade is 0.023%. Taking the above into consideration, the Ae_3 temperatures calculated according to Eq. (II.1) for the steels used in this investigation, are listed in Table II.1. The Ae_3 determined by the same procedure, but assuming a negligible influence of the Al and Ti are also included in Table II.1.

Table II.1 - Ae_3 temperature calculated using Andrews' expression (with and without Al and Ti)

Designation	Ae_3 temp. (°C)	Ae_3 temp. (°C) (without Ti and Al)
Low Al steel	863	870
High Al steel	849	870
Ti-treated steel	844	872
High Mn steel	864	869

By comparing the two columns in Table II.1, it is clear that the effects of Al and Ti are not "negligible". In the High Al and Ti treated steels, the influence of these elements alter the Ae_3 temperature by 21 and 28°C, respectively. Thus, using Eq. (II.1) but with the Al and Ti terms ommitted is not a possibility with the steels used in this work.

A further limitation of Andrews' analysis lies in the effect of Mn. Andrews notes that Eq. (II.1) is less accurate for Mn>1%. This degree of inaccuracy is illustrated by comparing Ae_3 values calculated using the computer program developed by Essadiqi [85] based on the thermodynamic considerations by Kirkaldy and Baganis [86]. This procedure also does not take the influences of Al and Ti into consideration. Therefore, as can be seen in Table 4.2 (in Chapter 4), the Ae_3 calculated by both procedures practically coincide for the Low Al steel, but differ by 13, 19 and 21°C for the High Al, Ti treated and High Mn steel respectively. Furthermore, for the High Mn steel, the Ae_3 determined by the method of Kirkaldy and Baganis is more consistent with the metallographic and ductility results obtained in this research.

Therefore, from the above analysis, the equation of Andrews for the Ae_3 can be used only for steels with low additions of Mn, and low levels of Al and Ti in solid solution. Consequently, in this study it was applicable only for the Low Al steel grade. The above restrictions do not apply for the Ae_1 temperature determination, and Eq. (II.2) was used in this work.